

**Duox NADPH oxidases in the airways:
regulation in health and malignancy**

Inaugural-Dissertation
zur Erlangung des Doktorgrades
der Mathematisch-Naturwissenschaftlichen
Fakultät der Universität zu Köln

vorgelegt von
Sylvia Luxen
aus Krefeld

Köln 2008

Berichtersteller:

Prof. Arnd Baumann
Prof. Sigrun Korsching

Tag der mündlichen Prüfung: 24.10.2008

meiner Familie

Table of Contents

Table of Contents	V
Figure Index	VIII
Table Index	X
Abbreviations	XI
1 Introduction.....	1
1.1 Reactive Oxygen Species in the Lung	1
1.2 Family of NADPH Oxidases	2
1.3 Duox1 and Duox2, novel members of the Nox family	5
1.3.1 DuoxA1 and DuoxA2, maturation factors for Duox1 and Duox2	6
1.3.2 Tissue localization of Duox	7
1.3.3 Function of Duox in other species	8
1.3.4 Potential functions for Duox in the airway epithelium	8
1.4 Duox in disease.....	9
1.5 Specific Aims.....	11
2 Materials and Methods	12
2.1 Chemicals and Reagents.....	12
2.1.1 Kits	13
2.1.2 Molecular Weight Markers.....	13
2.1.3 Buffers and Solutions.....	14
2.1.4 Antibodies.....	16
2.1.5 Rodent primers	16
2.1.6 Human Primers	17
2.2 Technical Equipment	18
2.2.1 Computer Programs	18
2.2.2 Internet Programs.....	19
2.3 Tissue Culture	19
2.3.1 Cell Culture Media	19
2.3.2 Cell Culture (2D).....	19
2.3.3 Polarized Airway System (3D).....	20
2.3.4 Treatments	20
2.3.5 Human and rodent tissue samples	20

2.4	Molecular Biology.....	21
2.4.1	Nucleic Acid Extraction	21
2.4.2	Determination of the concentration of RNA or DNA	22
2.4.3	cDNA Synthesis	22
2.4.4	Polymerase Chain Reaction (PCR)	22
2.4.5	Agarose Gel Electrophoresis.....	23
2.4.6	Bisulfite conversion of gDNA and methylation specific PCR	23
2.4.7	TOPO-cloning and Bisulfite sequencing.....	24
2.4.8	Lentivirus production and cell transduction.....	24
2.5	Immunodetection of Proteins	25
2.5.1	Protein isolation and quantification	25
2.5.2	Immunoblotting (IB)	25
2.5.3	Immunoprecipitation (IP)	26
2.5.4	Immunofluorescence (IF).....	26
2.5.5	Immunohistochemistry (IHC).....	26
2.6	Cell Biology Assays.....	27
2.6.1	Homovanillic acid (HVA) assay.....	27
2.6.2	Wound closure assay.....	27
2.6.3	Transwell Migration Assay.....	27
2.6.4	Cell Viability Assay	28
2.7	Statistical analysis	28
3	Results	29
3.1	Regulation and expression of Duox1 and Duox2	29
3.1.1	Expression analysis of Duox1 and Duox2 in primary lung epithelial cells	29
3.1.2	Duox proteins require DuoxA maturation factors for function.....	30
3.1.3	Duox and DuoxA co-localize at the same sub-cellular compartments	31
3.1.4	DuoxA maturation factors form complexes with Duox proteins	32
3.1.5	Characterization of DuoxA isoforms.....	34
3.1.6	Mismatch pairing of Duox and DuoxA.....	36
3.1.7	Generation of isoform-specific Duox1, Duox2 and DuoxA1 antibodies.....	38
3.1.8	Analysis of endogenous Duox and DuoxA expression	38
3.1.9	<i>in vivo</i> expression of Duox in lung epithelium.....	42
3.2	Duox-silencing in human lung cancer.....	43

3.2.1	Expression analysis of Duox and DuoxA in lung cancer cell lines	43
3.2.2	Restoration of Duox/DuoxA expression through global demethylation	44
3.2.3	Detailed methylation analysis of the <i>DUOX1</i> and <i>DUOX2</i> promoter	45
3.2.4	Expression of Duox in lung cancer tissues	47
3.2.5	Reconstitution of Duox leads to enhanced migration.....	50
3.3	Characterization of Duox expression in Rodents	54
3.3.1	Duox expression in murine airways.....	54
3.3.2	Duox expression in rat airways.....	55
4	Discussion	57
4.1	Regulation of Duox1 and Duox2.....	57
4.2	Duox in lung cancer	60
4.3	Outlook	63
5	Summary	65
6	Zusammenfassung.....	66
7	References.....	67
8	Acknowledgments	76
9	Erklärung	77
10	Curriculum Vitae.....	78

Figure Index

Figure 1: NADPH oxidase-derived ROS mediates intracellular signaling.....	2
Figure 2: Assembly and activation of the phagocytic NADPH oxidase Nox2	3
Figure 3: Transmembrane topology and domain structure of the family of NADPH oxidases.....	4
Figure 4: Transmembrane topology and functional domains of Duox proteins	6
Figure 5: Genomic arrangement of DUOX/DUOXA and topology of DuoxA maturation factors.....	7
Figure 6: Duox-based generation of a proton-gradient	9
Figure 7: Air-liquid system (3D)	20
Figure 8: Histology information.....	21
Figure 9: Bisulfite treatment and methylation-specific primer design	24
Figure 10: Expression analysis of Duox1 and Duox2 in primary human lung epithelial cells.....	29
Figure 11: Production of H ₂ O ₂ In primary lung epithelial cells.....	30
Figure 12: Duox-dependent H ₂ O ₂ production	31
Figure 13: Distinct localization of Duox1 and Duox2 in lung epithelial cells.....	32
Figure 14: Stable expression of functional Duox1 and Duox2.	33
Figure 15: Inhibition of heme-insertion into Duox1 and Duox2	34
Figure 16: Putative structure of DuoxA1 and DuoxA2	34
Figure 17: Endogenous levels of Duox and DuoxA.....	35
Figure 18: Reconstitution of Duox1 and DuoxA1-isoforms.....	36
Figure 19: Analysis of Duox-dependent H ₂ O ₂ production by matched and mismatched pairs of Duox and DuoxA	37
Figure 20: Duox2 localization is contingent on co-expression of DuoxA1-2 or DuoxA2.....	37
Figure 21: Heterodimer formation of Duox2 with DuoxA1-2	38
Figure 22: Validation of isoform-specific antibodies.....	38
Figure 23: Analysis of endogenous Duox expression in primary lung epithelial cells.....	39
Figure 24: Analysis of exogenous and endogenous Duox and DuoxA localization in primary human lung epithelial cells SAEC.....	40
Figure 25: Localization of endogenous Duox1, DuoxA1 and Duox2 in <i>in vitro</i> differentiated primary lung epithelial cells.....	41
Figure 26: Detection of endogenous Duox in human lung tissues.....	42
Figure 27: Expression analysis of <i>DUOX1</i> , <i>DUOX2</i> , <i>DUOXA1</i> , <i>DUOXA2</i> in lung epithelial cells and lung cancer cell lines	43

Figure 28: Analysis of the promoter regions upstream of <i>DUOX1</i> , <i>DUOX2</i> , <i>DUOXA1</i> and <i>DUOXA2</i>	44
Figure 29: Recovery of <i>DUOX1</i> , <i>DUOX2</i> , <i>DUOXA1</i> and <i>DUOXA2</i> expression after treatment with 5-aza-2'-deoxycytidine (Aza)	44
Figure 30: Recovery of Duox protein in lung cancer cells	45
Figure 31: Methylation specific PCR.....	46
Figure 32: Bisulfite sequencing.	47
Figure 33: Expression analysis of <i>DUOX1</i> , <i>DUOXA1</i> and <i>DUOX2</i> in 11 paired cancerous and adjacent normal lung tissue samples	48
Figure 34: Duox expression and promoter analysis in tumor specimen.....	49
Figure 35: Reintroduction of functional Duox into lung cancer cell lines	50
Figure 36: Duox1 increases directional migration and wound closure but not proliferation.....	51
Figure 37: Duox1 and Duox2 increase migration in NCI-H661.....	52
Figure 38: Localization of Duox proteins at the leading edge.....	53
Figure 39: Immunohistochemical detection of mouse Duox in C57BL/6 mice	54
Figure 40: Endogenous expression of mouse <i>DUOX1</i> , <i>DUOX2</i> , <i>DUOXA1</i> and <i>DUOXA2</i>	55
Figure 41: Endogenous expression of Duox in rat airways	56
Figure 42: Aberrant promoter hypermethylation as biomarker for lung cancer prediction	63

Table Index

Table 1: Tissue distribution and known regulatory factors of human Nox/Duox	5
Table 2: Antibody list.....	16
Table 3: Rodent primer list.....	16
Table 4: Human primer List	17

Abbreviations

%	percent
2D	two dimensional
3D	three dimensional
3'	three prime end of DNA sequences
5'	five prime end of DNA sequences
aa	amino acid
ALI	air-liquid interphase
APS	ammonium persulfate
ASI	airway surface liquid
ATP	adenosine triphosphate
Aza	5-Aza-2'- deoxycytidine
BCA	bicinchoninic acid
BEGM	bronchial epithelial growth media
bp	base pair
C	cytosine
°C	degrees Celsius
Ca ²⁺	Calcium ion
cAMP	cyclic adenosine monophosphate
cDNA	complementary DNA
CF	cystic fibrosis
CFTR	cystic fibrosis transmembrane conductance regulator
CO ₂	carbon dioxide
COPD	chronic obstructive pulmonary disease
Da	Dalton
DAPI	4',6-diamidino-2-phenylindole
ddH ₂ O	double distilled water
DEPC	diethylpyrocarbonate
DMSO	dimethylsulfoxide
DNA	desoxyribonucleic acid
dNTP	desoxynucleotide-triphosphate
DPI	Diphenyleneiodonium chloride
ds	double-stranded
DSP	dithiobis(succinimidyl-propionate)
DTT	1,4-Dithio-DL-threitol
Duox	dual oxidase
ECL	enhanced chemiluminescence
EDTA	ethylene-diaminetetraacetic acid
EGFR	epidermal growth factor receptor
ERK	extracellular signal-regulated kinase
FAD	flavin adenine dinucleotide
FCS	fetal calf serum
g	gram
G	guanine
GDP	guanosine diphosphate
GTP	guanosine triphosphate
H ₂ O ₂	hydrogenperoxide
HEPES	N-2-hydroxyethylpiperazine-N'-2-ethansulfonic acid

His	histidine
Hr	hour
HRP	horseradish peroxidase
IF	immunofluorescence
IFN- γ	interferon γ
IL	interleukin
IP	immunoprecipitation
kbp	kilobase pairs
kDa	kilodalton
LPS	lipopolysaccharide
mA	milliampere
mg	milligram
min	minute
ml	milliliter
MMP	matrix metalloproteinase
mRNA	messenger RNA
MTT	3-(4,5-Dimethylthiazol-2-yl)-2,5-diphenyltetrazolium bromide
MUC5AC	mucin 5AC
NaCl	sodium chloride
NADPH	nicotinamide adenine dinucleotide phosphate
NaF	sodium fluoride
NaN ₃	sodium azide
NaOH	sodium hydroxide
Na ₃ VO ₄	Sodium orthovanadate
NCI	national cancer institute
NEM	N-ethylmaleimide
NHBE	normal human bronchial epithelial cells
nm	nanometer
nmol	nanomole
NOX	NADPH oxidase
NP-40	Nonidet P-40
O ₂	oxygen
OSCN ⁻	hypothiocyanite
PBS	phosphate buffered saline
PCR	polymerase chain reaction
PDGF	platelet-derived growth factor
PFA	paraformaldehyde
PI3K	phosphatidylinositol-3 kinase
PIP ₂	Phosphatidylinositol-4,5-bisphosphate
PIP ₃	Phosphatidylinositol-3,4,5-trisphosphate
PMSF	Phenylmethylsulphonylfluoride
PTP	protein tyrosine phosphatase
RIPA	radioimmuno-precipitation assay buffer
RNA	ribonucleic acid
ROS	reactive oxygen species
rpm	revolutions per minute
RT	room temperature
SA	succinyl acetone
SAEC	small airway epithelial cells
SALE	small airway lung epithelial cells
SCN ⁻	thiocyanate

SDS	sodium dodecyl sulfate
sec	second
shRNA	small/short hairpin RNA
ss	single-stranded
TAE	Tris-acetic acid-EDTA buffer
Taq	Pol polymerase from <i>Thermus aquaticus</i>
TBS	tris buffered saline
TBS-T	tris buffered saline with tween
TE	Tris-EDTA buffer
TEMED	N,N,N',N'-tetramethylethylenediamine
Th1/2	T helper cell
Tris	2-amino-2-(hydroxymethyl)-1,3-propanediol
TWEEN	polyoxethylene-sorbitan-monolaureate
U	uracil
V	volts
v/v	volume per volume
w/v	weight per volume
μg	microgram
μl	microliter
μM	micromolar

1 Introduction

1.1 Reactive Oxygen Species in the Lung

The lung is a highly specialized organ and plays fundamental roles for the host organism. Based on its distinctive structure, it provides an enormous surface area to the ambient air, thereby allowing efficient gas exchange of vital oxygen (O₂) and the metabolic waste product carbon dioxide (CO₂). However, the lung does not only provide an entry for oxygen; its epithelium faces harmful oxidants, toxicants, pollutants as well as airborne pathogens. Many of these inhaled environmental challenges give rise to reactive oxygen species (ROS), which have been identified as major contributors to oxidative stress (Azad et al., 2008; van der Vliet, 2008).

ROS include radical components, such as superoxide (O₂^{•-}) or hydroxyl radicals (OH[•]), and non-radical components, such as hydrogen peroxide (H₂O₂), hydrochlorous acid (HOCl), ozone (O₃) or peroxyxynitrate (ONOO⁻) (Henricks and Nijkamp, 2001). ROS are generally highly reactive and have the ability to oxidize intracellular macromolecules, such as proteins, nucleic acids, lipids and membranes (Stadtman, 2006). Thus, ROS have been linked to DNA mutations, protein oxidation, lipid peroxidation and cell damage (Lambeth, 2004; Ryter et al., 2007). During inflammation excessive endogenous ROS levels are responsible for tissue injury, as they generate stable oxidation products. In the airways, ROS have been linked to acute respiratory distress syndrome and acute lung injury by either directly damaging the pulmonary structures or indirectly by initiating the release of other inflammatory mediators (Henricks and Nijkamp, 2001; Mills and Higgins, 1997). Prolonged oxidative stress can cause chronic lung diseases such as asthma, idiopathic pulmonary fibrosis and chronic obstructive pulmonary disease (COPD) (Barnes, 2000).

Environmental ROS are largely derived from air pollutants as well as cigarette smoke. In addition, ROS can also be derived endogenously. Low amounts of ROS were identified as accidental by-products of the mitochondrial respiratory chain; however, the mitochondria also can produce high ROS levels during hypoxia (Chandel et al., 1998; Chandel et al., 2000; Raha and Robinson, 2000). As a result, ROS have been viewed as harmful, yet unavoidable compounds.

Recent studies have provided evidence that small localized concentrations of ROS are generated deliberately by ROS-producing enzymes, such as NADPH oxidases. ROS act as secondary messengers in intracellular signaling cascades, which are implicated in proliferation and aging as well as anti-tumorigenic processes, such as senescence and apoptosis (Valko et al., 2006). This is accomplished by reversible inhibition of protein or lipid phosphatases (PTPs) such as PTP1B, SHP-1, SHP-2 or PTEN (Finkel, 1999). They all contain an invariant catalytic cysteine residue that is highly susceptible to oxidative inactivation through transiently produced H₂O₂, leading to the formation of intermolecular disulfides (R-SOH → R-SS-R). As a consequence, receptor tyrosine kinases (RTKs) are susceptible for activation by their ligands (EGF, PDGF), leading to downstream signaling (**FIGURE 1**).

Endogenous ROS has further been identified during inflammation, which was generated by neutrophils and macrophages. However, the best understood mechanism of inducible local ROS generation is a process known as respiratory burst. In this case, as part of an innate immunity defense mechanism, phagocytes produce superoxide in order to kill invading microorganisms (Babior, 1999).

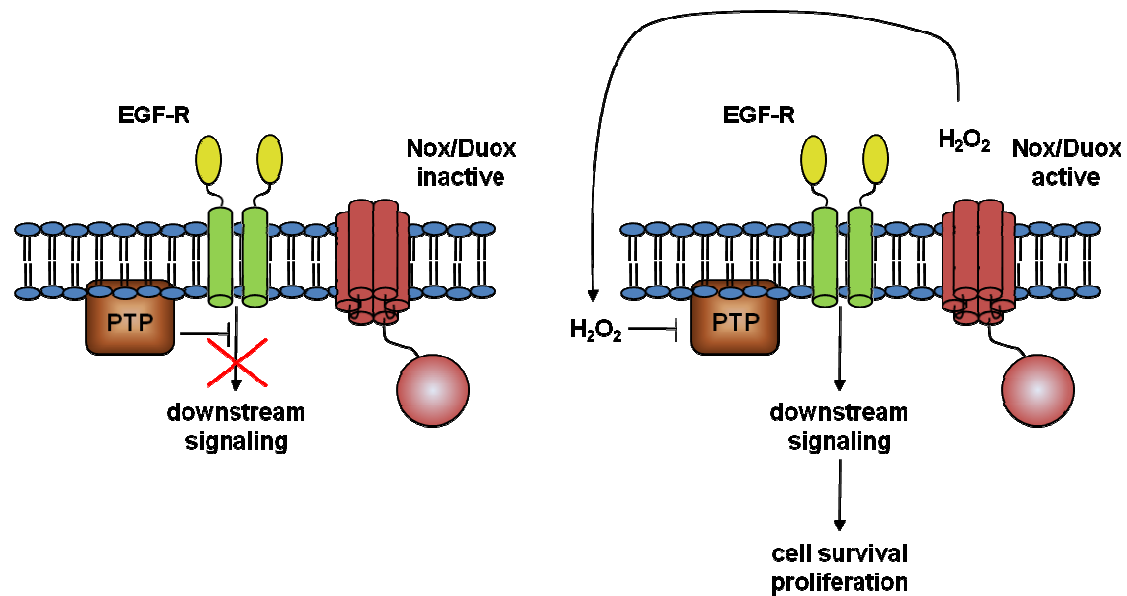


FIGURE 1: NADPH oxidase-derived ROS mediates intracellular signaling. Protein tyrosine phosphatases (PTPs) block downstream signaling of receptor tyrosine kinases (RTKs), such as epidermal growth factor-receptor (EGF-R). Transient production of H₂O₂ by NADPH oxidases leads to reversible oxidative inactivation of the PTP, through oxidation of an invariant catalytic cysteine residue. Consequently, downstream signaling of the RTKs is not blocked anymore and downstream affected pathways are activated. Adapted from (van der Vliet, 2008).

1.2 Family of NADPH Oxidases

The membrane-associated nicotinamide adenine dinucleotide phosphate (NADPH) oxidase (Nox) complex of phagocytes reduces molecular oxygen to superoxide through oxidation of NADPH. This oxidase complex consists of two membrane-bound proteins, the glycosylated catalytic component gp91^{phox} (Nox2) and the non-catalytic subunit p22^{phox}. They form a non-covalent dimer that is referred to as flavocytochrome b₅₅₈ (Wallach and Segal, 1996). The so-called “Nox-domain” of Nox2 comprises 6 transmembrane (TM) helices and contains subregions which form cavities for the binding of flavin adenine dinucleotide (FAD) and NADPH. In addition, Nox2 possesses two hemes, which are bishistidine-ligated in the parallel transmembrane helices 3 and 5, coordinated with His¹⁰¹-His¹¹⁵ and His²⁰⁹-His²²², respectively (Biberstine-Kinkade et al., 2001). The enzyme functions as an electron transferase by facilitating the transport of NADPH-derived electrons across the hemes towards extracellular molecular O₂, thus forming superoxide (Nauseef, 2008).

Nox2 activity is regulated by compartmentalization, as this enzyme has to assemble with 2 additional protein complexes in order to be fully active (FIGURE 2). These complexes reside in the cytoplasm and translocate to the membrane upon stimulation (Thrasher et al., 1994). The first complex consists of the three proteins p40^{phox}, p47^{phox} and p67^{phox}. p47^{phox} does not possess any intrinsic catalytic activity and acts as an organizing adaptor protein. p67^{phox} functions as an activating cofactor based on its domain that regulates the reduction of FAD by NADPH (Nisimoto et al., 1999). p40^{phox} interacts with p67^{phox} and participates in ROS production (Bissonnette et al., 2008). The second complex comprises the small GTPase Rac2, which is bound to RhoGDI, a GDP dissociation inhibitor for Rho GTPases. Activation of those two complexes leads to phosphorylation of p47^{phox} and RhoGDI (Nauseef, 2008). As a consequence, p47^{phox} can bind to p22^{phox} and RhoGDI dissociates from

Rac-GDP. Catalyzed by guanine nucleotide exchange factors (GEFs), GDP is exchanged with GTP, resulting in active Rac-GTP that independently translocates to the plasma membrane.

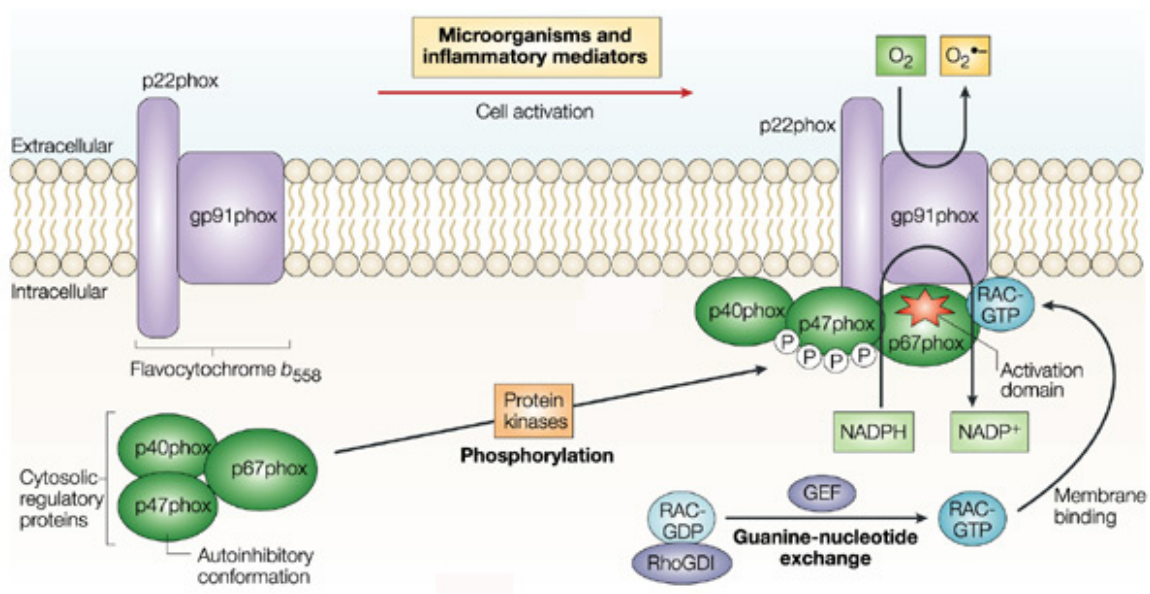


FIGURE 2: Assembly and activation of the phagocytic NADPH oxidase Nox2. The resting enzyme consists of the two membrane-bound components gp91^{phox} and p22^{phox}, which form the heterodimeric complex flavocytochrome b558. In order to be fully functional, the enzyme has to assemble with the cytosolic subunits p40^{phox}, p47^{phox}, p67^{phox} and Rac2. Upon activation, the cytosolic components translocate to the membrane, where they assemble with b558. Phosphorylation of p40^{phox} enables binding to p22^{phox}, while phosphorylation of RhoGDI leads to dissociation from inactive Rac (Rac-GDP). Rac-GDP is then activated (Rac-GTP), which promotes binding to p67^{phox} to form an active complex. Adapted from (Lambeth, 2004).

Mutations in any of these components (except of p40^{phox}) result in chronic granulomatous disease (CGD), a genetic immune disorder that results in an impaired ability of phagocytes to kill invading microorganisms (Kawahara et al., 2007; Lambeth, 2004; Nauseef, 2008; van der Vliet, 2008).

Low amounts of ROS have also been found in non-phagocytic cells and tissues. Inhibitor studies indicated that these ROS were not by-products of the mitochondrial respiratory chain, but actually flavoprotein-derived (Lambeth, 2004). Six other homologues of Nox2 were identified (Nox1, Nox3, Nox4, Nox5, Duox1, Duox2), which all possess the Nox-domain and now constitute the family of NADPH oxidases (**FIGURE 3**). Members can be divided into three groups, based on their similarity with gp91^{phox}. Nox1, Nox3 and Nox4 feature the same topology as Nox2. The slightly larger Nox5 possesses an N-terminal calmodulin-like domain, which contains four EF-hands. The EF-hand motif is ubiquitous in the genomes of eukaryotes and prokaryotes. It consists of a characteristic 30 amino acid long helix-loop-helix (HLH) structure and allows the binding of calcium. The two largest members of the Nox family, Duox1 and Duox2, build onto the structure of Nox5. These enzymes feature an additional amino terminal domain, which is homologous to peroxidases. This domain is connected to the intracellular calcium-binding region, which encodes two canonical EF-hands and an additional HLH-structure by a transmembrane α -helix (De Deken et al., 2000; Schwarzer et al., 2004).

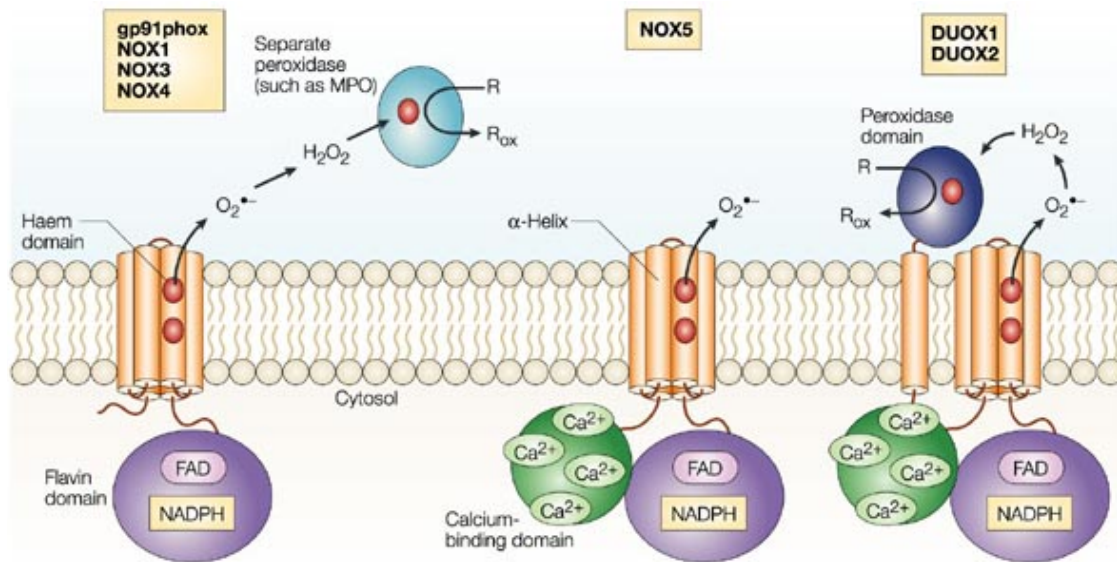


FIGURE 3: Transmembrane topology and domain structure of the family of NADPH oxidases. All members of the Nox-family feature the Nox-domain, which consists of the intracellular Flavin domain, containing binding sites for the co-enzymes FAD and NADPH, as well as an N-terminal hydrophobic domain, which forms 6 transmembrane (TM) α -helices. Two heme groups are bound to conserved histidines, which facilitate the electron transport from its donor NADPH to extracellular acceptor O_2 . Nox1, Nox3 and Nox4 have a similar structure as gp91^{phox} (Nox2). Nox5 contains an additional intracellular calcium-binding domain and Duox1/ Duox2 additionally comprise an extracellular peroxidase-homology domain TM-domain. Adapted from (Lambeth, 2004)

Not all members of the Nox family are regulated similar to Nox2. Only Nox1, Nox3 and Nox4 form a heterodimer with p22^{phox}, while Nox5, Duox1 and Duox2 do not require this subunit for function. Nox1 and Nox3 also associate with cytosolic factors, which are homologous to p47^{phox} and p67^{phox} and are termed Nox organizing (Noxo1 or p41) and Nox activating (Noxa1 or p51) protein, respectively. While both Nox1 and possibly Nox3 also need the GTPase Rac for function, Nox4, Nox5, Duox1 and Duox2 are Rac-independent (Kawahara et al., 2007; Nauseef, 2008). Nox5 function is entirely dependent on the elevation of intracellular calcium concentrations, resulting in phosphorylation of Thr⁴⁹⁴ and Ser⁴⁹⁸ and in conformational changes. The latter in turn leads to an interaction between the N-terminus and an unidentified C-terminal domain, facilitating electron delivery and superoxide production (Banfi et al., 2004; Jagnandan et al., 2007). Duox1 and possibly Duox2 are also predicted to undergo conformational changes via increase of intracellular calcium levels, resulting in ROS production upon dissociation from regulatory subunit Noxa1 (Pacquelet et al., 2008).

So far, the Nox family members have been divided into three groups, based on their similarity with gp91^{phox}. However, a recent study suggested a different classification (Kawahara et al., 2007). As Nox members are widely distributed from plants to mammals, 7 subfamilies of Nox/Duox enzymes were identified based on molecular taxonomy. No Nox-coding sequences were found in the genomes of prokaryotes, while – except for yeast – most eukaryotes (such as vertebrates, urochordates, echinodermates, nematodes, insects, fungi, plants, amoeba and red algae) encoded those genes. Nox5 and Duox are related to plant Nox, which also possess EF hands, demonstrating that the acquisition of calcium-binding domains occurred early in evolution. Indeed, the EF-hand-containing subfamilies comprise more than 50% of the taxonomic tree (Bedard et al., 2007; Kawahara et al., 2007; Torres et al., 1998).

Nox and Duox generate ROS in a regulated manner, producing reactive oxygen in various cells and tissues in response to growth factors, cytokines and Ca^{2+} -dependent signals. The expression pattern of these enzymes (**TABLE 1**) reveals tissue specificity and provides evidence that ROS generation by NADPH oxidases is a general feature of many, maybe all cells (Lambeth, 2004).

Enzyme	Highest level of expression	Known regulatory factors
Nox1	colon, uterus, prostate, vascular smooth muscle cell	Noxo1, Noxa1, p22 ^{phox} , Rac
Nox2 (gp91)	phagocytes	p47 ^{phox} , p67 ^{phox} , p40 ^{phox} , p22 ^{phox} , Rac
Nox3	inner ear, fetal kidney	p22 ^{phox} , Noxo1, p47 ^{phox} , p67 ^{phox}
Nox4	kidney, ovary, osteoclasts, heart, endothelial cells	p22 ^{phox}
Nox5	spleen, sperm, mammary gland, cerebrum	Calcium
Duox1	airways, thyroid, testis, tongue, cerebellum	Calcium, Noxa1
Duox2	thyroid, airways, colon, pancreatic islets	Calcium

TABLE 1: Tissue distribution and known regulatory factors of human Nox/Duox. Adapted from (Lambeth, 2004).

1.3 Duox1 and Duox2, novel members of the Nox family

Dual oxidases were first cloned from cDNA libraries of thyroid cells (De Deken et al., 2000; Dupuy et al., 1999) and were initially called Thox (thyroid oxidase) or Lnox (large NADPH oxidase). Duox1 was later also identified in the epithelia of the whole lung, trachea, testis, cerebellum and tongue, while Duox2 was also expressed in salivary gland, parotid gland, trachea, colon, prostate, lung and pancreas (Caillou et al., 2001; Edens et al., 2001; Forteza et al., 2005; Geiszt et al., 2003). The genes for both enzymes are located on the long arm of chromosome 15, at location 15q15.3, and are arranged head-to-head, divided by a 16 kb region (Pachucki et al., 2004). The gene for *DUOX1* is located more telomeric and spans 36 kb, encoding 35 exons, of which the first two are non-coding. The *DUOX2* gene consists of 34 exons, of which only the first exon is not coding and the whole sequence spans over 22 kb. Exons 4, 5 and 6 of *DUOX1* and *DUOX2* are more than 99% similar and the translated proteins, with respective open reading frames of 1551 and 1548 amino acids, display an 83% sequence similarity (Donko et al., 2005). The promoter regions of *DUOX1* and *DUOX2* are dissimilar. The Duox1 promoter lacks a TATA-box and features three putative binding sites for the transcription factor SP-1. Those sequences are commonly found within 100 bp of the transcriptional initiation site and are also referred to as a GC-box. While no such sequences are present in the *DUOX2* promoter, it exhibits a reverse TATA-box as well as a putative ATF/CRE-binding site, a stress-responsive element.

The Nox domain of Duox proteins is 47% similar to Nox2. In addition, these enzymes possess an N-terminal extracellular peroxidase-homology domain. Although this domain is 43% homologous with thyroperoxidase (TPO) and shares 25% identical amino acids with myeloperoxidase (MPO), its function is still a matter of controversy. Animal peroxidases contain hemes, which are bound via their iron to invariant histidine residues that provide proximal and distal axial bonds. However, the Duox peroxidase-homology domain lacks those key amino acids and encodes for serines instead (Donko et al., 2005; Nauseef, 2008). Surprisingly, when expressed in *E. coli* it could still form di- and trityrosines, a classical peroxidase feature (Edens et al., 2001). It has been suggested that this domain could also have a superoxide dismutase-like activity to promote exclusive H_2O_2 production (Morand et al., 2004), or that it functions as a docking site for secreted peroxidases, which use the Duox-based H_2O_2

(Wong et al., 2004). A long intracellular loop, which contains ER-retention signals (aa 596 to 685) and two EF-hands, links the first transmembrane domain with the Nox-domain. The latter contains, in accordance with the other members of the Nox-family two binding sites for FAD and four binding sites for NADPH (FIGURE 4).

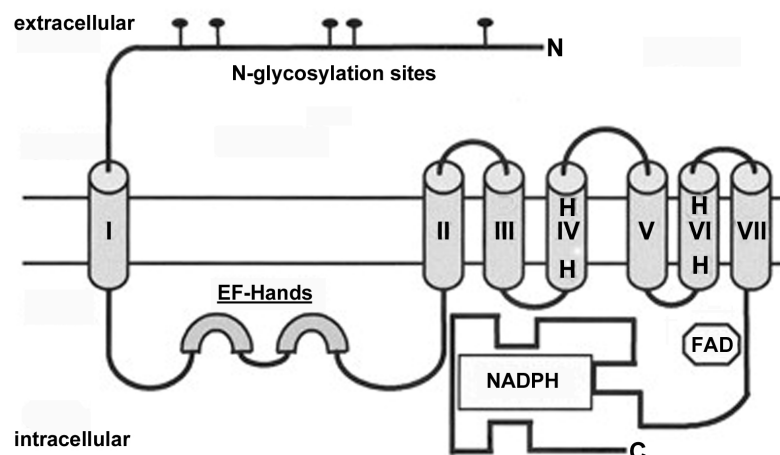


FIGURE 4: Transmembrane topology and functional domains of Duox proteins. Both Duox1 and Duox2 comprise seven membrane-spanning α -helices, of which six are part of the Nox domain. This domain contains conserved amino acids essential for heme binding, as well as intracellular binding sites for NADPH and FAD. The extracellular peroxidase-homology domain, which contains five N-glycosylation sites, is connected to the Nox domain via an intracellular sequence, comprising EF hands for Ca^{2+} -binding. Adapted from (De Deken et al., 2000).

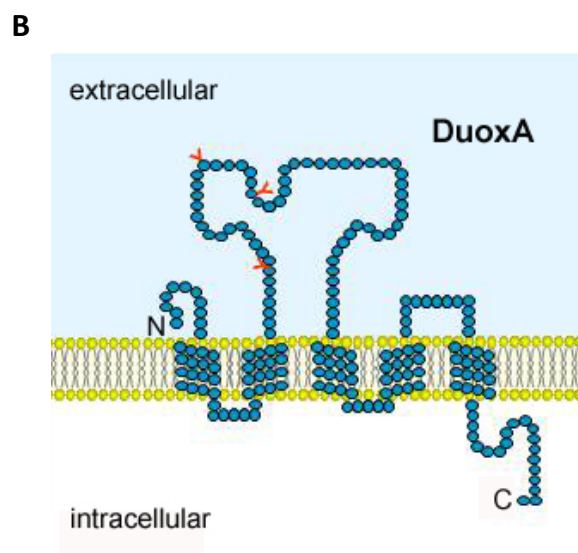
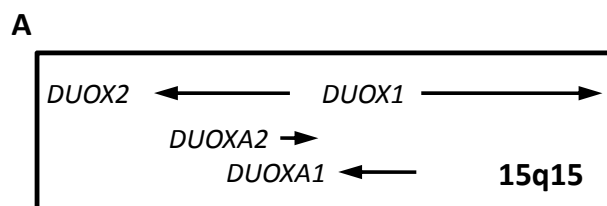
Both Duox1 and Duox2 are glycoproteins. When expressed in thyroid cells, they possess a molecular weight of 190 kDa, while a 180 kDa form is found in non-thyroid cells. Glycosylation accounts for about 10-20 kDa. Deglycosylated proteins have a molecular weight of about 160 kDa and are non-functional. It appears that glycosylation is an important step in folding and targeting the proteins to the proper compartment of the cell, thus allowing for full enzymatic activity of Duox (Caillou et al., 2001; De Deken et al., 2000).

Based on the presence of EF-hands, Duox1, as well as Duox2 and Nox5, require calcium for activity and therefore can be stimulated with ionomycin or thapsigargin. Both compounds increase intracellular calcium levels; thapsigargin primarily leads to intracellular calcium store-depletion while ionomycin works as an ionophore, allowing extracellular calcium to transit into the cell. ATP was also shown to stimulate Duox function via paracrine signaling, resulting in intracellular Ca^{2+} increase.

1.3.1 DuoxA1 and DuoxA2, maturation factors for Duox1 and Duox2

Attempts have been made to transiently reconstitute either form of Duox in non-thyroid cell lines. However, the proteins remained as an immature form in the ER rather than being translocated to the plasma membrane (Ameziane-El-Hassani et al., 2005; De Deken et al., 2002). A yeast two-hybrid screen identified EF hand-binding protein 1 (EFP1), a TPO-interacting thioredoxin-related protein, as a binding partner of Duox. However, co-expression of both EFP1 and Duox did not induce membrane targeting or Duox-dependent H_2O_2 production (Wang et al., 2005). Recently, maturation factors for Duox1 and Duox2, termed DuoxA1 and DuoxA2, were identified (Grasberger and Refetoff, 2006). They are located head-to-head with their respective oxidase in the 16 kb stretch between both DUOX genes (FIGURE 5A). This intergenic region was initially annotated as "homolog of *Drosophila* Numb-interacting protein (NIP)". A bidirectional promoter drives the transcription of Duox1/DuoxA1 and Duox2/DuoxA2, respectively. Bidirectional promoters account for 10% of all transcriptional units and

increase the probability of coordinated expression (Trinklein et al., 2004). Both DuoxA1 and DuoxA2 are integral membrane proteins and are predicted to possess 5 membrane-spanning α -helices. They



also feature an extended extracellular loop between transmembrane domain 2 and 3, which contains 3 putative N-glycosylation sites (FIGURE 5B). Co-expression of Duox1 or Duox2 with their respective maturation factor allowed Duox proteins to exit the ER and localize to the plasma membrane, resulting in inducible production of H_2O_2 (Grasberger and Refetoff, 2006).

FIGURE 5: Genomic arrangement of DUOX/DUOXA and topology of DuoxA maturation factors. (A), DUOX1 and DUOX2 are arranged head-to-head on chromosome 15, at position q15. Both maturation genes for DUOXA1 and DUOXA2 are located in the intergenic region, located head-to-head with their respective oxidase. (B), DuoxA1 and DuoxA2 are integral membrane proteins. They feature the same topological structure, encompassing 5 transmembrane (TM) domains, and contain 3 putative N-glycosylation (Y) sites in the extended extracellular loop between the second and the third TM domain. Adapted from (Grasberger and Refetoff, 2006).

1.3.2 Tissue localization of Duox

Although both isoforms can be found in the thyroid and in the lung, Duox1 and Duox2 are differentially expressed and regulated. In the thyroid Duox2 is up to six times more abundant than Duox1 (Pachucki et al., 2004). Duox2 co-localizes with thyroperoxidase (TPO) at the apical poles of thyrocytes and serves as a supplier of H_2O_2 for TPO-mediated oxidation of iodide and thyroxine synthesis in the thyroid (Donko et al., 2005; Geiszt and Leto, 2004). Duox1 is the major oxidase apically expressed in mucosal surfaces of the trachea, bronchi and large airways (Geiszt et al., 2003; Shao and Nadel, 2005). Duox1 is dramatically upregulated during alveolar maturation in the late gestational period in fetal lung epithelium and expression levels are then maintained in the adult lung (Fischer et al., 2007). In addition, other studies demonstrated that in lung epithelial cells message of Duox1 was modestly increased by Th2-specific cytokines interleukin (IL)-4 and IL-13, while the Th1-specific cytokine IFN- γ as well as bacterial infection markedly increased Duox2 transcripts (Ha et al., 2005; Harper et al., 2005).

In the airways a similar H_2O_2 -providing role has been suggested for Duox1 and Duox2 in conjunction with lactoperoxidase (LPO). LPO, which is largely found in milk, saliva, tears and mucosal secretions, can utilize H_2O_2 to oxidize the pseudohalide thiocyanate (SCN^-) into hypothiocyanate ($OSCN^-$), an oxidant which is highly effective against Gram-positive and Gram-negative bacteria (Forteza et al., 2005; Geiszt and Leto, 2004). Hence, like the phagocyte NADPH oxidase, Duoxs are thought to be involved in antimicrobial defense mechanisms in the lung. However, their roles may be

divergent, with Duox1 being the constitutive isoform monitoring long term changes and Duox2 as the inducible airway isoform, important for observation of pathologic changes (Harper et al., 2005).

1.3.3 Function of Duox in other species

NADPH oxidases have been conserved in many eukaryotes and Duox enzymes have been identified in other species. The murine isoform of Duox1 was associated with B-cell receptor (BCR) -dependent ROS generation and its suppression led to inhibition of the early ROS response, which is normally obtained upon triggering of the BCR (Singh et al., 2005). Urchin oxidase 1 (Udx1), a Duox isozyme found in sea urchins *Strongylocentrotus purpuratus* and *Lytechinus variegatus*, has a critical role during fertilization, as it supplies H₂O₂ that leads to cross-linking and therefore hardening of the fertilization envelope, thus preventing polyspermy and protecting the embryo (Wong et al., 2004). Another example of extracellular matrix-modifying activity of Duox enzymes is the process of protein cross-linking in *Caenorhabditis elegans*. Ce-Duox was shown to mediate oxidative cross-linking of tyrosine residues during cuticle biosynthesis, thereby stabilizing the extracellular matrix structure, which provides exoskeletal support for the nematode. A recent *in vivo* study demonstrated that the *Drosophila melanogaster* homologue of Duox1, termed dDuox, is indispensable for innate gut immunity. Silencing of dDuox in adult flies resulted in markedly elevated mortality rates, upon bacterial infection through contaminated food. Re-introduction of full-length dDuox reversed the phenotype. However, reconstitution of a dDuox-truncation variant lacking the extracellular peroxidase-homology domain did not augment the survival rates and flies were still as susceptible to infection as complete dDuox-deficient flies. ROS generated by dDuox was essential for the generation of an antimicrobial environment in the gut, thereby demonstrating for the first time that Duox is involved in oxidant-mediated antimicrobial response in mucosal barrier epithelia (Ha et al., 2005).

1.3.4 Potential functions for Duox in the airway epithelium

In analogy to the function of Ce-Duox, the human Duox enzymes might have a similar role in stabilizing the epithelial barrier. As they are abundantly expressed in the epithelial cells of the airways, the proteins might be able to oxidize matrix-proteins or other extracellular substrates through the peroxidase homology domain (Lambeth, 2004). Duox enzymes are further involved in homeostatic processes in the lung epithelium. Duox1 was recently linked to epithelial mucin expression, and accelerated cell migration and wound healing *in vitro* via a Duox1-H₂O₂-TACE-proligand-EGF receptor cascade (Koff et al., 2006; Kuwahara et al., 2007; Shao and Nadel, 2005; Wesley et al., 2007). Further, Duox1 was connected to acidification of the airway surface liquid (ASL) via epithelial generation of H⁺ (FIGURE 6). The composition of the airway surface liquid and its pH (pH_{ASL}) are of critical importance for the normal function of the airways, including mucociliary clearing and microbial killing (Schwarzer et al., 2004). Abrogation of the pH_{ASL} can negatively impact homeostatic functions in the epithelium, such as ciliary beating, ion transport and epithelial integrity. Activity of the NADPH oxidase domain generates intracellular H⁺ accumulation, resulting in a gradient across the apical plasma membrane. This drives acid secretion and can therefore be utilized to fine tune the pH of the ASL (pH_{ASL}) (Schwarzer et al., 2004). Moreover, intracellular acidification activates Na⁺/H⁺ exchangers, NHE, which are ubiquitously expressed and regulate cell volume, shape, migration, adhesion and proliferation (van der Vliet, 2008). In addition, Duox might actively contribute to host defense by killing invading microorganisms which escaped the primary destruction in the airway surface liquid in a Nox2-similar manner (Kyle et al., 1990; Lambeth, 2004).

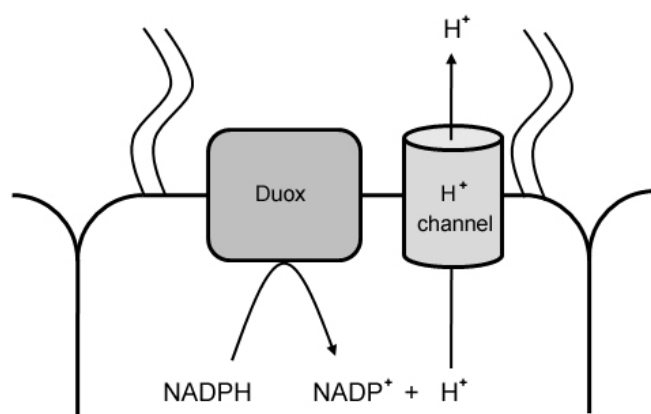


FIGURE 6: Duox-based generation of a proton-gradient. Duox enzymes in the apical membrane of the airway epithelium oxidize NADPH, resulting in intracellular acidification. Proton channels facilitate the exit of intracellular H^+ into the extracellular milieu, leading to acidification of the airway surface liquid. Adapted from (Schwarzer et al., 2004).

1.4 Duox in disease

Based on their ability to produce ROS, which in turn are involved in a multiplicity of cellular pathways, it is conceivable that a de-regulation of Duox enzymes could have severe consequences for a cell, tissue, organ or consequently, the host. Indeed, it has been demonstrated that Duox2 has an essential role in hormone biosynthesis. To date, 12 point mutations in the sequence of Duox2 have been identified, which all lead to nonsense mutations or premature stop codons, deleting the functional domains of the enzyme (Figueiredo et al., 2001; Moreno et al., 2002; Ohye et al., 2008; Pfarr et al., 2006; Varela et al., 2006; Vigone et al., 2005). The phenotype of these mutations is dominant and biallelic mutations of the gene result in severe hypothyroidism, while a heterozygous mutation still causes mild hypothyroidism. Similarly, homozygous mutation of DuoxA2, encoding for a truncated protein that lacks the fifth transmembrane domain and the cytoplasmic C-terminus, leads to hypothyroidism (Zamproni et al., 2008). This disease is solely attributable to inactivity of Duox2. Duox1 is not able to compensate for mutations of Duox2, suggesting that both enzymes have different roles in the thyroid.

Expression levels of both, Duox1 and Duox2, have not been found to be altered in other diseases of the thyroid, including Graves' thyroid tissue, toxic adenoma, multinodular goiter and hypofunctioning adenoma. In thyroid carcinomas, however, Duox levels were variable and the proteins showed a cytoplasmic localization, in contrast to the apical membrane location in normal thyroid tissue. Duox expression was increased in papillary thyroid carcinoma, although the expression levels could not be linked to certain stages of the disease (Gerard et al., 2003; Lacroix et al., 2001).

No direct causality has yet been shown between Duox de-regulation and lung disease. However, several studies have shown that transcriptional levels of Duox1 and Duox2 are affected during the emergence of certain lung pathologies and diseases. Cystic fibrosis, which is also known as mucoviscidosis, is a hereditary disease characterized by thick mucus production and compromised airway immunity, resulting in recurrent lung infections. The disease is caused by mutations in the cystic fibrosis transmembrane conductance regulator (CFTR), a channel that facilitates the transport of anions such as chloride (Cl^-) or thiocyanate (SCN^-) across the membrane. Inactivating mutations of the CFTR channel lead to a defect in SCN^- secretion. Consequently, LPO cannot use Duox-based H_2O_2 to catalyze the oxidation of SCN^- into the powerful antimicrobial hypothiocyanite ($OSCN^-$), resulting in impaired immunity in the lung (Moskwa et al., 2007). In addition, a recent study demonstrated a

significant downregulation of Duox2 in cystic fibrosis *in vivo*, thus further substantiating the relationship between impaired host defense and the Duox-LPO airway defense system (Wright et al., 2006). Defective Cl⁻ transport triggers deficient water transport into the airway surface liquid due to annihilated osmotic force. This causes thick and sticky mucus, which in turn slows clearance of the mucus and promotes formation of mucus plaques that provide nests for infection (Donaldson et al., 2006).

In asthma, levels of the Th2 cytokines IL-4 and IL-13 are upregulated, leading to enhanced Duox1 expression. A connection has been suggested between its expression and the disease, as Duox1 has been associated with airway acidification, enhanced EGFR activation and mucus hypersecretion, which are all characteristics of asthma and other inflammatory airway diseases, such as cystic fibrosis and COPD (van der Vliet, 2008). Chronic obstructive pulmonary disease (COPD) is an umbrella term for lung diseases such as emphysema, chronic bronchitis, bronchiectasis and refractory asthma, which are all delineated by permanent, incurable reduction of lung capacity. COPD is caused by smoking and characterized by shortness of breath, chronic cough, excessive production of phlegm (mucus), wheezing, recurring respiratory infections and damage to the lungs (Barnes, 2000). A direct impact of chronic smoking and the development of COPD has been shown, as both Duox1 and Duox2 are downregulated in COPD patients, which have been former smokers. Long-term exposure to cigarette smoke alone diminished only Duox1, while Duox2 was upregulated (Nagai et al., 2008). Cigarette smoke contains many cancerous and toxic substances, of which particularly thiol-reactive compounds were linked to H₂O₂ production in airway cells through activation of Duox (Jaimes et al., 2004; Lavigne and Eppihimer, 2005).

Owing to their ability to generate ROS, Duox de-regulation could lead to an increase of DNA strand breaks, mutations and deletions. As many chronic diseases of the respiratory tract are associated with increased oxidative stress and enhanced ROS production, Duox enzymes are an interesting candidate in connection with the onset of lung cancer and its progression.

1.5 Specific Aims

The family of NADPH oxidases has been associated with cell transformation, differentiation, inflammation and host defense. Based on their expression in the airway epithelium of the lung and their ability to generate ROS, Duox1 and Duox2 specifically have to be taken into consideration as mediators of host defense and pro-inflammatory effects. To date, not much is known about the spatio-temporal regulation of these enzymes, nor if lung malignancy involves Duox de-regulation. Therefore, this thesis focuses primarily on two aspects of Duox biology in the airway epithelium – Duox regulation in lung epithelial cells and its expression in lung cancer. Expression of Duox will also be analyzed in rodents, as particularly mice and rats have proven to be indispensable models for studies of human diseases. This study will include the following goals:

Objective 1: Function, regulation and expression of Duox enzymes in lung epithelial cells

To elucidate the localization and regulation of functional Duox proteins, human lung cancer cells will be utilized for exogenous expression of Duox and DuoxA protein. Further, primary lung epithelial cells will be used for analysis of endogenous expression of Duox in undifferentiated cells as well as highly differentiated, three dimensional systems.

Objective 2: Characterization of Duox expression in primary human lung cancer

To decipher if Duox expression is altered in human lung cancer, cancer cell lines and primary lung epithelial cells will be probed for expression of Duox and DuoxA. Using tissue samples derived from patients with primary lung carcinomas, expression will also be analyzed *in vivo*. If Duox expression is altered, its contribution to cell transformation will be investigated *in vitro*.

Objective 3: Evaluation of Duox expression and function in potential lung disease models

To evaluate if rodent models are applicable for studies of lung disease with respect to Duox expression and function, expression of the Duox and DuoxA homologs will be analyzed in the airways of mice and rats. Functional studies will allow correlation between the human and the rodent isoform. This might facilitate the generation of disease models, in which Duox function could be linked to certain stages or types of lung pathologies.

2 Materials and Methods

2.1 Chemicals and Reagents

Albumin Standard from BSA	Pierce, Rockford, IL
Albumin bovine serum, fatty acid free, low endotoxin	Sigma-Aldrich CO, St. Louis, MO
Ampicillin (Na salt)	Sigma-Aldrich CO, St. Louis, MO
Aprotinin	Sigma-Aldrich CO, St. Louis, MO
APS (ammonium persulfate)	Sigma-Aldrich CO, St. Louis, MO
5-Aza-2'-deoxycytidine	Sigma-Aldrich CO, St. Louis, MO
β -mercaptoethanol	Sigma-Aldrich CO, St. Louis, MO
Bromophenolblue	Sigma-Aldrich CO, St. Louis, MO
Catalase	Sigma-Aldrich CO, St. Louis, MO
Collagen (human placenta, type VI)	Sigma-Aldrich CO, St. Louis, MO
Coverslips (BD Biocoat Collagen glass coverslips)	BD Biosciences, San Jose, CA
Coverslips (photoetched)	Bellco Glass, Vineland, NJ
DAPI (4',6-diamidino-2-phenylindole)	Sigma-Aldrich CO, St. Louis, MO
DEPC (diethyl pyrocarbonate)	Sigma-Aldrich CO, St. Louis, MO
DMSO (dimethyl sulfoxide)	Sigma-Aldrich CO, St. Louis, MO
dNTP	Promega, Madison, WI
DPI (Diphenyleneiodonium chloride)	Sigma-Aldrich CO, St. Louis, MO
DSP (dithiobis(succinimidyl-propionate))	Pierce, Rockford, IL
Ethanol	Aaper Alcohol, Shelbyville, KY
Ethidiumbromide	Sigma-Aldrich CO, St. Louis, MO
EDTA (ethylenediaminetetraacetic acid)	Sigma-Aldrich CO, St. Louis, MO
Fibronectin (bovine plasma)	Sigma-Aldrich CO, St. Louis, MO
Fluoromount G	Southern Biotech, Birmingham, AL
Glacial acetic acid	Fisher Scientific, Hampton, NH
Glycerol	Sigma-Aldrich CO, St. Louis, MO
Glycine	J.T. Baker, Phillipsburg, NJ
Goatserum	Gibco Invitrogen, Carlsbad, CA
GoTaq DNA Polymerase	Promega, Madison, WI
H ₂ O ₂ (Hydrogen peroxide)	Fisher Scientific, Hampton, NH
Homovanillic Acid	Sigma-Aldrich CO, St. Louis, MO
Horseradish peroxidase	Sigma-Aldrich CO, St. Louis, MO
Ionomycin	Calbiochem, San Diego, CA
Leupeptin	Sigma-Aldrich CO, St. Louis, MO
Lipofectamine reagent (2mg/ml)	Invitrogen, Carlsbad, CA
Mayer's Hematoxylin	Sigma-Aldrich CO, St. Louis, MO
Methanol	Fisher Scientific, Hampton, NH
MTT	Sigma-Aldrich CO, St. Louis, MO
Na-Cholate	Sigma-Aldrich CO, St. Louis, MO
Na-Citrate	Fisher Biotech, Fair Lawn, NJ
NaCl (sodium chloride)	Fisher Scientific, Hampton, NH
NaF (sodium fluoride)	Sigma-Aldrich CO, St. Louis, MO
NaN ₃ (sodium azide)	Sigma-Aldrich CO, St. Louis, MO
NaOH (sodium hydroxide)	Sigma-Aldrich CO, St. Louis, MO
Na ₃ VO ₄ (Sodium orthovanadate)	Sigma-Aldrich CO, St. Louis, MO
NEM (N-ethylmaleimide)	Calbiochem, San Diego, CA
NP-40 (Nonidet P-40)	Calbiochem, San Diego, CA
NuSerum V	BD Biosciences, San Jose, CA

Paraformaldehyde	Electron Microscopy Sciences, PA
PBS (phosphate-buffered saline)	Gibco Invitrogen, Carlsbad, CA
PLUS Reagent (3 mg/ml)	Invitrogen, Carlsbad, CA
PMA (Phorbol-12-myristate-13-acetate)	Sigma-Aldrich CO, St. Louis, MO
PMSF (Phenylmethylsulphonylfluoride)	Sigma-Aldrich CO, St. Louis, MO
Polybrene (hexadimethrine bromide)	Sigma-Aldrich CO, St. Louis, MO
Poly-L lysine	Sigma-Aldrich CO, St. Louis, MO
Protease inhibitor, complete mini, EDTA-free	Roche Diagnostics, Indianapolis, IN
ProtoGel	Nat. Diagnostics, Atlanta, GA
Restore Western Blot Stripping Buffer	Thermo Scientific, Waltham, MA
Ponceau's S	Fisher Scientific, Hampton, NH
Sae Kem LE Agarose	Lonza Walkersville, Walkersville, MD
Scott's Tap water Substitute	Fisher Scientific, Pittsburgh, PA
SDS (sodium dodecyl sulfate)	Sigma-Aldrich CO, St. Louis, MO
SA (succinyl acetone)	Sigma-Aldrich CO, St. Louis, MO
Superoxidedismutase (Marchetti et al.)	Sigma-Aldrich CO, St. Louis, MO
SuperSignal West Dura Extended Duration Substrate	Pierce, Rockford, IL
TaqMan Universal PCR Master Mix (no AmpErase UNG)	Applied Biosystems, Foster City, CA
TaqMan Fast Universal PCR Master Mix (no AmpErase UNG)	Applied Biosystems, Foster City, CA
TEMED (N,N,N',N'-tetramethylethylenediamine)	Sigma-Aldrich CO, St. Louis, MO
Thapsigargin	Invitrogen, Carlsbad, CA
TSA (Trichostatin A)	Sigma-Aldrich CO, St. Louis, MO
Trans-Blot, pure nitrocellulose	Bio-Rad Laboratories, Hercules, CA
Tris base	Calbiochem, San Diego, CA
Trizol	Invitrogen, Carlsbad, CA
Triton X-100	Sigma-Aldrich CO, St. Louis, MO
Tween-20 (Polyoxyethylene-sorbitan-mono-laurate)	Sigma-Aldrich CO, St. Louis, MO
Xelenes	Sigma-Aldrich CO, St. Louis, MO

2.1.1 Kits

Aminoethyl carbazole (AEC) Staining Kit	Sigma-Aldrich CO, St. Louis, MO
BCA Protein Assay Reagent A+B	Pierce, Rockford, IL
DNeasy Mini Kit	Qiagen, Valencia, CA
EZ DNA Methylation Kit	Zymo Research, Orange, CA
High Capacity cDNA Reverse Transcription Kit	Applied Biosystems, Foster City, CA
PureLink Quick Gel Extraction Kit	Invitrogen, Carlsbad, CA
QIAprep Spin Miniprep Kit	Qiagen, Valencia, CA
Qiashreder	Qiagen, Valencia, CA
Quick-Dip Stain	Mercedes Medical Inc., Sarasota, FL
RNeasy Mini Kit	Qiagen, Valencia, CA
SuperScript™ II Reverse Transcriptase	Invitrogen, Carlsbad, CA
TOPO TA Cloning Kit	Invitrogen, Carlsbad, CA

2.1.2 Molecular Weight Markers

100bp DNA ladder	NEB Biolabs, Beverly, MA
Benchmark Pre-Stained protein ladder	Invitrogen, Carlsbad, CA
PageRuler Plus Prestained protein ladder	Fermentas, Hanover, MD

2.1.3 Buffers and Solutions

Antibody diluent	50 ml	10x TBS
	5 g	BSA
	15 ml	goat serum
	1 ml	Tween-20
	ad 500 ml	dH ₂ O
Blocking buffer	50 ml	10x TBS
	15 g	BSA
	50 ml	goat serum
	50 µl	20% NaN ₃
	ad 500 ml	dH ₂ O
DEPC - H ₂ O	200 µl	DEPC
	ad 100 ml	ddH ₂ O
HVA - solution	100 µM	homovanillic acid
	4 U/ml	horseradish peroxidase (HRP)
	in PBS with Ca ²⁺ , Mg ²⁺	
HVA - stop buffer	0.1 M	NaOH
	25 mM	EDTA
	0.1 M	glycine, pH 12.0
IP-buffer (2x)	50mM	Tris/HCl (pH 7.4)
	300mM	NaCl
	100mM	glycine
	1%	TritonX-100
Laemmli buffer (4x)	40 ml	0.5M Tris-HCl, pH 6.8
	20 ml	glycerol
	40 ml	10% SDS in dH ₂ O
	4 ml	β-mercaptoethanol
	pinch	Bromophenolblue
Ponceau's S	0.5 g	Ponceau S
	1 ml	glacial acetic acid
	100 ml	dH ₂ O
Relaxation buffer	100 mM	KCl
	3 mM	NaCl
	3.5 mM	MgCl ₂
	1 mM	EGTA
	10 mM	HEPES (pH 7.4)
RIPA lysis buffer	150 mM	NaCl
	50 mM	Tris-HCl, pH 7.5
	1%	Na-cholate
	1%	NP-40
	0.1%	SDS
	in ddH ₂ O	

SDS running buffer (10x)	30 g 140 g 10 g ad 1000 ml	Tris base Glycine SDS dH ₂ O
TAE (50x)	242 g 57.1 ml 100 ml ad 1000 ml	Tris base glacial acetic acid 0.5 M EDTA, pH 8.0 ddH ₂ O
TBS	0.2 M 1.4 M in dH ₂ O	Tris base NaCl
TBS-T (10x)	0.2 M 1.4 M 0.5% in dH ₂ O	Tris base NaCl Tween-20, pH 7.5
TE :	1 M 0.5 M in dH ₂ O	Tris-HCl (pH 7.5 or 8.0) EDTA
Transfer buffer (10x) :	250 mM 1.92 M in dH ₂ O	Tris base glycine
Transfer buffer (1x):	100 ml 150 ml 4 ml 750 ml	10x transfer buffer methanol 10% SDS ddH ₂ O

2.1.4 Antibodies

Antibody	Isotype	Dilution	Vendor
α -tubulin (DM1)	Mouse	1:1000 (WB)	Sigma
β - tubulin IV	Mouse	1:200 (IF)	Sigma
Alexa Fluor 488	Rabbit	1:500 (IF)	Invitrogen
Alexa Fluor 568	Rabbit	1:500 (IF)	Invitrogen
Alexa Fluor 568	Mouse	1:500 (IF)	Invitrogen
anti-rabbit HRP	Goat	1:10000 (WB)	Southern Biotech
anti-mouse HRP	Goat	1:10000 (WB)	Southern Biotech
Duox1/2 (aa 775-1026 of hDuox1)	Rabbit	1:200 (IF); 1:1000 (WB)	homemade
Duox1 (aa 988-1011 of hDuox1)	Rabbit	1:200 (IF); 1:1000 (WB)	homemade
Duox2 (aa 634-648 of hDuox2)	Rabbit	1:200 (IF); 1:1000 (WB)	homemade
DuoxA1 (aa 280-299 of hDuoxA1-2)	Rabbit	1:500 (IF); 1:5000 (WB)	OpenBiosystems
GFP	Mouse	1:100 (IP)	Genetex
GFP	Rabbit	1:1000 (WB)	Invitrogen
GST	Mouse	1:200 (IP)	Santa Cruz
MUC5A (45M1)	Mouse	1:200 (IF)	Neomarker
c-myc (9E10)	Mouse	1:200 (IF)	Upstate
c-myc	Rabbit, mono	1:200 (IF); 1:1000 (WB)	Cell Signaling
Biotinyl, IgG conjugate	Rabbit	1:200 (IHC)	Zymed Laboratories
Streptavidin, HRP conjugate		1:200 (IHC)	Molecular Probes

TABLE 2: ANTIBODY LIST

2.1.5 Rodent primers

Name	Sequence (5' → 3')	Annealing Temperature
β -actin Fwd (rat+mouse)	TGACGGGGTCACCCACACTGTGCCCATCTA	60°C
β -actin Rev (rat+mouse)	CTAGAAGCATTTGCGGTGGACGATGGAGGG	
Mouse Duox1 Fwd	CTGTACAATCAGGACCTGTCTCGGCT	64°C
Mouse Duox1 Rev	TGAGCCTGCCATCCACTACTCGAATC	
Mouse Duox2 Fwd	CCCGAAGGAAGGTTTCAGACAG	60°C
Mouse Duox2 Rev	GTAGTCAATCACAGTAACAGGCG	
Mouse DuoxA1 Fwd	GCGGCGTCAACATCACCTTC	62°C
Mouse DuoxA1 Rev	GTCCTCTGAACTCAGGTTGAAG	
Mouse DuoxA2 Fwd	CGTGGGACGGGGTGCTAC	62°C
Mouse DuoxA2 Rev	GCAGACCGACATGGACTTGAAC	
Rat Duox1 Fwd	ATCAAGCAGATGCAGGGACTC	61°C
Rat Duox1 Rev	GGGGATGACGCTGTCTTCG	
Rat Duox2 Fwd	CCGTTGGAACTATTCTTGG	60°C
Rat Duox2 Rev	AGTTGGATGGTACGGAGCAC	
Rat DuoxA1 Fwd	GGCTGCTACGGGTGGTGAC	60°C
Rat DuoxA1 Rev	GCAGCGGGCAGGACATGAG	
Rat DuoxA2 Fwd	GGCTGGAGGGCGTTAATATC	64°C
Rat DuoxA2 Rev	CTCGAAGGACGCTGGGTC	

TABLE 3: RODENT PRIMER LIST

2.1.6 Human Primers

Name	Sequence (5' → 3')	Annealing Temperature
β-actin Fwd	TGACGGGGTCACCCACACTGTGCCCATCTA	60°C
β-actin Rev	CTAGAAGCATTTGCGGTGGACGATGGAGGG	
Duox1 Fwd	GCAGGACATCAACCCTGCACTCTC	65°C
Duox1 Rev	CTGCCATCTACCACACGGATCTGC	
Duox2 Fwd	CCGGCAATCATCTATGGAGGT	58°C
Duox2 Rev	TTGGATGATGTCAGCCAGCC	
DuoxA1-1 Fwd	GAGCTTCAGTTCCCAAATTTGCTAC	63°C
DuoxA1-1 Rev	GACAGCCTAGTACACTCTCCGC	
DuoxA1-2 Fwd	GTCAGCACCAACACATCATAACAAGG	65°C
DuoxA1-2 Rev	GGGTGTGCCTCTTTACAGTATGC	
DuoxA1-3 Fwd	GTCAGCACCAACACATCATAACAAGG	66°C
DuoxA1-3 Rev	CTGGACCAAAGCGCCAAGGAC	
DuoxA2 Fwd	CTTCCTGCTCATCTTGCCGG	59°C
DuoxA2 Rev	GAGAGCAGCACGTTGGAGAGG	
Alu Fwd	ACGCCTGTAATCCCAGCACTT	63°C
Alu Rev	TCGCCCAGGCTGGAGTGC	
Duox1-Universal-a Fwd	AGTTTTATGGGATTTGTGAAGG	54°C
Duox1-Universal-a Rev	ACCTAACTACCAACTAAACC	
Duox1-MSP-a Fwd	CGTTAGATTTTATTTTCGTTTTATTGCGTTTCGTTTC	64°C
Duox1-MSP-a Rev	GATACCTCTACAACCTCTACACCGAAACGAACG	
Duox1-USP-a Fwd	GATGGAATATTTTTATTTGTGTTTTG	58°C
Duox1-USP-a Rev	CCAATACCTCTACAACCTCTACACCAA	
Duox1-Universal-b Fwd	ATGGGATTTGTGAAGGYGGATTTG	60°C
Duox1-Universal-b Rev	CTTATCTCCRACCTAACTACCAACTAAAC	
Duox1-MSP-b Fwd	TGCGTTTTCGGGAGTTTTTCGTC	70°C
Duox1-MSP-b Rev	CTCTACGCCGAAACGAACG	
Duox2-Universal-a Fwd	GATGAGTAGGAAGTTTGTGTTG	54°C
Duox2-Universal-a Rev	CACCTCACCTTTCTCTC	
Duox2-MSP-a Fwd	GTAGTCGTTATTTTTTTGGTTTTGTC	63°C
Duox2-MSP-a Rev	CTAAAACCTCACCTCCTACCGTA	
Duox2-USP-a Fwd	AGTAGTGGAATGTTGAAGTTTGTG	64°C
Duox2-USP-a Rev	ACTAACTTACCTACCCACCTACATA	
Duox2-Universal-b Fwd	TGGGTTGGTGAAGTTTGAAGTTTGT	60°C
Duox2-Universal-b Rev	CCAACCTCAAACCAACCCCTAAACT	
Duox2-MSP-b Fwd	TTTAGTCGGCGAGCGAAATTA	70°C
Duox2-MSP-b Rev	CGTATAACACGTCGCCAC	
BSP-Duox1 Fwd	GGGGTGTGATTAAAGAGGGAA	59°C
BSP-Duox1 Rev	CCCAAACTCCCTCCCTAATATAT	
BSP-Duox2 Fwd	GGAAAGGGGTGTTTGTGTTAG	58°C
BSP-Duox2 Rev	AAACCCTTATTTACACAACCTCTTC	

TABLE 4: HUMAN PRIMER LIST

2.2 Technical Equipment

2100 Rainbow laser scanning confocal microscope	Bio-Rad (Zeiss), Hercules, CA
5415C Eppendorf Centrifuge	Brinkman Instruments Inc, Westbury, NY
5810R Eppendorf Centrifuge	Brinkman Instruments Inc., Westbury, NY
AB 104 Scale	Mettler Toledo, Switzerland
AccuBlock Digital Dry Bath	Labnet International Inc., Edison, NJ
Accumet AB15 pH meter	Fisher Scientific, Hampton, NH
Alphaimager 2200	Alpha Innotech, San Leandro, CA
Autoclave Amsco Scientific series	STERIS Corporation, Mentor, Ohio
Axiovert 100 Microscope	Zeiss, Göttingen, Germany
Beckman GS-6KR	Beckman Coulter, Fullerton CA
Beckman J2-HC	Beckman Coulter, Fullerton CA
Biological Safety Cabinets	Nuaire, Plymouth, MN
Bio-Rad Power Pac 1000	Bio-Rad, Hercules, CA
Dry Bath Incubator	Fisher Scientific, Hampton, NH
Fisher Stirring Hotplate	Fisher Scientific, Hampton, NH
Fisher Vortex Genie 2	Fisher Scientific, Hampton, NH
HE 33 mini horizontal submarine unit	Hoefer Inc., San Francisco, CA
Incubator, NAPCO CO2	Fisher Scientific, Hampton, NH
Isotemp Incubator	Fisher Scientific, Hampton, NH
IsoTemp 215 waterbath	Fisher Scientific, Hampton, NH
LS55 Chemiluminescence Photometer	Perkin Elmer Instruments, Wellesley, MA
Microfuge 22R Centrifuge	Beckman Coulter, Fullerton, CA
Microplate Luminometer LB 96 V	EG + G Berthold, Bad Wildbach, Germany
NanoDrop ND-1000 Spectrophotometer	NanoDrop Technologies, Wilmington, DE
Nikon Eclipse E800	Nikon, Melville, NY
Nikon Eclipse TE2000-U	Nikon, Melville, NY
Olympus IX70 Microscope	Olympus, Center Valley, PA
Optima Microcentrifuge	Beckman Coulter, Fullerton, CA
PB3002 Scale	Mettler Toledo, Switzerland
PCR-Express	Thermo Hybaid, Heidelberg, Germany
ProteinPower Pac 200	Bio-Rad, Hercules, CA
Protein Bio-Rad Mini Protean II cell	Amersham Bioscience, Uppsala, Sweden
PS 500 XT DC Power Supply	Hoefer Scientific Instruments
Rocker Platform	Bellco Glass, Vineland NJ
SRX-101A Medical Film Processor	Konica Minolta, Wayne, NJ
STX2 Electrode	World Precision Instruments, Sarasota, FL
Synergy HT	Bio-Tek Instruments Inc., Winooski, VT
Tissue Tearor	Biospec Products, Inc., Bartlesville, OK
UV/Visible Spectrometer Ultrospec 3000	Pharmacia Biotech, Cambridge UK
VERSAmax Microplatereader	Molecular Devices, Sunnyvale, CA

2.2.1 Computer Programs

AxioVision AC 4.2	Zeiss, Göttingen, Germany
Bio-Rad LaserSharp 2000	Bio-Rad, Hercules, CA
EndNote X	EndNote, Carlsbad, CA
Imaris 5	Bitplane Inc., Saint Paul, MN
Image J	NIH, Bethesda, MD
LSM Image Analyzer	Zeiss, Göttingen, Germany
Methamorph	Molecular Devices Corp., Downingtown, PA
Spectra Alias	DeltaSoft/Biomaterials, Princeton, NJ

pDRAW32
Prism 5.0

AcaClone software
GraphPad Software, Inc., La Jolla, CA

2.2.2 Internet Programs

<http://bisearch.enzim.hu/>
<http://blast.ncbi.nlm.nih.gov/Blast.cgi>
<http://ca.expasy.org/>
<http://cpgislands.usc.edu/>
<http://genome.ucsc.edu/cgi-bin/hgBlat>
<http://phobius.sbc.su.se/>
<http://psort.ims.u-tokyo.ac.jp/form2.html>
<http://symatlas.gnf.org/SymAtlas/>
<http://www.basic.northwestern.edu/biotools/oligoCalc.html>
<http://www.ebi.ac.uk/Tools/clustalw2/index.html>
<http://www.ensembl.org/index.html>
<http://www.enzim.hu/hmmtop/index.html>
<http://www.ncbi.nlm.nih.gov/>
<http://www.ncbi.nlm.nih.gov/sites/entrez?db=protein&cmd=search&term=>
<http://www.urogene.org/methprimer/index1.html>

2.3 Tissue Culture

2.3.1 Cell Culture Media

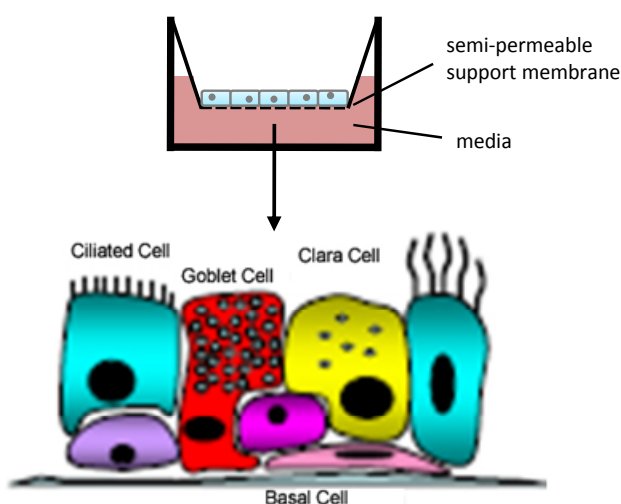
RPMI 1640 with Glutamax	Gibco Invitrogen, Carlsbad, CA
MEM	Gibco Invitrogen, Carlsbad, CA
DMEM (4.5g/L D-glucose) with Glutamax	Gibco Invitrogen, Carlsbad, CA
Ham's F12 Medium	Gibco Invitrogen, Carlsbad, CA
Trypsin-EDTA (1x) 0.05%	Gibco Invitrogen, Carlsbad, CA
HEPES Buffer solution 1 M	Gibco Invitrogen, Carlsbad, CA
Sodium pyruvate 100mM	Gibco Invitrogen, Carlsbad, CA
Sodium bicarbonate solution 7.5%	Sigma-Aldrich CO, St. Louis, MO
Dulbecco's Phosphate-Buffered Saline	Gibco Invitrogen, Carlsbad, CA
SABM + SAGM single quotes	Lonza Walkersville Inc., Walkersville, MD
BEBM + BEGM single quotes	Lonza Walkersville Inc., Walkersville, MD

2.3.2 Cell Culture (2D)

Human lung cancer cell lines NCI-H69, NCI-H82, SHP-77, NCI-H292, NCI-H272, NCI-H441, UCLA-P3, NCI-H460, NCI-H661 and NCI-H157 were grown in RPMI 1640 media. Lung cancer cell lines Calu-3, A549 were cultured in MEM and Ham's F12 media, in the presence of 1.5g/L sodium bicarbonate. HeLa and HEK293T cells were kept in DMEM media. All aforementioned media were supplemented with 10% FCS and 0.01mM HEPES. Human primary lung epithelial cells NHBE and SAEC as well as immortalized normal human lung epithelial cells BEAS-2B and SALE were cultured in SABM media, supplemented with SAGM SingleQuotes. All cells were maintained in humidified tissue culture incubators at 37°C and 5% CO₂.

2.3.3 Polarized Airway System (3D)

NHBE and SAEC were cultured in SABM media supplemented with 30µg/ml bovine pituitary extract, 0.5µg/ml hydrocortisone, 0.5ng/ml human recombinant epidermal growth factor, 0.5µg epinephrine, 10µg/ml transferrin, 5µg/ml insulin, 0.1ng/ml retinoic acid, 6.5ng/ml triiodothyronine, 50µg/ml gentamicin, 50ng/ml amphotericin-B and 0.5mg/ml bovine serum albumin-fatty acid free (SingleQuots). Upon 80% confluency cells were split using the Reagent Pack (Lonza) and cells were resuspended in differentiation media, consisting of 50% DMEM and 50% BEBM media, supplemented with 200µg/ml bovine pituitary extract, 0.5µg/ml hydrocortisone, 0.5ng/ml human recombinant epidermal growth factor, 0.5µg epinephrine, 10µg/ml transferrin, 5µg/ml insulin, 1.5µg/ml bovine serum albumin fraction V, 6.5ng/ml triiodothyronine, 50µg/ml gentamicin and 50ng/ml amphotericin-B. The media was also complemented with freshly prepared 50nM all-trans retinoic acid, which induces differentiation. $1.8-2.0 \times 10^5$ cells were seeded on semi-permeable support



membranes (24-well; Costar Transwell-clear culture insert, polyester, 0.4µm pore, Corning Costar), which were coated with human placenta collagen, type IV (15µg/cm²). After 2 days the media on top of the membrane was removed and cells were grown and differentiated at an air-liquid interphase (ALI) for up to 21 days.

FIGURE 7: Air-liquid system (3D). Primary lung epithelial cells are grown at the air-liquid interphase and differentiate into several cell types as indicated. Adapted from Dr. Mandy Lehmann (The Scripps Research Institute).

2.3.4 Treatments

5-Aza-2'-deoxycytidine (Aza): Lung cancer cell lines were cultured in appropriate medium supplemented with 5% FCS in the absence or presence of 1µM Aza. Due to its instability at warmer temperatures (Lin et al., 1981), the media was changed daily and replenished with fresh Aza.

Trichostatin A (TSA): Lung cancer cells were grown in 5% medium and 5ng/ml TSA was added for 48 hours. Control cells were grown in the presence of vehicle alone.

Succinylacetone (SA): NCI-H661 cells were grown for 4 days in RPMI, containing Hepes and 1% NuSerum V in the presence or absence of 10µg/ml SA.

2.3.5 Human and rodent tissue samples

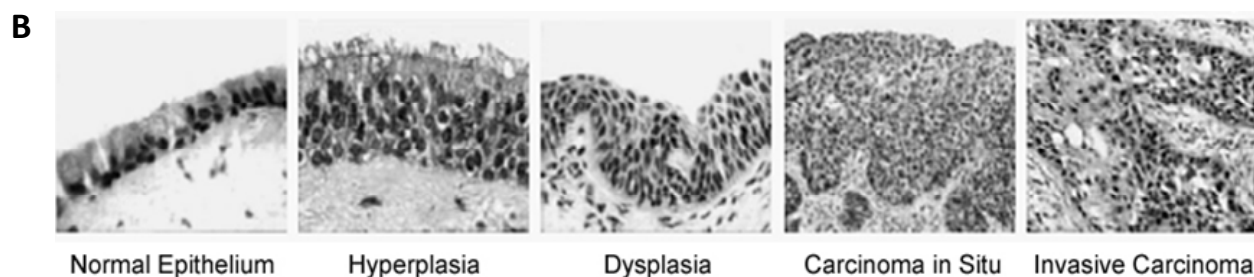
Human Samples: A total of eleven paired specimen of primary lung carcinomas and adjacent non-cancerous tissue were obtained from the Cooperative Human Tissue Network (Western Division, Vanderbilt University Medical Center, Nashville, TN), which is funded by the National Cancer Institute. Other investigators may have received specimens from the same subjects. The tissue samples were collected from surgical resections and quick-frozen in liquid nitrogen immediately after excision and stored at -80°C until further use. The histological type of the cancer and the

corresponding differentiation state is listed in (FIGURE 8A). Those specimens were used for promoter methylation studies and immunohistochemistry. In addition, 39 primary adenocarcinomas from the Lovelace Respiratory Research Institute (Albuquerque, NM) were analyzed for promoter methylation. Tissue sections from normal human upper lung and diseased lung (cystic fibrosis) were obtained from Pantomics, Inc. (San Francisco)

A

Patient	Histology	TNM Mapping	Stage Grouping
1	Large Cell Carcinoma	T3N1	IIIA
2	Squamous Cell Carcinoma	T1NO	IA
3	Squamous Cell Carcinoma	T2NO	IB
4	Squamous Cell Carcinoma	T2NO	IB
5	Squamous Cell Carcinoma	T2NO	IB
6	Squamous Cell Carcinoma	T2N2	IIIA
7	Adenocarcinoma	T2NO	IB
8	Adenocarcinoma	T2NO	IB
9	Adenocarcinoma	T2NO	IB
10	Adenocarcinoma	T1NO	IA
11	Adenocarcinoma	T2NO	IB

FIGURE 8: Histology information. (A), Histology of the eleven non-small cell lung cancer patients analyzed for expression of DUOX/DUOXA. (B), Sequential pathogenetic changes involved in lung cancer development. Hyperplasia is an early event in the development of lung cancer, while dysplasia and carcinoma *in situ* are regarded as intermediate and late events, respectively. Adapted from (Spira and Ettinger, 2004).



Rodent samples: Mice (strains: C57BL/6 and BALB/c) and rats (strain: Sprague Dawley) were obtained from the core rodent breeding facility at The Scripps Research Institute (TSRI) and Harlan Sprague Dawley, Inc. (San Diego, CA), respectively and were housed in a pathogen-free facility. Animals were sacrificed by CO₂ inhalation and tissues were excised and immediately processed. All animal procedures were reviewed by the Institutional Animal Care & Use Committee (IACUC) of TSRI and approved by the Animal Welfare Act.

2.4 Molecular Biology

2.4.1 Nucleic Acid Extraction

2.4.1.1 Total RNA and genomic DNA extraction from cell culture

Total RNA from primary cells and cell lines was isolated using an RNA extraction kit (RNeasy Mini Kit, Qiagen). Cells were lysed in RLT buffer (provided in the kit) containing β-mercaptoethanol. The cell lysate was applied to a Qias shredder column (Qiagen) and homogenized via microcentrifugation. Total RNA was eluted with 30 μl DEPC-treated RNase-free water. DEPC reacts with reactive residues (such as amines, thiol- and hydroxy-groups) of proteins, thus inactivating their biological activity. Genomic DNA (gDNA) was extracted from 2*10⁶ cells using a DNA extraction kit (DNeasy Tissue Kit, Qiagen). Integrity of gDNA was determined by Alu-PCR.

2.4.1.2 Total RNA and genomic DNA extraction from tissue specimen

Total RNA from tissue specimen was isolated with a combination of phenol/chloroform and spin-column purification. 10-20mg of frozen lung tissue was homogenized in 1ml Trizol reagent, using a tissue homogenizer. The aqueous phase was mixed with 1 volume of 75% ethanol after phase separation and transferred to an RNeasy column. RNA was bound to the column and eluted in 50µl RNase-free water. Genomic DNA from tissue specimen was isolated at the same time as total RNA. After complete removal of remaining aqueous phase, gDNA was precipitated from the interphase and underlying organic phase by addition of 300µl 100% ethanol. Samples were inverted and centrifuged at 2,000g for 5 minutes at room temperature. The DNA pellet was washed twice with 1ml 10% ethanol in 0.1M trisodium citrate for 30 minutes at room temperature. Subsequent to each wash, DNA was spun down for 5 minutes at 2,000g at 4°C. After the second wash, the pellet was suspended in 1ml 75% ethanol in order to remove the pinkish color from the DNA. The pellet was briefly air-dried after ethanol removal and resuspended in 50µl 8mM sodium hydroxide by pipetting up and down. Insoluble material was removed by centrifugation at 12,000g for 10 minutes.

2.4.2 Determination of the concentration of RNA or DNA

Concentration of RNA or DNA was determined by measuring the absorbance at 260nm on a Nanodrop spectrophotometer. The following equation was used to calculate the concentration.

$$c[\mu\text{g}/\mu\text{l}] = \frac{A_{260} \cdot \text{dilution factor} \cdot X}{1000}$$

The value for X depends on the type of nucleic acid analyzed: 50 (dsDNA), 40 (RNA), 30 (ssDNA).

2.4.3 cDNA Synthesis

Complementary DNA (cDNA) was synthesized from total RNA using two different approaches, depending on the downstream application. Total RNA (2µg) from cultivated cells was reverse transcribed using 200 units SuperScript II (SSII) and oligo(dT) (both Invitrogen). Reverse transcription was carried out for 50 minutes at 42°C in a 20µl reaction volume, containing First-strand buffer, 0.01 M DTT (both supplied with SSII) and RNase inhibitor (40 units, Roche Diagnostics, Indianapolis, IN). Remaining RNA was removed through subsequent incubation with 2 units RNase H (Invitrogen). cDNA generated this way was used for semi-quantitative PCR. Total RNA (1µg) from tissue specimen was reverse transcribed using the High Capacity cDNA reverse transcription Kit (Applied Biosystems, Foster City, CA) according to the manufacturer's protocol. The cDNA (in a final volume of 20µl) was subject to quantitative (real-time) PCR.

2.4.4 Polymerase Chain Reaction (PCR)

The polymerase chain reaction was used to amplify a single or few copies of a DNA fragment. Reactions were performed in a Thermocycler for generally 35 cycles. Particular variations are mentioned in the text.

2.4.4.1 Qualitative (semi-quantitative) PCR

One µl of cDNA from cultivated cells was used for qualitative PCR amplification. For all PCR reactions a master mix was prepared that contained a multiple of the following (25µl total reaction volume):

Reaction mix:	5.0µl	Green GoTaq Flexi buffer	(5X)
	1.5µl	MgCl ₂	(25mM)
	0.5µl	dNTPs	(10mM)
	0.5µl	Forward primer	(10µM)
	0.5µl	Reverse primer	(10µM)
	0.125µl	GoTaq DNA polymerase (5U/µl)	
	1.0µl	cDNA template	
	16.88µl	H ₂ O	
Program:	<u>94°C - 5 min</u>		
	94°C - 30 sec		
	X°C - 30 sec	35 repeats	
	<u>72°C - 60 sec</u>		
	72°C - 5 min		
	4°C - hold		

2.4.4.2 Quantitative (real-time) PCR

cDNA from tissue specimen and SAEC (differentiated for a time course of 21 days) was subject to quantitative real-time PCR analysis utilizing TaqMan™ technology. The cDNA was diluted in water to a final concentration of 10ng/µl, assuming 100% reverse-transcription efficiency during cDNA synthesis. 5µl of the diluted cDNA were mixed with 12.5µl 2xTaqMan® Universal PCR Master Mix (no AmpErase® UNG), 1.25µl 20x gene expression assay probe and 6.25µl sterile water. Each sample (in a 25µl reaction volume) was pipetted in triplicate into a 96-well reaction plate and 3 samples per specimen or time point were analyzed. Gene-specific PCR products were continually measured with an ABI PRISM 7700 or 7900 Sequence Detection System (Applied Biosystems). The probes for *Duox1* (Hs00213694_m1, Applied Biosystems), *DuoxA1* regulation, *Duox2* (Hs00204187_m1) and human β -actin (Hs99999903_m1) were labeled with 6FAM™ dye - MGB and were designed over an exon-exon boundary to eliminate the possibility of genomic DNA amplification. Relative *DUOX1*, *DUOX2* and *DUOXA1* mRNA amounts in the different samples were standardized against the amount of actin mRNA and expressed as $\Delta CT = (CT_{\beta\text{-actin}} - CT_{GOI})$. The mRNA copy ratio of GOI to actin was calculated as $2^{\Delta CT}$ and normalized to the highest (tissue specimen) or lowest (SAEC) expression of the respective GOI.

2.4.5 Agarose Gel Electrophoresis

DNA fragments were separated according to their size in 1% (w/v) agarose in 1x TAE buffer, containing 0.5 mg/ml ethidium bromide. 8-10µl PCR product was electrophoresed at 100V. Integrity of total RNA (0.5-2.0µg) was also assessed by electrophoresis, as non-degraded RNA shows 2 distinct bands, corresponding to ribosomal subunits 28S and 18S.

2.4.6 Bisulfite conversion of gDNA and methylation specific PCR

Isolated gDNA (2µg) from cell lines and tissue specimen was subject to bisulfite treatment using the EZ DNA Methylation Kit (Zymo Research, Orange), converting unmethylated cytosines into uracil (**FIGURE 9A**). CpG islands in the promoter regions of *DUOX1*, *DUOX2*, *DUOXA1* and *DUOXA2* were identified by utilizing CpG island searcher (Takai and Jones, 2003). A CpG island was defined by the following criteria: GC >55%, observed CpG/expected CpG >0.65, and length >500bp. In the first step of the nested methylation specific PCR, universal primers, which are unbiased for potential CpG conversion sites, were used to amplify a fragment of the *DUOX1* and *DUOX2* promoter, respectively,

spanning the region of interest. One μl of the universal PCR product was used as template for subsequent methylation (MSP) and unmethylation (USP) specific PCR (**FIGURE 9B**). Primer sequences are shown in (**TABLE 4**).

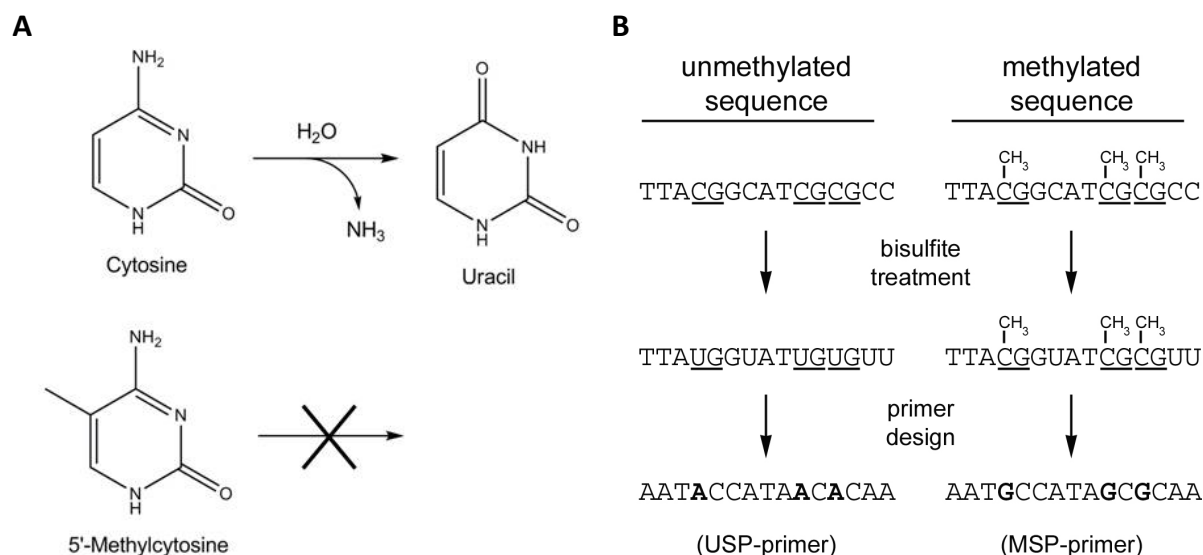


FIGURE 9: Bisulfite treatment and methylation-specific primer design. (A), bisulfite converts unmethylated cytosines stoichiometrically to uracil via deamination. Methylated cytosines (5'-methylcytosine) are resistant to bisulfite conversion. (B), isolated genomic DNA is treated with bisulfite, which leads to conversion of all unmethylated cytosines into uracil (U), while methylated cytosines (CH₃) remain as cytosine in the sequence. Two primer sets, which are used in two individual PCR reactions, are designed for the same DNA region, based on the assumption that cytosines of given CpG dinucleotides are unmethylated (USP) or methylated (MSP).

2.4.7 TOPO-cloning and Bisulfite sequencing

The region between -894 to +1411 of the *DUOX1* and -755 to -52 of the *DUOX2* promoter was amplified from the bisulfite modified gDNA, using BSM primers. These sequences comprise 72 (*DUOX1*) and 39 CpG sites (*DUOX2*), respectively. As PCR purification is not sufficient to selectively purify the correct sized product, the desired PCR products were gel purified with the Pure Link Quick Gel Extraction Kit and subsequently cloned into the pCR4-TOPO vector (Invitrogen), according to the manufacturer's instructions. The plasmid vector is supplied linearized with single 3'-thymidine (T) overhangs, thus allowing for easy ligation with the PCR amplicon, as Taq polymerases always add a single deoxyadenosine (A) to the 3' ends of PCR products, due to their nontemplate-dependent terminal transferase activity. Upon ligation of the insert with the vector, the construct was chemically transformed into One Shot Mach1™-T1R Competent *E. coli* cells. Positive selection was achieved through 50 $\mu\text{g}/\text{ml}$ ampicillin. Colonies were picked for plasmid purification and at least 8 positive clones per condition were sequenced using M13 primers (supplied with the kit).

2.4.8 Lentivirus production and cell transduction

Human Duox1, DuoxA1-2, Duox2 and DuoxA2 were cloned into CGW lentiviral expression vector. Virus particles were produced by transient transfection of HEK293T cells. Approximately 24 hours

prior to transfection, cells were seeded in 5% DMEM high glucose media (2×10^6 cells/10 cm dish, pre-coated with 20 $\mu\text{g}/\text{ml}$ poly-L-lysine). The following mix was prepared in a 5ml FACS tube:

Per 10 cm dish: 10 μg transfer vector plasmid
 6.5 μg GAG/pol plasmid
 3.5 μg VSV.G plasmid
 2.5 μg pRSV-rev plasmid
 Ad 450 μl with 0.1x TE

While vortexing, 500 μl warm 2xHBS and 50 μl 2.5M CaCl_2 were added dropwise and the mixture was immediately added to the cells. Fresh media was added to the cells after approximately 16 hours. The supernatant was collected 24 and 48 hours post-transfection, sterile filtered through a 0.22 μm filter and centrifuged at 19400 rpm for 2.2 hours at 4°C. The liquid was discarded and the virus-pellet resuspended in 5% BSA/PBS, aliquotted and frozen at -80°C. Lung cancer cell lines and primary lung cells were incubated with viral supernatant for 48-72 hours in the presence of 4 $\mu\text{g}/\text{ml}$ polybrene (Rizzi et al., 2007; Swan et al., 2006).

2.5 Immunodetection of Proteins

2.5.1 Protein isolation and quantification

For isolation of total cell lysate (TCL) cells were frozen at -80°C for a minimum of 30 minutes to disrupt the cell structure. Ice-cold RIPA buffer (containing 10 μM Aprotinin, 10 μM Leupeptin, 1mM PMSF) was added to the cells and the lysate was scraped off into a microcentrifuge tube, vortexed and incubated on ice for 10 minutes. Cell debris was parted from the solubilized protein by centrifugation at 14,000rpm for 10 minutes at 4°C. Protein concentrations were determined using a BCA assay (Smith et al., 1985). It is critically important that the cell lysates are kept ice-cold at all times, to prevent aggregation of Duox-protein. For isolation of cytosolic and membrane fractions cells were lysed in relaxation buffer (containing 1 mM PMSF, 100 μM leupeptin, 10 μM aprotinin, 1 mM Na_3VO_4 , 25 mM NaF) and briefly sonicated. Cell debris was removed after centrifugation at 2150rpm for 10minutes at 4°C. The supernatant was transferred into microfuge tubes and lysates were ultracentrifuged at 49,000rpm (100,000g) for 30 minutes. The remaining pellet, which corresponds to membrane-associated proteins, was separated from the cytosolic proteins in the supernatant, washed and finally resuspended in Laemmli-buffer.

2.5.2 Immunoblotting (IB)

Frozen protein extracts were thawed on ice. TCL (30 μg) was mixed with ice-cold 4x Laemmli buffer and immediately loaded onto 8% (v/v) discontinuous denaturing polyacrylamide gel (Laemmli, 1970). Heating of the lysates must be avoided, as Duox proteins aggregate and will be only detectable as high molecular weight smear. The proteins were transferred to nitrocellulose membranes (2 hours, 0.3A), blocked for 1 hour with 5% non-fat dry milk/TBS-T and subsequently probed with primary antibodies (generally 1:1,000 in 1% BSA/TBS-T) for 1 hour at RT or over night at 4°C. After washing for 3 x 5 minutes with TBS-T, appropriate secondary antibodies (HRP-labeled; 1:10,000) were applied for 1 hour. Membranes were washed again 3 x 5 minutes with TBS-T, followed by short incubation with SuperSignal West Dura Extended Duration Substrate and exposed to autoradiography film.

2.5.3 Immunoprecipitation (IP)

Cells were washed with PBS and proteins were crosslinked by incubation with 2mM DSP in PBS (prepared freshly) at 37°C for 20 minutes. All following steps were carried out at 4°C or on ice. The cells were washed with ice-cold PBS and their proteins were alkylated for 15 minutes with 20mM NEM in PBS. The cells were scraped into a microcentrifuge tube and incubated for 15 minutes with an equal volume of 2x IP buffer (containing 20µM Aprotinin, 20µMLeupeptin, 2mM PMSF). Cell debris was separated from the lysate via centrifugation for 10 minutes at 14000rpm and the supernatant was transferred to a new microcentrifuge tube. An aliquot of the lysate was stored at -80°C and the remainder was cleared by incubation with 1:1 slurry of BSA-coated protein G beads, rotating for 1 hour. The cleared lysate was incubated with primary antibody (monoclonal anti-myc or anti-GFP) and control antibody (monoclonal anti-GST) rotating for 1.5 hours. Subsequently, BSA-coated protein G beads were added and incubated while rotating for 45-60 minutes. Bound antibody was precipitated through centrifugation for 10 minutes at 3000rpm and the beads were washed 3 times with IP buffer. Immunoprecipitated proteins were separated from the beads by addition of 4x Laemmli buffer and vigorous vortexing.

2.5.4 Immunofluorescence (IF)

For localization studies of exogenous and endogenous protein, cells were seeded on collagenized coverslips, if needed transfected or transduced, and fixed with 4%PFA/PBS for 10 minutes at RT. After permeabilization with 0.5% Triton-X cells were blocked with blocking buffer for 1 hour RT or at 4°C over night. Coverslips were transferred to a light-impermeable humidified chamber and primary antibodies were applied directly onto the coverslip for 1 hour RT. Generally, primary antibodies were diluted 1:200 in antibody diluent. Before and after the addition of the Alexa-conjugated fluorescent antibodies for 1 hour RT (1:500 in antibody diluent), the coverslips were washed with PBS. The nucleus was stained for 10 minutes with 1µg/ml DAPI and the coverslips were mounted on glass slides with Fluoromount G. Samples were dried at RT over night and images were acquired with a 2100 Rainbow laser scanning confocal microscope (Nikon 60x oil, Plan-Apo-1.4 NA; Nikon 100x oil Plan-Apo-1.4 NA). 3D-differentiated cells were processed identically, except that fixation and permeabilization were conducted for 20 minutes. Images were analyzed for colocalization with Image J and LSM Analyzer software. Orthogonal planes were illustrated by Metamorph software.

2.5.5 Immunohistochemistry (IHC)

50 to 200mg of frozen tissue from patient specimen or whole organs (trachea, upper lung, lower lung) were fixed in zinc formalin for 12 hours minimum and subsequently embedded in paraffin wax. For histological assessment, 3µm thick sections were H&E and PAS stained according to standard procedures. Sections containing airway cross cuts were deparaffinized in xylenes, rehydrated in graded alcohol (two minutes each in ethanol 100%, 95%, 70%, 50%, 30%; followed by two minutes in PBS) and autoclaved (10 minutes, 120 psi) in 0.01M sodium citrate buffer (pH 6.0) for antigen retrieval. Use of citrate buffer older than four weeks can result in decreased antigen retrieval. Endogenous peroxidase activity was inhibited through 30 minute incubation with 3% hydrogen peroxide in methanol. After blocking with 2% non-fat dry milk in water the sections were incubated with serial dilutions of polyclonal rabbit anti-Duox serum in blocking solution for 16 hours at 4°C (1:1000 for human sections, 1:200 for rodent sections). The antibody was raised in rabbits to amino acid residues 775 to 1,026 of hDuox1. The slides were washed in PBS containing 0.1% Tween-20 (PBS-T) and incubated with biotinylated anti-rabbit IgG for 60 minutes at room temperature (1:200 in blocking solution). After three short washes with PBS-T, streptavidin conjugated HRP was applied for

60 minutes at room temperature (1:200 in ddH₂O) and subsequently the labeled antigen was visualized with 3-amino-9-ethylcarbazole (AEC) as chromogen with a brownish color indicating the area of Duox expression. The slides were counterstained with Mayer's Hematoxylin and washed with Scott's water for 7 minutes before mounting. As negative controls, slides were incubated with preimmune serum, but otherwise were treated identically. Images were taken with a Nikon Eclipse E800 microscope (Nikon 10x air, 0.3 NA; Nikon 40x air, 0.75 NA).

2.6 Cell Biology Assays

2.6.1 Homovanillic acid (HVA) assay

Release of H₂O₂ into the extracellular milieu was measured by H₂O₂-dependent horseradish peroxidase-mediated oxidation of HVA (3-methoxy-4-hydroxyphenylacetic acid) into a highly fluorescent dimer (2,2'-dihydroxy-3,3'-dimethoxydiphenyl-5,5'-diacetic acid). Cells were grown in 6 well plates and incubated for 30 minutes with 1ml HVA-solution in the presence or absence of 2 μ M ionomycin or 1 μ M thapsigargin. 500 μ l supernatant were transferred into a microcentrifuge tube and mixed with 75 μ l Stop buffer. Fluorescence was read on a Perkin Elmer Luminescence Spectrometer LS50B (320nm excitation, 420nm emission, slit width = 3). A preparation of a standard curve allowed for the accurate determination of H₂O₂ produced by the cells. For this, H₂O₂ concentrations ranging from 0 μ M to 5 μ M, were incubated in HVA solution for the duration of the assay and fluorescence of the standards were read at the same time as the samples.

2.6.2 Wound closure assay

For the quantitative analysis of wound closure cell lines transduced with Duox1/DuoxA1-2 or EV-control cell lines were grown on Fibronectin-coated photoetched coverslips until 100% confluency was reached. The cells were starved over night in their respective media, containing 0.5% FCS and the monolayer was wounded with a 10 μ l pipette tip in a linear fashion. Floating cells were removed through subsequent washes with sterile PBS and the cells on the coverslips were incubated in 10% media for 2-4 hours. For better statistics, at least 9 fields were imaged per condition and pictures of the same areas were taken hourly using a phase-contrast microscope. Wound areas were measured using Metamorph software and were expressed as percent closed wound of the average wound area of Duox1+DuoxA1-2. For IF studies, cells were grown on standard collagenized coverslips. The cells were fixed after 1 hour upon wounding and stained using the standard IF protocol.

2.6.3 Transwell Migration Assay

Migration experiments were performed in semi-permeable support membranes (24well; Costar Transwell-clear culture insert, polycarbonate, 8.0 μ m pore, Corning Costar), which were coated with 20 μ g/ μ l bovine fibronectin or 0.15 μ g/ μ l human placenta collagen, type IV. Transduced lung cancer cell lines expressing control vector, DuoxA1 or Duox1/DuoxA1 were washed twice in plain media and resuspended at 5x10⁵ cells/ml in media containing 0.5% FCS. 1x10⁵ cells were seeded on top of the insert and were allowed to attach for 30 min. Directional migration was induced by addition of 0.8ml 10% FBS-containing medium into the bottom chamber. Cells were cultured in a humidified incubator at 37°C and 5% CO₂ for up to 3.5 hours. The remaining cells on top of the insert were removed with a cotton swab and cells adherent to the bottom membrane were fixed and stained with Quik-Dip Stain according to the manufacturer's instructions and quantified with an Axiovert 100 microscope.

2.6.4 Cell Viability Assay

Lung cancer cell lines were seeded in triplicate and grown for up to 5 days in low-serum conditions. Proliferation was measured by means of mitochondrial activity, which reduces yellow water-soluble MTT (3-(4,5-Dimethylthiazol-2-yl)-2,5-diphenyltetrazolium bromide, Sigma) into water insoluble purple formazan. The MTT stock solution (5 mg/ml in water) was diluted 10-fold in pre-warmed culture medium and added to the cells. After incubation for 30 minutes at 37°C, the solution was aspirated and the cells were carefully washed with PBS. The violet formazan precipitate was solubilized in DMSO and the absorbance (540nm) of the solution was determined spectrophotometrically (Synergy HT).

2.7 Statistical analysis

Data are presented as mean \pm SEM and were graphed using GraphPad Prism 4.0 software. Differences in hydrogen peroxide production per milligram of protein per hour were analyzed by using a two-tailed Student's *t* test. Differences in mRNA expression between cancerous and non-cancerous matched human lung specimen and in 3D cultures were also assessed using the Student's *t*-test and the equality of variances was determined by the F-test. $P < 0.05$ was considered as statistically significant. Significance levels were *, $P < 0.05$; **, $P < 0.01$; ***, $P < 0.001$.

3 Results

3.1 Regulation and expression of Duox1 and Duox2

Dual oxidases were first identified in human and porcine glands, where they supply H_2O_2 for thyroperoxidase-mediated iodination and cross-linking of thyroglobulin tyrosine residues (De Deken et al., 2000; Geiszt and Leto, 2004). However, Duox enzymes seem to be distributed in a differential manner, as Duox2 is predominantly expressed in the thyroid and the highest levels of Duox1 were found in the lung (Caillou et al., 2001; Geiszt et al., 2003). Yet, not much is known about their cellular localization in lung epithelial cells and their dependence on other factors needed for correct processing and transfer of full enzymatic activity.

3.1.1 Expression analysis of Duox1 and Duox2 in primary lung epithelial cells

In order to get qualitative information about Duox1 and Duox2 levels in lung epithelial cells, their expression was characterized in human primary small airway epithelial cells (SAEC) and normal human bronchial epithelial (NHBE) cells. RT-PCR revealed expression of *DUOX1* and *DUOX2* in both cell types, with *DUOX2* being less abundantly expressed (**FIGURE 10A**). Total cell lysates (TCL) were probed with a Duox-specific and a distinct band of approximately 180 kDa was detected (**FIGURE 10B**), which corresponds to the glycosylated and mature form of Duox (Caillou et al., 2001; De Deken et al., 2002; Morand et al., 2003). As only fully matured Duox is functional and localizes to the plasma membrane, endogenous Duox was analyzed in SAEC via confocal microscopy (**FIGURE 10C**). Interestingly, a clear stain was visible at particular regions of the cell, reminiscent of protrusions of the leading edge.

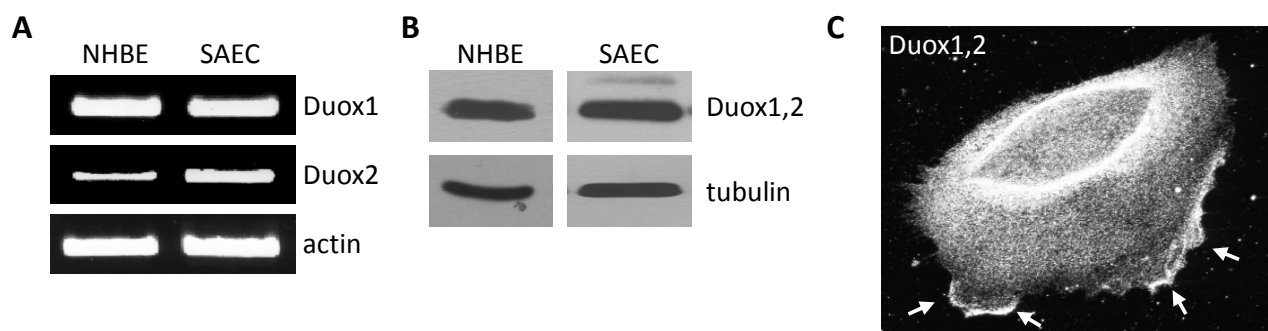


FIGURE 10: Expression analysis of Duox1 and Duox2 in primary human lung epithelial cells. (A), RT-PCR with specific primers for human Duox1 and human Duox2 was performed on normal human bronchial epithelial (NHBE) and small airway epithelial cells (SAEC). Actin was used as internal control. (B), Immunoblot analysis of total Duox expression in NHBE and SAEC. Total cell lysates (TCL) were probed with a Duox-specific antibody, which does not discriminate between the two isoforms. Tubulin served as loading control. (C), Localization of total Duox in SAEC was determined by immunofluorescence.

Functional analysis of Duox enzymatic activity demonstrated Ca^{2+} -inducible H_2O_2 production in primary lung epithelial cells (Geiszt et al., 2003). However, based on their structural homology with gp91^{phox}/Nox2, it is also conceivable that Duox enzymes are able to produce superoxide ($\text{O}_2^{\bullet-}$), which then rapidly dismutates into hydrogen peroxide (see **FIGURE 3**). To test for both types of reactive oxygen species (ROS), SAEC and NHBE cells were stimulated with ionomycin, which leads to an amplification of intracellular Ca^{2+} . Duox enzymes contain two EF-hand motifs, a structural domain for calcium-binding, and consequently an increase of Ca^{2+} should lead to their activation. Both primary human lung epithelial cell types produced H_2O_2 upon stimulation with ionomycin, which was determined by oxidation of homovanillic acid (HVA assay; **FIGURE 11**), thus suggesting an involvement of EF hand-containing Duox enzymes. Treatment of these cells with DPI, a flavoprotein inhibitor, led to complete inhibition of ROS production despite stimulation with ionomycin. While this inhibitor is not specific for NADPH oxidases, it still indicates the involvement of a flavoenzyme in ROS generation. The addition of catalase diminished detectable H_2O_2 upon stimulation with ionomycin. Because this enzyme promotes the conversion of hydrogen peroxide to water and molecular oxygen, this result suggested that the produced ROS was indeed H_2O_2 .

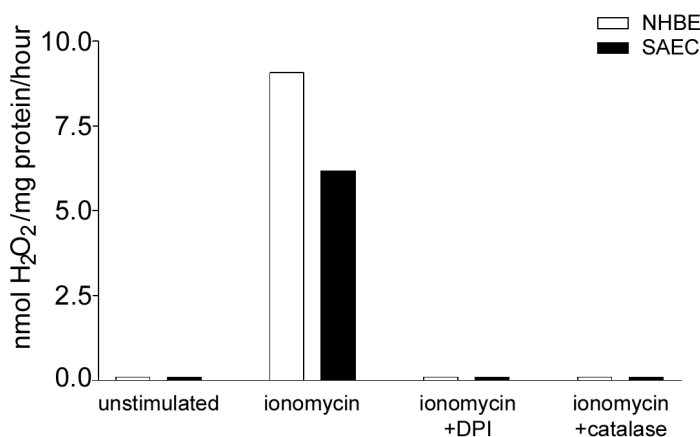


FIGURE 11: Production of H_2O_2 In primary lung epithelial cells. SAEC and NHBE were stimulated with ionomycin ($3\mu\text{M}$) for one hour. Catalase was added to determine the nature of the generated ROS and DPI ($10\mu\text{M}$) was used to inhibit NADPH oxidase activity. This experiment was repeated several times and one representative experiment is shown.

In summary, Duox1 and possibly Duox2 are expressed in primary human lung epithelial cells and are localized to the plasma membrane. The inducibility with Ca^{2+} and utilization of FAD as cofactor suggest that Duox is the likely source of H_2O_2 in lung airway epithelial cells.

3.1.2 Duox proteins require DuoxA maturation factors for function

Attempts have been made to reconstitute Duox enzymes in several different cell types; yet, functional enzyme was only recovered if Duox proteins were re-introduced into thyroid cells (De Deken et al., 2002; Morand et al., 2004). A recent study however, described a maturation factor for Duox2, termed DuoxA2, which enabled the translocation of the oxidase from the ER to the plasma membrane, thus allowing the functional reconstitution of Duox2 in HeLa cells (Grasberger and Refetoff, 2006). The authors also identified a putative maturation factor for Duox1, termed DuoxA1. Since no functional studies on Duox1/DuoxA1 were conducted, a model system for lung epithelial cells was established. Lung cancer cells NCI-H661, which are deficient of Duox1, Duox2, DuoxA1 and

DuoxA2 (see **FIGURE 27**), were transiently transfected with either Duox1 and DuoxA1 (343aa) or Duox2 and DuoxA2. Since both Duox enzymes possess intracellular EF-hands (see **FIGURE 4**), the cells were stimulated with either ionomycin or thapsigargin. Both compounds raise cytosolic calcium concentration via Ca^{2+} influx from intracellular calcium stores. A significant amount of H_2O_2 was released into the extracellular milieu upon stimulation, in both Duox1/DuoxA1 and Duox2/DuoxA2 reconstituted cells (**FIGURE 12**). These results correlate well with the already published data for Duox2/DuoxA2 (Grasberger and Refetoff, 2006) and confirm a similar dependence of Duox1 on DuoxA1.

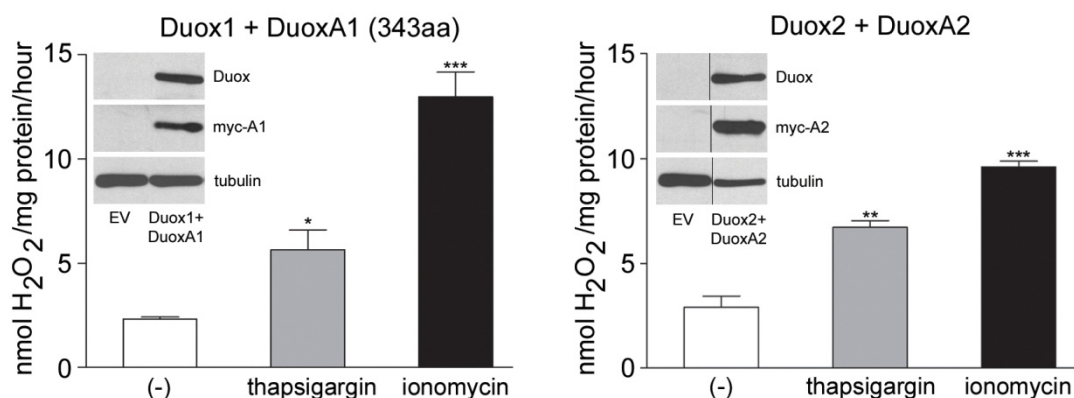


FIGURE 12: Duox-dependent H_2O_2 production. Duox1 and DuoxA1 (343aa) or Duox2 and DuoxA2 were transiently expressed in Duox-deficient lung cancer cells NCI-H661. Release of H_2O_2 was measured in response to thapsigargin ($1\mu\text{M}$) or ionomycin ($2\mu\text{M}$). Immunoblots from TCL were probed for Duox and myc-DuoxA expression. Tubulin served as loading control. Graphs show mean \pm SEM.

3.1.3 Duox and DuoxA co-localize at the same sub-cellular compartments

Duox proteins have been identified in the apical membrane of follicular cells in the thyroid (Caillou et al., 2001) and within the epithelium of the airways (Geiszt et al., 2003). However, the detailed localization of both oxidases and their maturation factors at the single cell level has not been determined yet. Since Duox1/DuoxA1 and Duox2/DuoxA2 reconstituted NCI-H661 cells produced similar amounts of H_2O_2 , it is conceivable that both oxidases localize to same cellular locations. Confocal immunofluorescence revealed that Duox1 was expressed at the plasma membrane, where it co-localized with DuoxA1 (343aa) (**FIGURE 13**, left panel). As shown by staining for calnexin, a marker for the ER, no co-localization was detected with either Duox1 or DuoxA1. Surprisingly, Duox2 mostly co-localized with DuoxA2 in vesicular structures and the ER, while some Duox2/DuoxA2 was also targeted to the plasma membrane (**FIGURE 13**, right panel). These findings are in contrast to previous reports in HeLa cells (Grasberger et al., 2007; Grasberger and Refetoff, 2006; Zamproni et al., 2008), where DuoxA proteins did not co-localize with Duox at plasma membrane-associated compartments, but were rather completely retained in the ER. Lung cells might possess other yet unknown factors which allow DuoxA proteins to exit the ER. Hence, it is possible that HeLa cells lack those tissue specific factors, as they were derived from a carcinoma of the cervix, a tissue not expressing endogenous Duox.

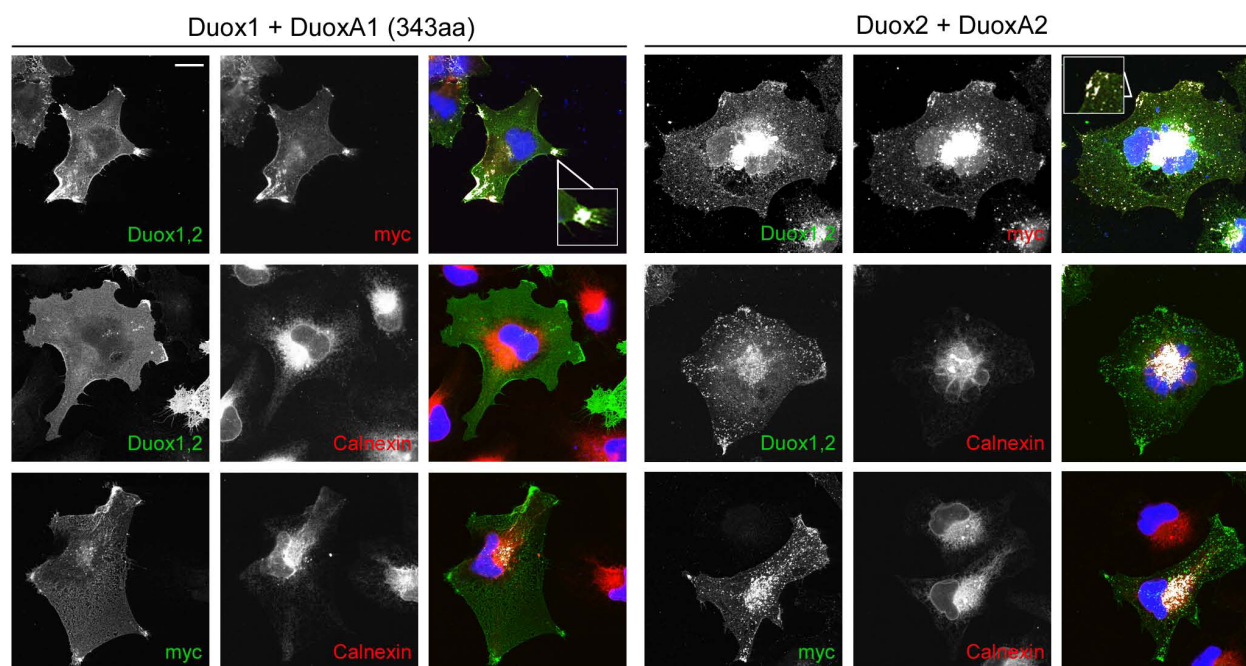


FIGURE 13: Distinct localization of Duox1 and Duox2 in lung epithelial cells. Duox1 and DuoxA1 (343aa) or Duox2 and DuoxA2 were transiently expressed in NCI-H661 cells. Cells were stained for Duox (Duox1,2), DuoxA (myc) or the ER marker calnexin as indicated. Nuclei were visualized by blue DAPI staining. Inserts depict distinct localizations of Duox1/DuoxA1 and Duox2/DuoxA2. Co-localization is indicated in white. Bar, 10 μ m.

3.1.4 DuoxA maturation factors form complexes with Duox proteins

The co-localization of Duox with DuoxA indicates a close spatial proximity of those two proteins. Since Duox1 and Duox2 need the presence of DuoxA1 and DuoxA2, respectively, to be fully mature and active, it is likely that they form a functional complex. In order to test for heterodimer formation, NCI-H661 cells were first stably transduced with lentiviruses encoding for Duox1 and DuoxA1 (343aa) or Duox2 and DuoxA2, thus allowing integration and stable, low-level expression. The cells produced similar amounts of H₂O₂ upon stimulation with ionomycin or thapsigargin compared to transiently transfected cells, when reconstituted with functional Duox1 or Duox2 (**FIGURE 14A**). Expression of empty vector (EV), DuoxA1 or DuoxA2 alone resulted only in background levels of H₂O₂, as maturation factors alone cannot generate ROS. Next, DuoxA proteins were immunoprecipitated using anti-myc monoclonal antibody, since both maturation factors were C-terminally fused to a myc-tag (**FIGURE 14B**). Both Duox1 and Duox2 co-immunoprecipitated with their respective DuoxA maturation factor, as indicated by positive Duox-detection in the myc-immunoprecipitates. No Duox protein was detectable in the control lanes, suggesting specific co-immunoprecipitation of Duox with DuoxA. Positive detection of myc (DuoxA) in the immuno-precipitates confirmed the presence of DuoxA proteins, thus ruling out that Duox protein was bound unspecifically to the beads in the pull down process.

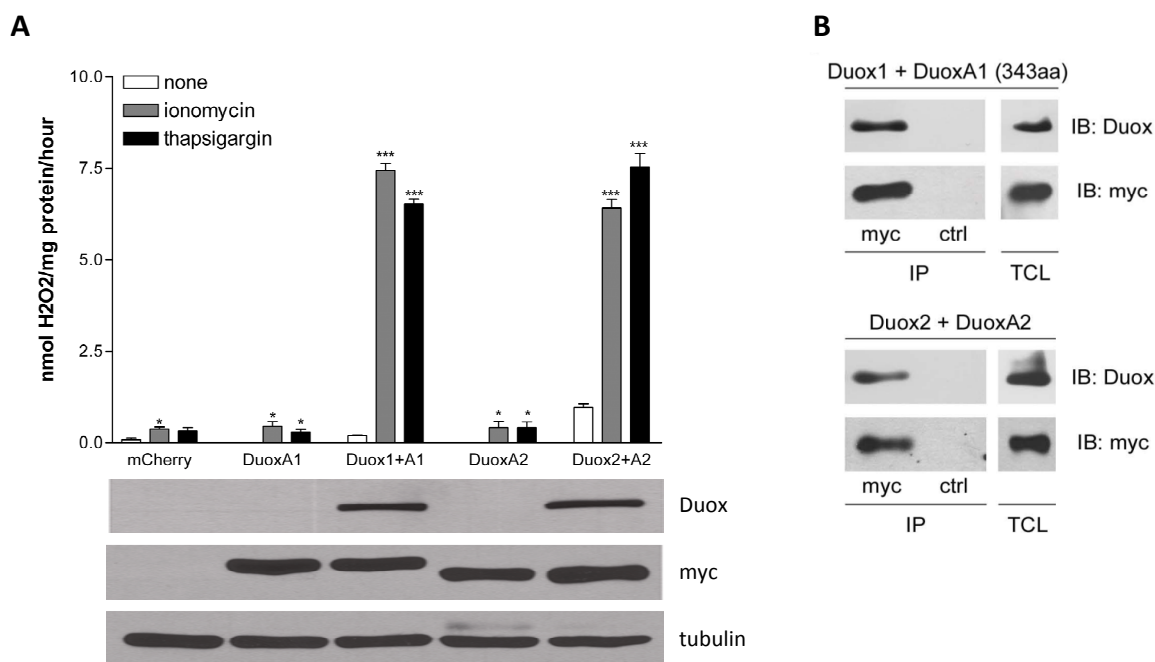


FIGURE 14: Stable expression of functional Duox1 and Duox2. Lung cancer cells NCI-H661 cells were transduced with lentiviruses encoding for Duox1 and DuoxA1 (343aa) or Duox2 and DuoxA2. (A), Duox-dependent H₂O₂ production was determined in response to ionomycin (2 μ M) or thapsigargin (1 μ M). The immunoblots depict Duox1 or Duox2 (Duox), DuoxA1 or DuoxA2 (myc) and tubulin expression in cell lysates. (B), after anti-myc immunoprecipitation (IP) immunoblotting for Duox and DuoxA (myc) was performed. Control IP (ctrl) was done with anti-GST. Immunoblotting (IB) on TCL was performed to confirm expression of Duox and DuoxA (myc).

The formation of heterodimers has been identified for other members of the Nox family, particularly Nox2/p22 (DeLeo et al., 2000; Yu et al., 1997). The incorporation of heme into Nox2 was shown to be essential for the interaction of both proteins, a phenomenon, which was also crucial for homodimer formation of inducible Nitric oxide synthases (Espinosa and Alfano) (Espinosa and Alfano, ; Panda et al., 2005). To analyze if the acquisition of heme by Duox is also necessary for association with DuoxA, the stably transduced cells were cultured in the presence or absence of succinyl acetone (SA), a specific inhibitor of heme biosynthesis. Indeed, co-immunoprecipitation of Duox with DuoxA was diminished in SA-treated cells (**FIGURE 15A**). Also, the enzymatic activities of both Duox1 and Duox2 were significantly reduced in cells treated with SA compared to untreated cells and only background levels of H₂O₂ were detectable (**FIGURE 15B**).

These results demonstrate that DuoxA1 and DuoxA2 are not only maturation factors for Duox1 and Duox2, but they are rather an integral part of the functional oxidase complex at the plasma membrane or other particular Duox1- or Duox2-containing membrane-associated compartments. Moreover, the insertion of heme into Duox1 and Duox2 is essential for the formation of the heterodimer and its disruption leads to the abrogation of H₂O₂ production.

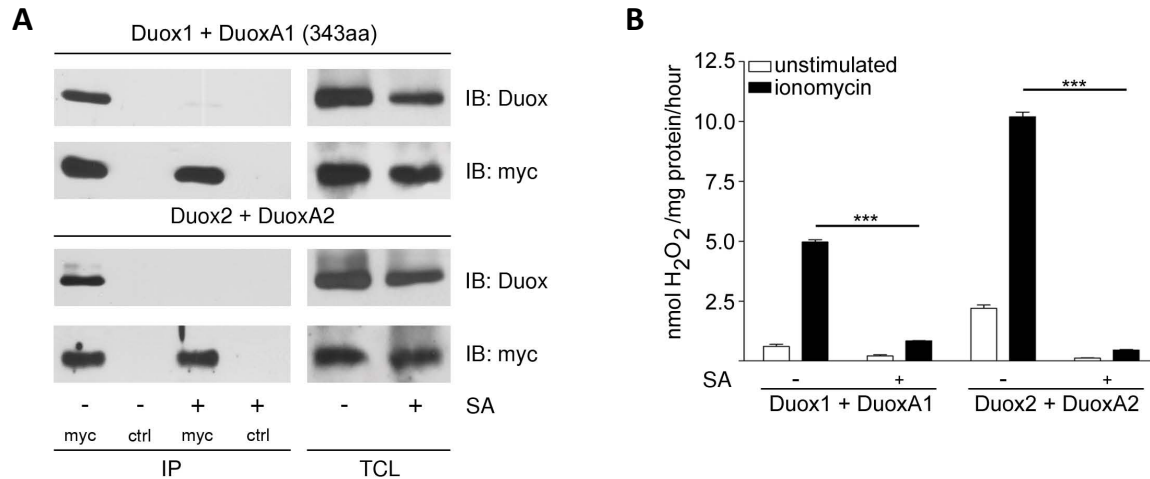


FIGURE 15: Inhibition of heme-insertion into Duox1 and Duox2. NCI-H661 cells stably expressing Duox1/DuoxA1 (343aa) or Duox2/DuoxA2 were cultured for 4 days in low serum media in the presence or absence of the heme synthesis inhibitor succinyl acetone (SA; 10 μ g/ml). (A), Immunoblotting (IB) for Duox and DuoxA (myc) was performed after immunoprecipitation of DuoxA (myc IP). Control IP was done with anti-GST. TCL were probed for expression of Duox and DuoxA (myc). (B), H₂O₂-production was measured upon stimulation with ionomycin (2 μ M). Graphs show mean \pm SEM.

3.1.5 Characterization of DuoxA isoforms

DuoxA1 and DuoxA2 are predicted to comprise five membrane-integral regions and harbor three NX(S/T) consensus sites for N-glycosylation within an extended extracellular loop between transmembrane (TM) domains two and three (**FIGURE 16A**). A search for both proteins in the Entrez Protein Database yields one DuoxA2 protein comprised of 320aa (NM_207581.2), while three isoforms of DuoxA1 were found: DuoxA1-1 (298aa; BC020841.1), DuoxA1-2 (343aa, DQ489735.1) and DuoxA1-3 (483aa, BC029819.1) (**FIGURE 16B**). All three DuoxA1 isoforms share the putative 5 transmembrane structure. DuoxA1-1 lacks two of the three N-glycosylation sites and DuoxA1-3 features an extended intracellular C-terminus.

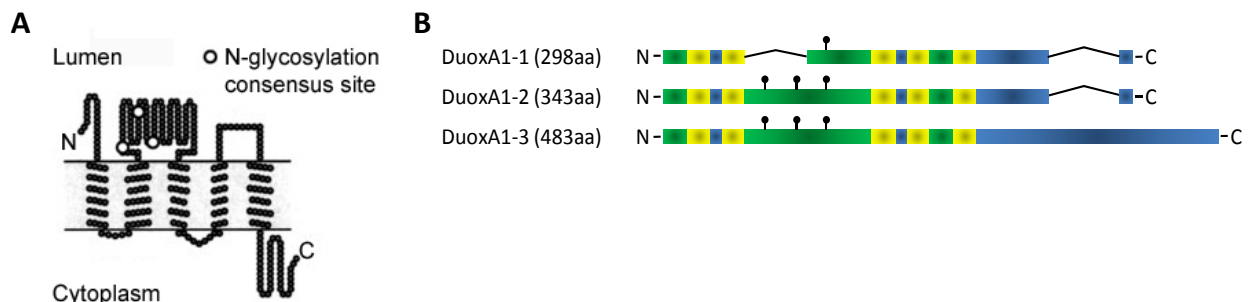


FIGURE 16: Putative structure of DuoxA1 and DuoxA2. (A), suggested topology model for DuoxA proteins features 5 transmembrane (TM) domains. The longer extracellular loop between TM2 and TM3 contains 3 putative N-glycosylation sites (Grasberger and Refetoff, 2006). (B), schematic representation of the three identified DuoxA1-variants, which all share the presumed five TM structure. DuoxA1-1 (298aa) lacks two of three putative N-glycosylation sites. DuoxA1-3 possesses an extended C-terminus. Green, extracellular regions; yellow, TM domains; blue, intracellular regions; •, N-glycosylation sites.

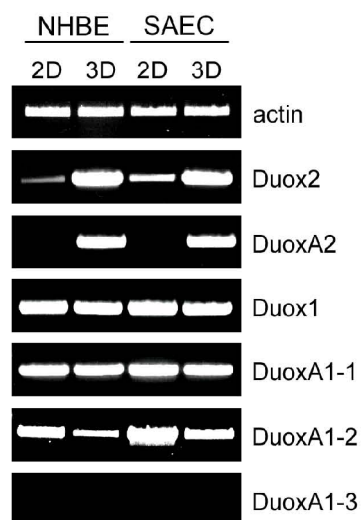


FIGURE 17: Endogenous levels of Duox and DuoxA. RT-PCR was done with specific primers on undifferentiated (2D) und ALI-differentiated (14 days; 3D) human primary lung epithelial cells SAEC and NHBE.

To date, no extensive functional analysis of DuoxA1 was published. Expression of all three DuoxA1 isoforms, as well as expression of *DUOXA2*, *DUOX2* and *DUOX1*, was analyzed in primary lung epithelial cells NHBE and SAEC (**FIGURE 17**). Cells were either grown in normal tissue culture conditions (2D) or in air-liquid interphase condition for 14 days (3D), as polarized epithelia are known to differentiate and upregulate certain genes (de Jong et al., 1994; Gray et al., 1996; Wu et al., 1997). Semi-quantitative PCR of *DUOXA1-1* revealed constant expression levels, suggesting a possible housekeeping role. *DUOXA1-2* expression was slightly decreased in 3D. The transcript of *DUOXA1-3* was not detected in any of the samples. Primer specificity and PCR-conditions were confirmed via transfection with the full length construct (data not shown). Since this isoform was initially identified from pooled libraries of brain, lung and testis, it is possible that the longest of the three DuoxA1 isoforms is not expressed in the lung. Also, the polarized epithelium lacks alveolar type II cells, which could be the source for this protein (Fischer et al., 2007; Nagai et al., 2008). Expression of *DUOX2* and *DUOXA2* was greatly enhanced in differentiated cells.

To investigate if all three DuoxA1 proteins can contribute to Duox1 function, Duox1 was co-expressed with each isoform in NCI-H661 cells (**FIGURE 18A**). Reconstitution of DuoxA1-3 induced only modest Duox1-dependent H_2O_2 production compared to DuoxA1-2 (see also **FIGURE 12**). Surprisingly, reconstituted DuoxA1-1 did not support Duox1 function, suggesting a potentially different role for this protein than DuoxA1-2 or DuoxA1-3. Confocal analysis revealed different cellular localization of all three isoforms and of the heterodimer (**FIGURE 18B**). DuoxA1-1 remained exclusively in the ER, where it co-localized with Duox1 and Calnexin (data not shown). It is possible that the lack of two of the three potential N-glycosylation sites in the putative extracellular loop hinders maturation of this isoform, resulting in ER retention. While DuoxA1-3 resided mostly in the ER, it also localized partially to the plasma membrane. This correlates well with the functional assay, as most Duox1 seemed to remain in the ER rather than being transported to the plasma membrane and consequently H_2O_2 -production was only moderate in Duox1/DuoxA1-3 reconstituted cells. Only co-transfection of DuoxA1-2 allowed Duox1 to exit the ER completely. The notion of a functional interaction of Duox1 with DuoxA1-2 and DuoxA1-3, respectively was further substantiated as Duox1 did only co-immunoprecipitate with those two proteins, but not with DuoxA1-1 (**FIGURE 18C**).

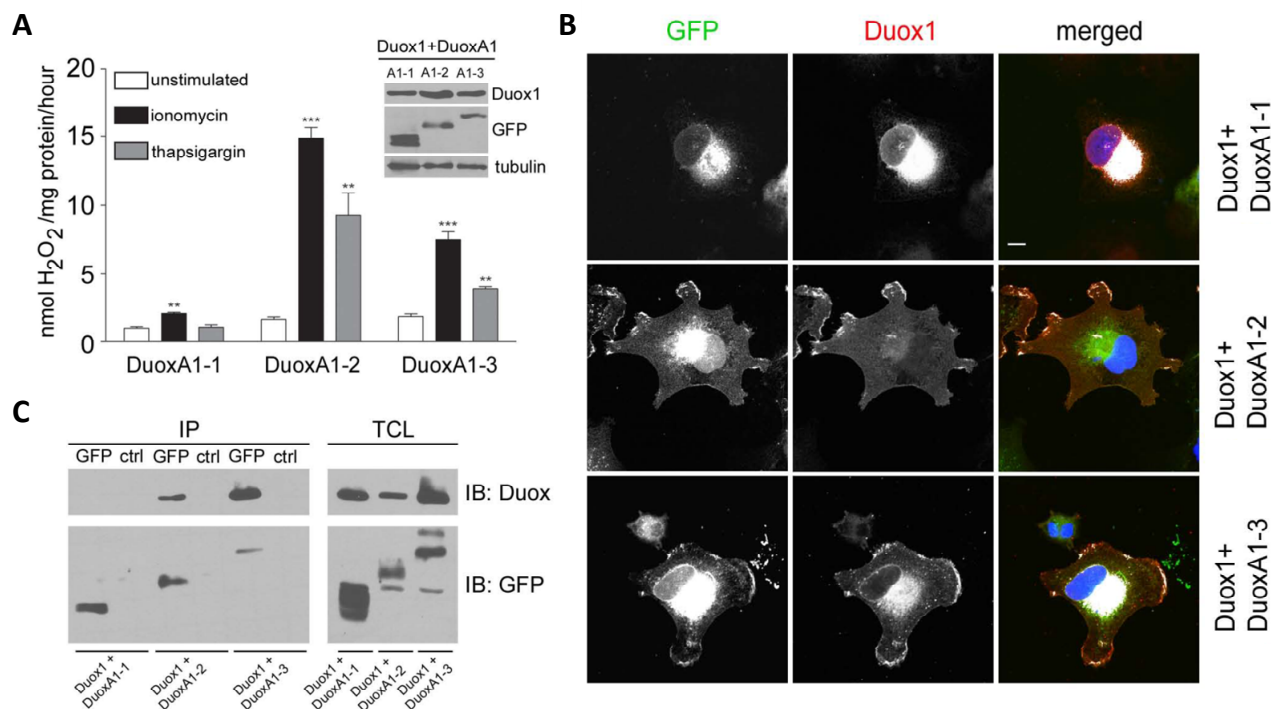


FIGURE 18: Reconstitution of Duox1 and DuoxA1-isoforms. NCI-H661 cells were transiently transfected with Duox1 and DuoxA1-1, DuoxA1-2 and DuoxA1-3, respectively. All three DuoxA1 isoforms were fused to eGFP. (A), Duox1-dependent H₂O₂ production was determined in response to stimulation with ionomycin (2 μ M) or thapsigargin (1 μ M). Data are presented as mean values \pm SEM. Expression of Duox1 and DuoxA1 (GFP) was confirmed by immunoblotting. Tubulin served as loading control. (B), Detection of Duox1 and the three DuoxA1 isoforms by immunofluorescence. Cells were stained with Duox antibody. DuoxA1-(1-3) detection was based on the eGFP fusion protein. Co-localization is shown in white. Bar, 10 μ m. (C), Immunoblotting for Duox1 and DuoxA1 (GFP) was conducted upon anti-GFP immunoprecipitation. Control IP was done with anti-GST. TCL were probed for Duox1 and DuoxA1-1, DuoxA1-2 and DuoxA1-3 (GFP) expression.

Taken together, these findings demonstrate that the localization and consequentially the function of Duox1 are dependent on the DuoxA1-isoform. While both DuoxA1-3 and DuoxA1-2 form a heterodimer with Duox1, only the latter enables complete translocation of the heterodimer to the plasma membrane, which is essential for Duox1/DuoxA1 activity.

3.1.6 Mismatch pairing of Duox and DuoxA

The aforementioned experiments showed that reconstitution of Duox1 and Duox2 with their respective maturation factor, Duox A1-2 and DuoxA2, resulted in the highest ROS production (FIGURE 12, 14, 18). Those two maturation factors share the predicted 5 transmembrane structure (see FIGURE 5, 16) and are 52% identical in their primary structure. To test if both could support function of the paralog of their respective oxidase, DuoxA1-2 and Duox2 were co-expressed with Duox1 and DuoxA2, respectively. Surprisingly, DuoxA1-2 could sustain Duox2-dependent H₂O₂ production, with levels similar to those of the combination Duox2/DuoxA2 (FIGURE 19A). However, pairing of Duox1 with DuoxA2 did not result in any substantial H₂O₂ release. In contrast, a recent report showed a minimal rescue of Duox2 function when expressed together with DuoxA1-2 (Zamproni et al., 2008). Therefore, this experiment was repeated in Duox-deficient HeLa cells, the cell type used by Zamproni and coworkers (FIGURE 19B). Only minimal levels of basal and ionomycin-stimulated H₂O₂ were

produced by the mismatch, indicating cell-type specific differences in functional dimer formation. It is possible that HeLa cells lack additional lung-cell-specific factors, thus preventing functional recovery of the mismatched Duox2/DuoxA1-2 pair.

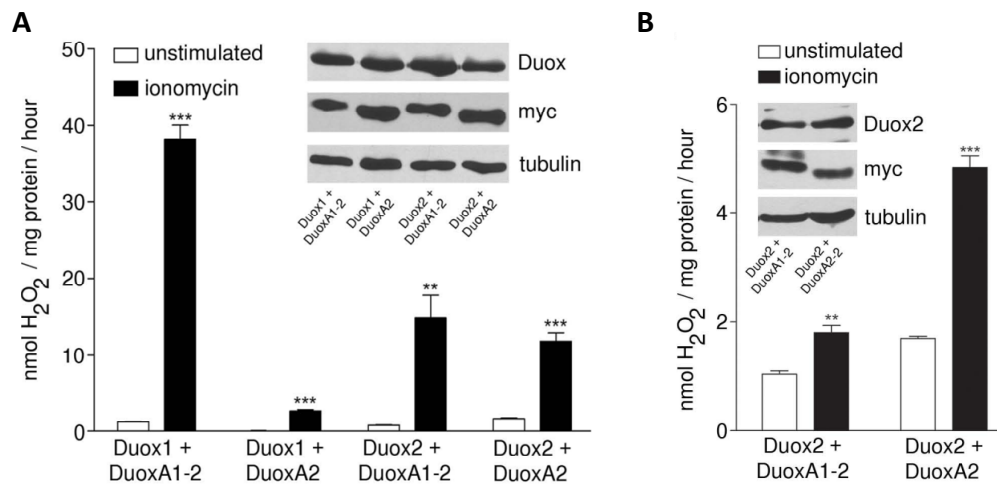


FIGURE 19: Analysis of Duox-dependent H₂O₂ production by matched and mismatched pairs of Duox and DuoxA. Duox1 and Duox2, respectively, was transiently co-expressed with DuoxA1-2 or DuoxA2 in NCI-H661 (A) or HeLa (B) cells. The release of H₂O₂ was measured upon stimulation with ionomycin (2 μ M). Shown are mean values \pm SEM. Levels of Duox and DuoxA expression were determined by immunoblotting. Tubulin served as loading control.

Immunostaining of NCI-H661 cells expressing Duox2 in the presence of DuoxA1-2 showed distinct localization of both proteins at the plasma membrane, whereas Duox2 localized mainly in vesicular structures when co-expressed with DuoxA2 (FIGURE 20, left panel, see also FIGURE 13).

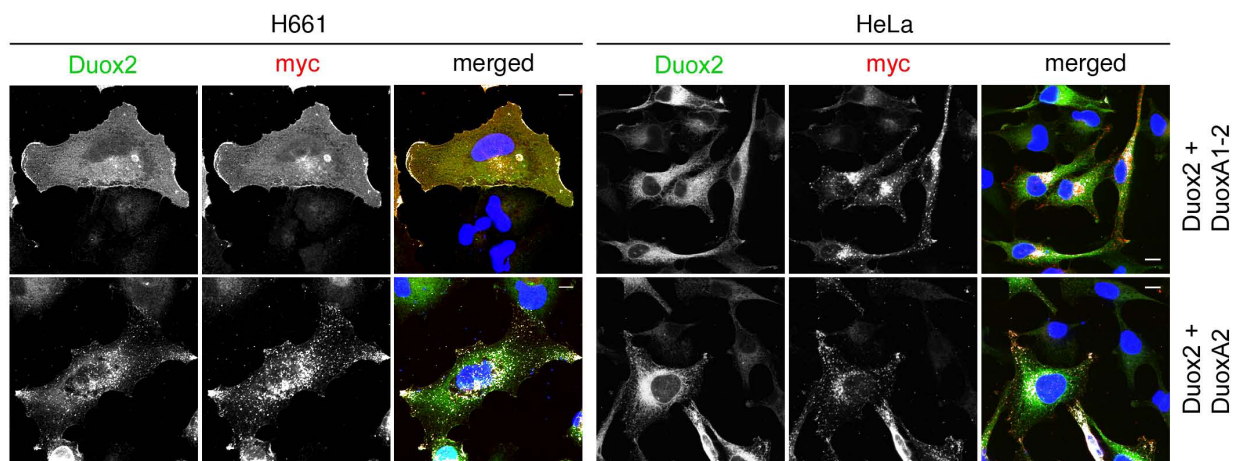


FIGURE 20: Duox2 localization is contingent on co-expression of DuoxA1-2 or DuoxA2. Duox2 localization was analyzed via confocal microscopy in NCI-H661 and HeLa cells, which were transiently transfected with Duox2/DuoxA1-2 or Duox2/DuoxA2 and stained with Duox and myc antibodies. Co-localization is shown in white. Bar, 10 μ m.

In HeLa cells Duox2 was not targeted to the plasma membrane when co-expressed with DuoxA1-2 and remained almost exclusively in the ER (FIGURE 20, right panel). The formation of a mismatched Duox2/DuoxA1-2 heterodimer in lung cells was further confirmed via co-immunoprecipitation. Duox2 was detected after pull down of both DuoxA2 and DuoxA1-2, confirming a close interaction of Duox2 with either maturation factor (FIGURE 21).

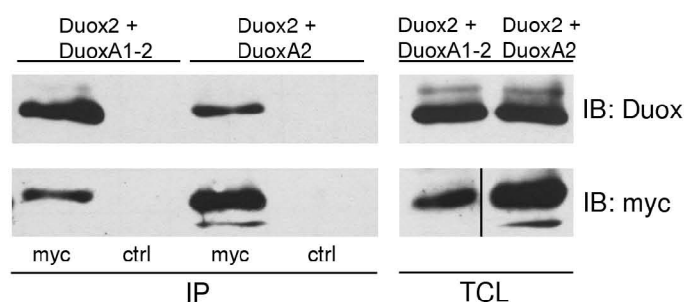


FIGURE 21: Heterodimer formation of Duox2 with DuoxA1-2. Immunoprecipitation of DuoxA1-2 and DuoxA2 was conducted on lysates from NCI-H661 cells, which were transiently transfected with Duox2 and DuoxA1-2 or DuoxA2. Immunoprecipitates and TCL were probed for Duox2 and DuoxA (myc). Control IP was done with anti-GST.

These results suggest that lung cells can utilize not only DuoxA2 but also DuoxA1-2 to support Duox2-dependent H_2O_2 production. Also, the particular interaction of Duox2 with either DuoxA subunit seems to define the subcellular localization of the oxidase, which could possibly impact the spatiotemporal generation of ROS. In addition, these findings demonstrate that results can vary depending on the model cells used. Hence, this emphasizes the use of cells, which are derived from the same tissue as the protein of interest.

3.1.7 Generation of isoform-specific Duox1, Duox2 and DuoxA1 antibodies

To investigate endogenous expression of Duox and DuoxA, antibodies specific for human Duox1, Duox2 and DuoxA1 were generated in the lab, finally allowing for differential expression analysis of those proteins (**FIGURE 22**). Isoform specificity was confirmed by detection of total Duox (using anti-Duox1,2) and DuoxA (using anti-myc). The anti-DuoxA1 antibody does not discriminate between any of the three DuoxA1 isoforms.

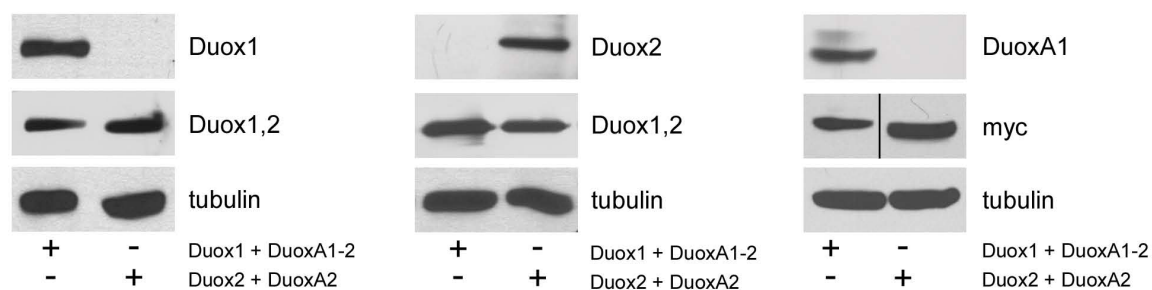


FIGURE 22: Validation of isoform-specific antibodies. TCL from cells expressing Duox1/DuoxA1-2 or Duox2/DuoxA2 were probed with isoform-specific antibodies for Duox1, Duox2 and DuoxA1. The latter does not discriminate between any of the DuoxA1-isoforms. Detections of total Duox using the isoform-unspecific antibody (Duox1,2) and of total DuoxA (myc) served as expression control. Tubulin-probing confirmed equal loading.

3.1.8 Analysis of endogenous Duox and DuoxA expression

Quantitative PCR of SAEC, which were cultured and differentiated for a time course of 21 days, showed no change in *DUOX1* transcript levels, whereas *DUOX2* mRNA was significantly increased over time (**FIGURE 23A**). Western blot analysis revealed an increase of Duox1 protein, which might be a result of increased protein stability in differentiated cells (**FIGURE 23B**). Despite the fact that *DUOX2* mRNA was markedly upregulated during differentiation (**FIGURE 17, FIGURE 23A**) Duox2 protein could not be detected in the lysates (data not shown). It is possible that the protein levels were still below

the detection limit of the antibody, at least for immunoblotting applications, especially because overexpressed Duox2 was readily detectable.

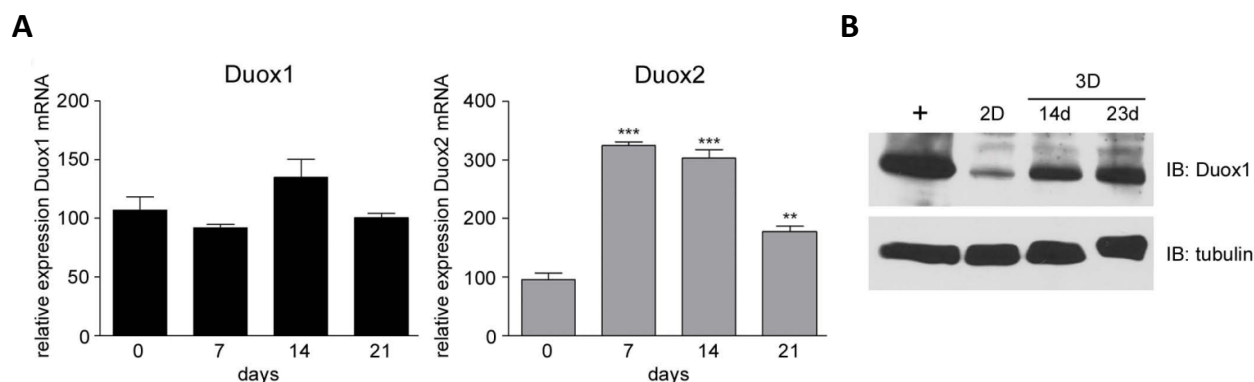


FIGURE 23: Analysis of endogenous Duox expression in primary lung epithelial cells. (A), real-time PCR specific for Duox1 or Duox2 was performed on SAEC, which were either undifferentiated (day 0) or differentiated in ALI-culture for 7, 14 and 21 days. Per sample, two inserts were pooled for extraction of total RNA. Data points consisted of three samples each and were individually normalized to actin, which served as internal control. Data were expressed in relation to transcript levels at day 0 and are presented as mean \pm SEM. (B), detection of endogenous Duox1 protein in lysates from SAEC, which were either undifferentiated (2D) or ALI-differentiated (3D) for 14 and 23 days (d), by probing with the specific anti-Duox1 antibody. Lysates from cells transiently transfected with Duox1/DuoxA1-2 were used as positive expression control (+). Tubulin served as loading control.

Previous results have shown distinct localization patterns for both Duox1 and Duox2, when co-expressed with DuoxA maturation factors (FIGURE 13, FIGURE 20). Since these localization experiments were conducted in transformed lung cancer cells, these findings were further validated in the context of normal lung epithelial cells. Primary SAEC were transduced with lentivirus, encoding for Duox1, Duox2, DuoxA1-2 and DuoxA2 or empty vector (EV) as control. Cells were stained with anti-Duox1,2 and anti-myc antibodies, which detect both Duox isoforms and the myc epitope tag of DuoxA, respectively. Confocal analysis revealed the same heterodimer co-localization in SAEC compared to the previous observations in NCI-H661, with Duox1/DuoxA1-2 and Duox2/DuoxA1-2 being expressed at the plasma membrane and Duox2/DuoxA2 being localized to vesicular structures and the ER (FIGURE 24). When antibodies specific for Duox1, Duox2 and DuoxA1 were used, the same pattern was detected. Endogenous Duox1 and DuoxA1 were detected at the plasma membrane in cells expressing either EV or DuoxA1 alone. Duox2 could not be visualized, as it is not expressed in undifferentiated SAEC (FIGURE 17).

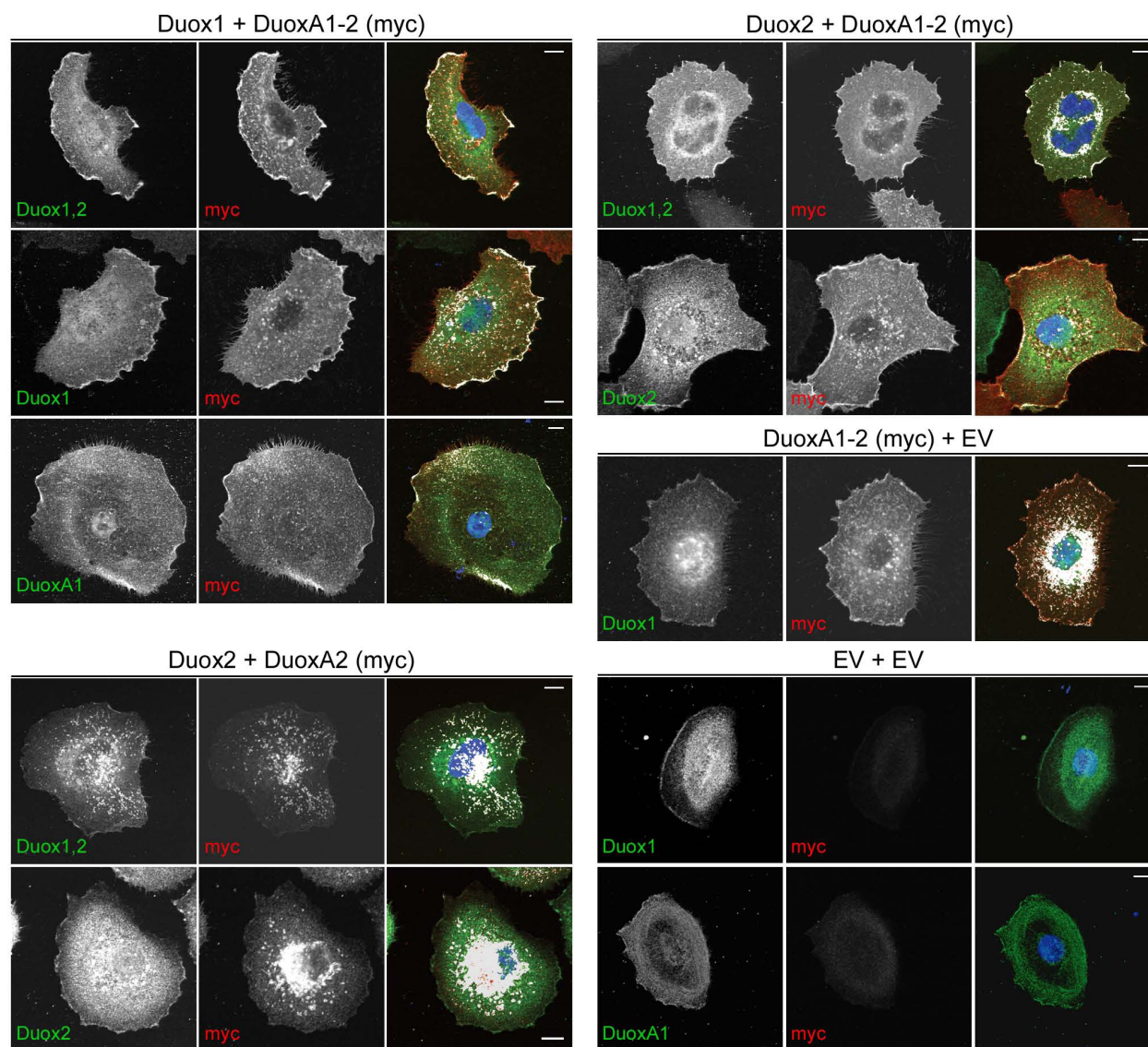


FIGURE 24: Analysis of exogenous and endogenous Duox and DuoxA localization in primary human lung epithelial cells SAEC. Cells were lentivirally transduced with Duox1/DuoxA1-2, Duox2/DuoxA2, Duox2/DuoxA1-2, DuoxA1-2/empty vector (EV) or EV/EV and stained with specific antibodies as indicated. Co-localization is illustrated in white. Bar, 10µm.

Thus far, not much is known about the intracellular distribution of Duox1 and Duox2 in *in vitro* polarized cells. The generation of the specific antibodies in our lab allowed for the detection of not only the presence of Duox1, Duox2 and DuoxA1, but also their localization in differentiated cells. As a first step SAEC were grown and differentiated for 2 weeks in ALI culture and stained with markers for mucus (MUC5A) and ciliated (β -tubulin IV) cells, as well as for Duox1, Duox2 and DuoxA1 (**FIGURE 25**). A Z-series of confocal images revealed expression of Duox1, Duox2 and DuoxA1 on the apical side of the multiple cell layer. Surprisingly, Duox2 was also expressed in ciliated cells, where it colocalized with β -tubulin in the cilia. Some DuoxA1 and little Duox1 was also detectable in the cilia but to a much lesser extent than Duox2. Duox1 was not found in mucus-expressing cells.

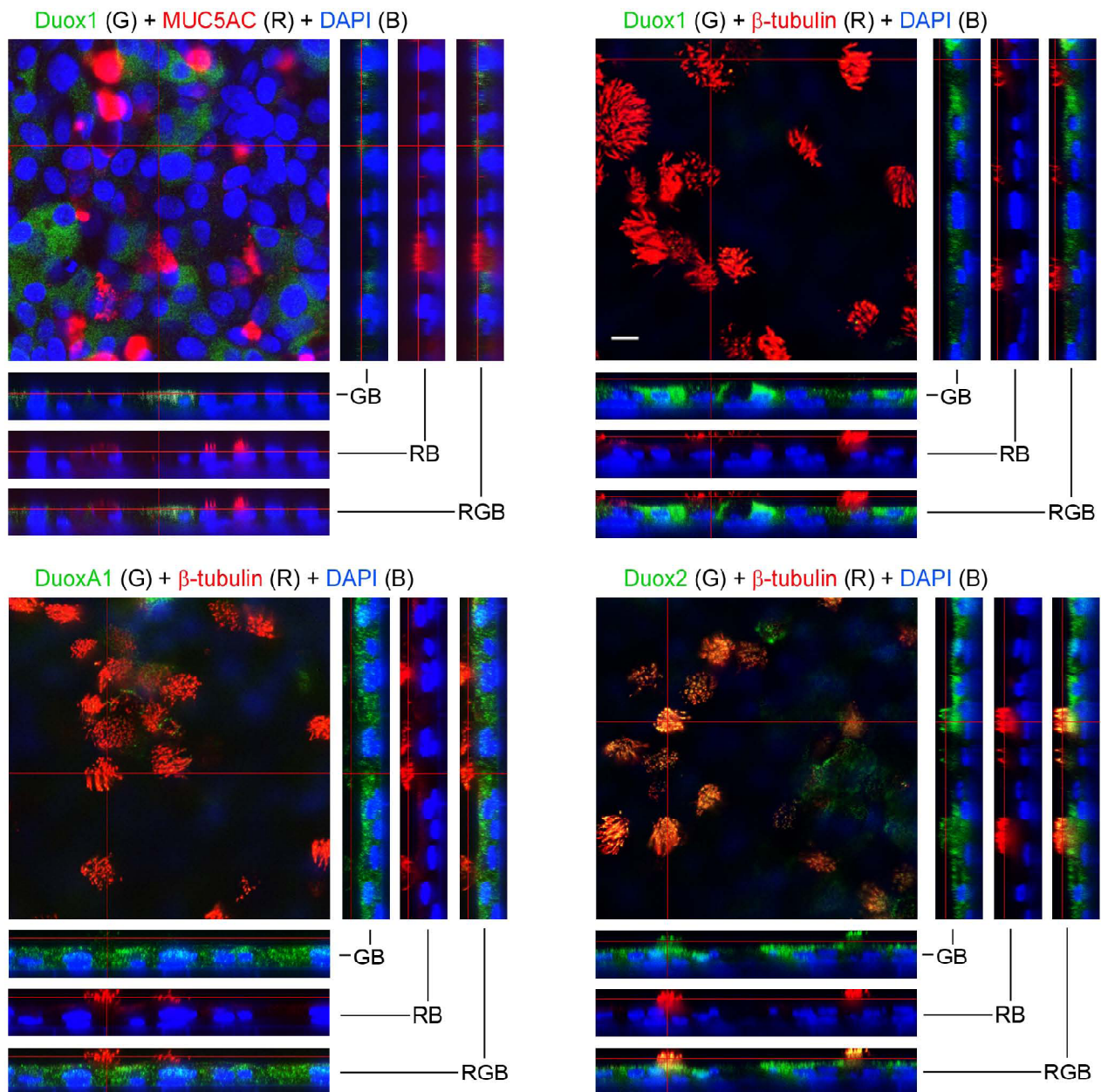


FIGURE 25: Localization of endogenous Duox1, DuoxA1 and Duox2 in *in vitro* differentiated primary lung epithelial cells. SAEC were differentiated for 14 days in ALI-culture and stained for mucus-containing cells (MUC5A, red, R), ciliated cells (β -tubulin, red, R) and Duox1, DuoxA1 and Duox2 (all green, G) as indicated. Nuclei were stained with DAPI (blue, B). Z-sections at 0.3 μ m intervals were taken throughout the entire depth of the multiple cell layer at several positions of the insert. Orthogonal views correspond to crosslines depicted in the rectangular overview and show two color overlays of green and blue (GB), red and blue (RB) and three color merge (red, green, blue; RGB), with co-localization indicated in yellow. Bar, 10 μ m.

3.1.9 *in vivo* expression of Duox in lung epithelium

In order to get information about Duox expression *in vivo*, sections from human normal upper lung were stained for Duox1,2 expression. The red stain indicative for Duox protein revealed localization within the pseudostratified epithelium of the airways, oriented towards the lumen (**FIGURE 26A**).

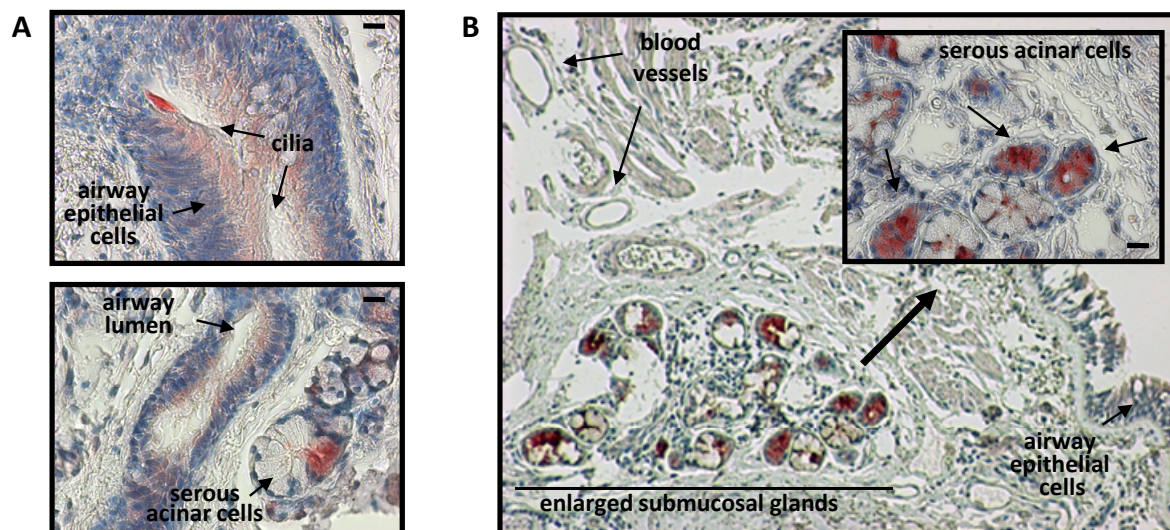


FIGURE 26: Detection of endogenous Duox in human lung tissues. Immunohistochemical staining for Duox1,2 was performed on human tissue sections from a normal donor (A) and a patient with cystic fibrosis (B). Duox protein is indicated by a red stain. (A), Duox protein was predominantly expressed in the ciliated airway epithelial cells, which are directed towards the lumen of the airways. (B), strong staining for Duox1,2 was detected in serous acinar cells, depicted in the inset. They are localized in enlarged submucosal glands, in close proximity to the airways. Bar, 10μm.

Duox was also detected in airway epithelial cells of lung tissue sections from a donor with cystic fibrosis (CF) (**FIGURE 26B**). Additionally, a very strong red stain was visible in serous acinar cells. These cells are located in submucosal glands, which were enlarged in this patient, a typical phenotype of CF (Kamio et al., 2005; Yang et al., 1988).

As this data show Duox-specific staining in serous acinar cells, they suggest an additional site for Duox expression *in vivo*, in addition to the already established localization to airway epithelial cells (Geiszt et al., 2003).

3.2 Duox-silencing in human lung cancer

ROS are known to damage biomolecules, such as proteins, DNA or lipids, and this in turn can potentially lead to abnormalities of cellular function and regulation (Lambeth, 2004). Since Duox enzymes produce ROS and are the predominant NADPH oxidases in the lung, it is possible that an upregulation of those proteins could lead to oxidative stress and cellular damage, potentially promoting lung cancer development and progression.

3.2.1 Expression analysis of Duox and DuoxA in lung cancer cell lines

To investigate potential differences between normal and cancerous lung epithelial cells, expression of *DUOX* was analyzed in primary (SAEC, NHBE) and immortalized primary (BEAS-2B, SALE) lung cells as well as lung cancer cell lines, which were derived from primary small cell lung carcinomas (NCI-H69, NCI-H82, SHP-77), and non-small cell lung carcinomas (Adenocarcinoma: NCI-H292, NCI-H727, Calu-3, NCI-H441, UCLA-P3, A549; Squamous cell carcinoma: NCI-H460, NCI-H661; Large cell carcinoma: NCI-H157) (FIGURE 27).

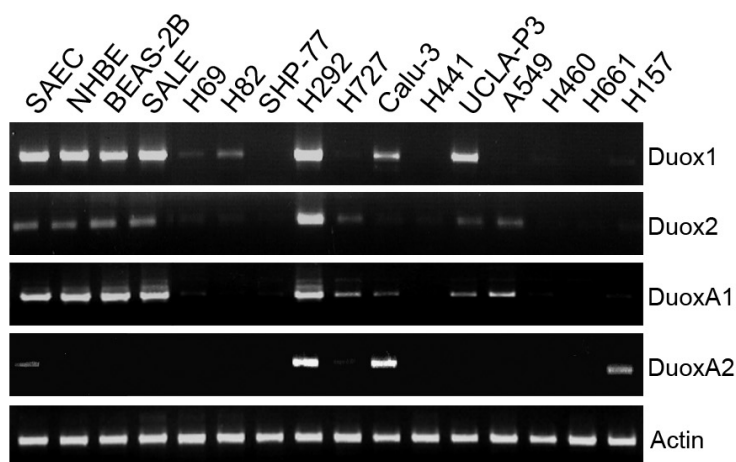


FIGURE 27: Expression analysis of *DUOX1*, *DUOX2*, *DUOXA1*, *DUOXA2* in lung epithelial cells and lung cancer cell lines. RT-PCR was performed on primary human lung epithelial cells (SAEC, NHBE), immortalized normal lung epithelial cells (BEAS-2B, SALE), three small cell lung cancer cell lines (H69, H82, SHP-77) and 9 non-small cell lung cancer cell lines (Adenocarcinoma: H292, H727, Calu-3, H441, UCLA-P3, A549; Squamous cell carcinoma: H460, H661; Large cell carcinoma: H157). DuoxA1 mRNA was detected with primers detecting DuoxA1-2 and DuoxA1-3. Actin was used as internal control.

Surprisingly, *DUOX1* message was reduced or absent in 9 out of 12 lung cancer cell lines, while it was expressed in primary and immortalized primary lung epithelial cells. Because *DUOX2*, *DUOXA1* and *DUOXA2* are localized at the same locus as *DUOX1* on chromosome 15q15 (see FIGURE 5A), their expression was analyzed as well. *DUOX2* was clearly detectable in normal lung cells, although the levels were lower than *DUOX1*. This correlates well with previous data that also showed lower *DUOX2* transcript levels in cells, which were grown in normal 2D tissue culture conditions (see FIGURE 17). The endogenous levels of *DUOXA1* demonstrated a similar expression pattern as its corresponding oxidase, while *DUOXA2* was not present in primary lung cells and most cell lines.

3.2.2 Restoration of Duox/DuoxA expression through global demethylation

Since reduced *DUOX* message was detected in most lung cancer cell lines, we hypothesized aberrant promoter hypermethylation being involvement in *DUOX* silencing. Promoter hypermethylation has been identified as a frequent key event in both early- and late-stage lung carcinoma pathogenesis (Bowman et al., 2006; Machida et al., 2006; Palmisano et al., 2000; Tsou et al., 2002; Widschwendter et al., 2004). Since this epigenetic mechanism almost exclusively occurs in CpG-islands, areas with a high density of CpG dinucleotides, the regions -1000bp upstream of the transcriptional start site (TSS) of *DUOX1*, *DUOX2* and -2000bp upstream of *DUOX1*-2 and *DUOX2* were analyzed (FIGURE 28).

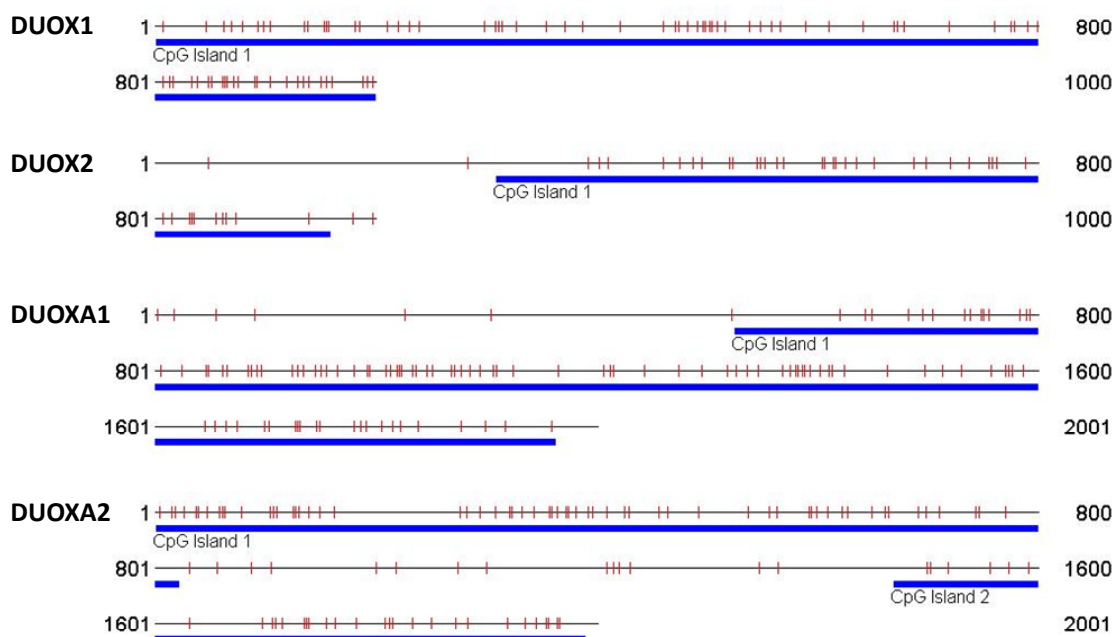
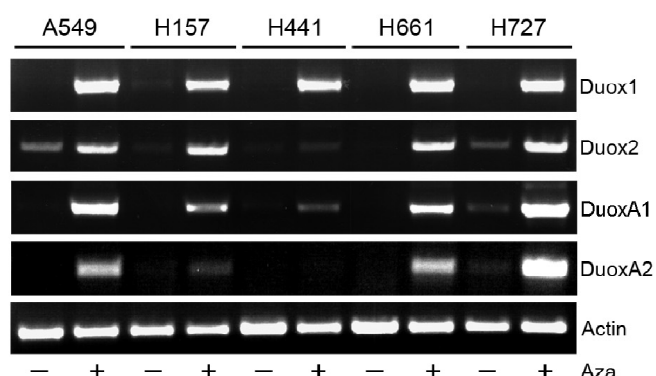


FIGURE 28: Analysis of the promoter regions upstream of *DUOX1*, *DUOX2*, *DUOX1A1* and *DUOX2A2*. Contingent on the stringent criteria described by (Takai and Jones, 2003) CpG islands were detected within the analyzed 1000bp upstream of the TSS of *DUOX1* and *DUOX2*. Similarly, CpG islands were also detected in the 2000bp upstream of the TSS of *DUOX1A1* and *DUOX2A2*.

The regions of all four genes are CpG-rich and contain CpG islands. Hence, it is likely that their promoters are subject to non-random hypermethylation. It has been shown that inhibition of the cellular DNA methyltransferase (DNA (cytosine-5)-methyltransferase 1; Dnmt1) recovered expression of genes that were silenced by promoter hypermethylation. Therefore, in order to analyze if *DUOX* genes are also affected by the epigenetic phenomenon, selected *DUOX*-deficient cell lines were



treated with 5'-aza-2'-deoxycytidine (Aza) (FIGURE 29).

FIGURE 29: Recovery of *DUOX1*, *DUOX2*, *DUOX1A1* and *DUOX2A2* expression after treatment with 5-aza-2'-deoxycytidine (Aza). *DUOX*-deficient lung cancer cell lines were grown for 5 days in the presence (+) or absence (-) of Aza (1 μ M). Gene expression was analyzed by RT-PCR. Actin served as internal control.

Indeed, expression of *DUOX1* was restored in all tested lung cancer cell lines upon inhibition of Dnmt1. Aza-treatment also induced expression of *DUOX2*, *DUOX1A1* and *DUOX1A2* in four out of five cell lines. It is possible that in NCI-H441 cells other epigenetic mechanisms, such as histone acetylation, are responsible for the transcriptional repression of the investigated genes. TCL of cell lines A549 and NCI-H661 cultured in the presence or absence of Aza were probed for total Duox expression and a band of 180kDa was detected (**FIGURE 30A**). However, even upon Ca²⁺ mobilization via stimulation with ionomycin, no increase of H₂O₂ was detectable (**FIGURE 30B**). It is possible that Duox recovery through Aza is too modest to support function, a notion that was supported by comparison of exogenous levels of Duox versus endogenous amounts achieved by Aza treatment (**FIGURE 30C**). While Duox protein was easily observed after one second of enhanced chemiluminescence (ECL) exposure in NCI-H661 transiently transfected with Duox1/DuoxA1-2, Aza-recovered Duox was barely detectable after 20 seconds. It is possible that several concomitant events are taking place in cancer cells, besides inhibition of Duox protein expression, which prevent the re-establishment of the functional oxidase.

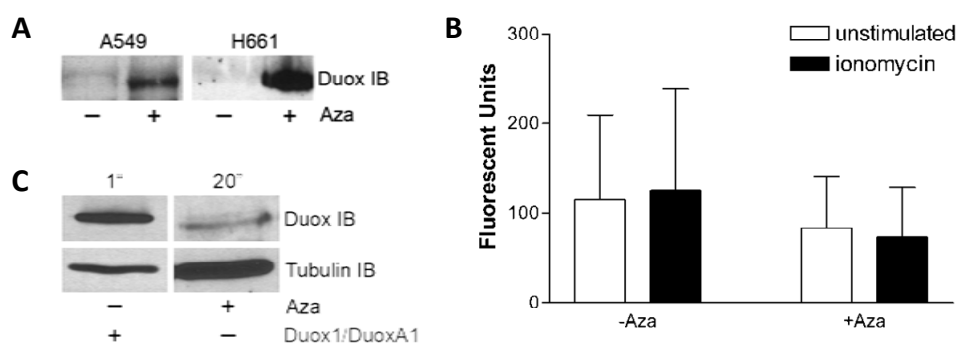


FIGURE 30: Recovery of Duox protein in lung cancer cells. Duox-deficient lung cancer cell lines A549 and NCI-H661 were grown in the presence or absence of Aza (1 μ M) for 5 days. (A), 150 μ g total lysate were loaded on each lane and membranes were probed for total Duox expression. (B), H₂O₂ production was analyzed in NCI-H661 upon stimulation with ionomycin (2 μ M). Shown are mean values \pm SEM. $n=3$. (C), NCI-H661 cells were either transfected with Duox1/DuoxA1-2 for 48h or grown in the presence of 1 μ M Aza for 5 days. 50 μ g of total cell lysate for each treatment were loaded per lane. Immunoblots were probed with anti-Duox and anti-tubulin antibodies and proteins were visualized by ECL with exposure times ranging from 1 to 20 seconds.

3.2.3 Detailed methylation analysis of the *DUOX1* and *DUOX2* promoter

The promoter of Duox1 encompasses three binding sites for Sp1. This transcription factor is an activator of RNA polymerase II-driven transcription (Yeh et al., 2006). Its consensus binding sequence (CCGCCC) does enclose one CpG site, which could be methylated. In turn, this could lead to sterical inhibition of the RNA-Polymerase complex during transcription. Since Aza causes global demethylation throughout the entire cell, so far no conclusions could be drawn regarding the definite methylation status of the promoter regions of *DUOX*. In order to analyze specific CpG islands, genomic DNA (gDNA) was treated with sodium bisulfite, resulting in deamination of cytosines into uracil. Methylated cytosines, however, are not affected and remain in the DNA as cytosines (see methods for details). A larger region of the promoter was amplified with universal primers, which are unbiased for CpG sites. The product of this PCR reaction was subsequently probed with primers specific for either methylated (MSP) or unmethylated (USP) sequences, revealing the methylation status of few CpG sites close to the TSS of both *DUOX1* and *DUOX2* (**FIGURE 31**). Methylated

sequences were identified in 4 out of 5 Duox-negative cell lines (A549, NCI-H157, NCI-H441, NCI-H661). As expected, Duox-expressing cells (NHBE, SAEC, NCI-H292) were negative for methylation in this region and were positive for unmethylated sequences. Cell line NCI-H727 was negative for MSP, however, *DUOX1* message was restored upon Aza-treatment (see **FIGURE 29**). This could indicate that methylation occurred at a different CpG-rich region of the promoter, which was not covered by the MSP primers used in this assay, or that other epigenetic modifications, such as histone acetylation, are responsible for the inactivation of *DUOX1* in these cells. Cancer cell line NCI-H157 was positive for both methylated and unmethylated sequences, indicative for partial methylation throughout the cell population. MSP of the *DUOX2* promoter was negative in primary and immortalized primary cells and all but one investigated cell line (NCI-H441) were partially methylated.

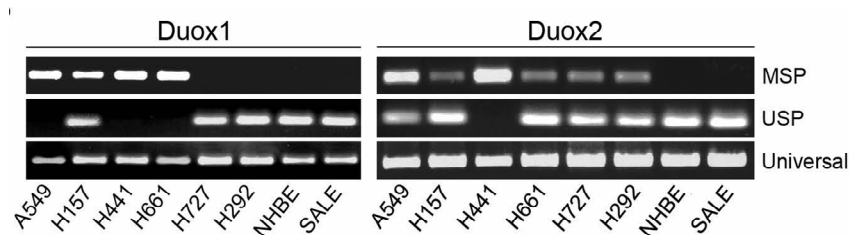


FIGURE 31: Methylation specific PCR. The methylation status of lung cancer cell lines and normal lung epithelial cells was characterized using primers specific for methylated (MSP) and unmethylated sequences. The promoter regions of *DUOX1* and *DUOX2* were amplified with Universal-a primers, followed by PCR with MSP-a and USP-a primers. Primer locations: Duox1-Universal-a: -263 and +58; Duox1-MSP-a: -96 and +19; Duox1-USP-a: -186 and +21; Duox2-Universal-a: -566 and +65; Duox2-MSP-a: -199 and -18; Duox2-USP-a: -517 and -402.

MSP only allows for the analysis of a few CpG sites, which are determined by the chosen primer sequences. In order to get information about the methylation status of all existent CpG-dinucleotides in a given sequence, the regions 1000bp upstream of the TSS of *DUOX1* and *DUOX2* were sequenced following bisulfite modification. The sequencing of at least eight individual clones disclosed very dense hypermethylation of the 72 CpG dinucleotides within the *DUOX1* promoter in cell lines NCI-H661 and A549 (**FIGURE 32**, left panel). Only 30-35% of the CpG sites were methylated in NCI-H157 cells, correlating very well with the MSP results (**FIGURE 31**). *DUOX1*-expressing primary cells NHBE showed virtually no methylated CpG sites. The bisulfite sequencing of the three investigated cell lines revealed less overall methylation within the 39 CpG sites of the *DUOX2* promoter, especially in NCI-H157 and NCI-H661 (**FIGURE 32**, right panel). Since both cell lines showed an explicit recovery of *DUOX2* upon Aza-treatment, it is possible that not all alleles present in the whole cell population of those cell lines were characterized by the bisulfite sequencing. It is also conceivable that other *cis*- or *trans*-acting stretches of DNA outside the investigated sequence, are methylated in these cells, leading to a signaling-inhibition upstream of *DUOX2* transcription.

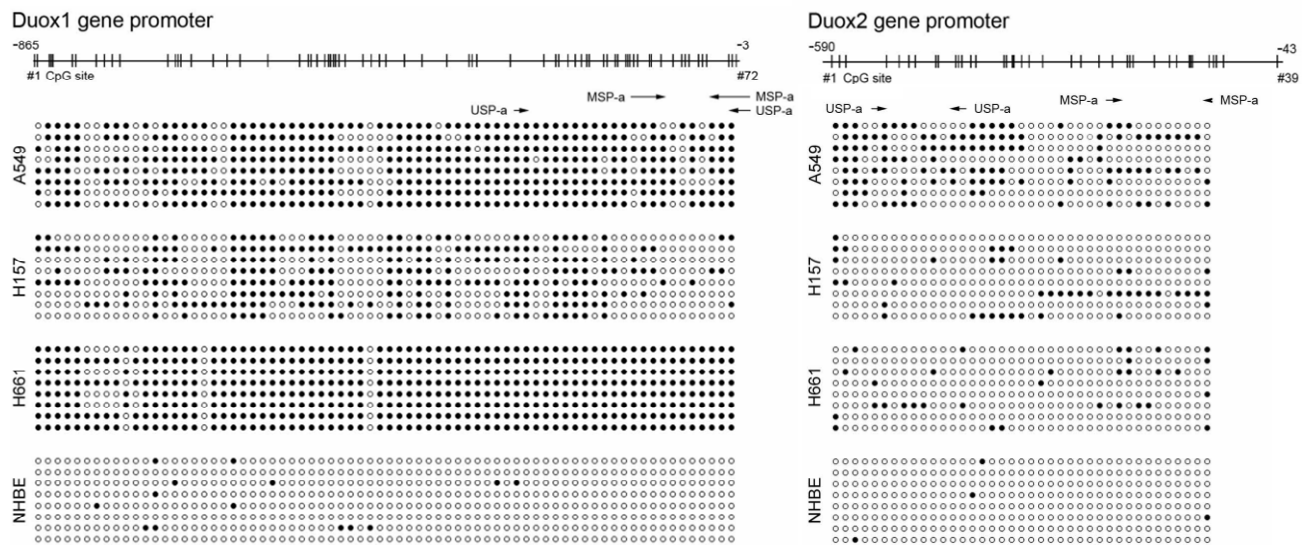


FIGURE 32: Bisulfite sequencing. Genomic DNA of three *DUOX*-deficient lung cancer cell lines and primary lung epithelial cells NHBE were treated with sodium bisulfite. BSP primers located outside the investigated sequences were used to amplify the regions of interest. PCR products containing the 72 and 39 CpG sites of the *DUOX1* and *DUOX2* promoter, respectively, were cloned and eight individual clones per sample were sequenced. Each row represents one sequenced clone and each circle represents one CpG dinucleotide. The promoter regions upstream of *DUOX1* and *DUOX2* are shown at the top, with each vertical bar representing one CpG dinucleotide. ○, unmethylated CpG site; ●, methylated CpG site. Arrows indicate the location of MSP-a and USP-a primers, used in Figure 31.

3.2.4 Expression of *Duox* in lung cancer tissues

Particularly squamous and small cell lung cancer cell lines preserve resemblance with their equivalent tumor (Virtanen et al., 2002). Nevertheless, molecular changes can arise in the establishment and maintenance of cell culture lines. In fact, cell lines developed from adenocarcinomas have been shown to alter their phenotype *in vitro* (Virtanen et al., 2002; Wistuba et al., 1999). Moreover, established cancer cell lines show significantly higher levels of CpG methylation compared to their corresponding tumor tissue (Flatau et al., 1983). Therefore, to rule out artefacts which can only be observed *in vitro*, mRNA levels of *DUOX1*, *DUOX2* and *DUOX1A1* were analyzed in 11 primary non-small cell lung carcinomas and paired adjacent normal tissues. Real-time PCR was performed on three different regions of each specimen to average the results per tissue sample. When probed for *DUOX1* expression, 9 out of 11 patients showed a statistically significant downregulation in tumor tissue compared to the corresponding adjacent tissue (**FIGURE 33A**). One patient showed lower *DUOX1* levels in tumorigenic tissue, but failed to be statistically significant (patient 2), while one patient had elevated *DUOX1* levels in the cancer tissue compared to adjacent tissue (patient 6). Interestingly, the pattern of *DUOX1A1* is highly similar to that of *DUOX1* (**FIGURE 33B**). Analysis of *DUOX2* revealed statistically significant lower transcript levels in 7 out of 11 patients (**FIGURE 33C**). Two patients (patient 5 and 7) retained expression of *DUOX2*, while *DUOX1/DUOX1A1* were reduced in the cancer tissue. Since *DUOX* and *DUOX1A1* genes are arranged head-to-head on chromosome 15q15 (see **FIGURE 5A**), a linked deregulation of these genes is possible.

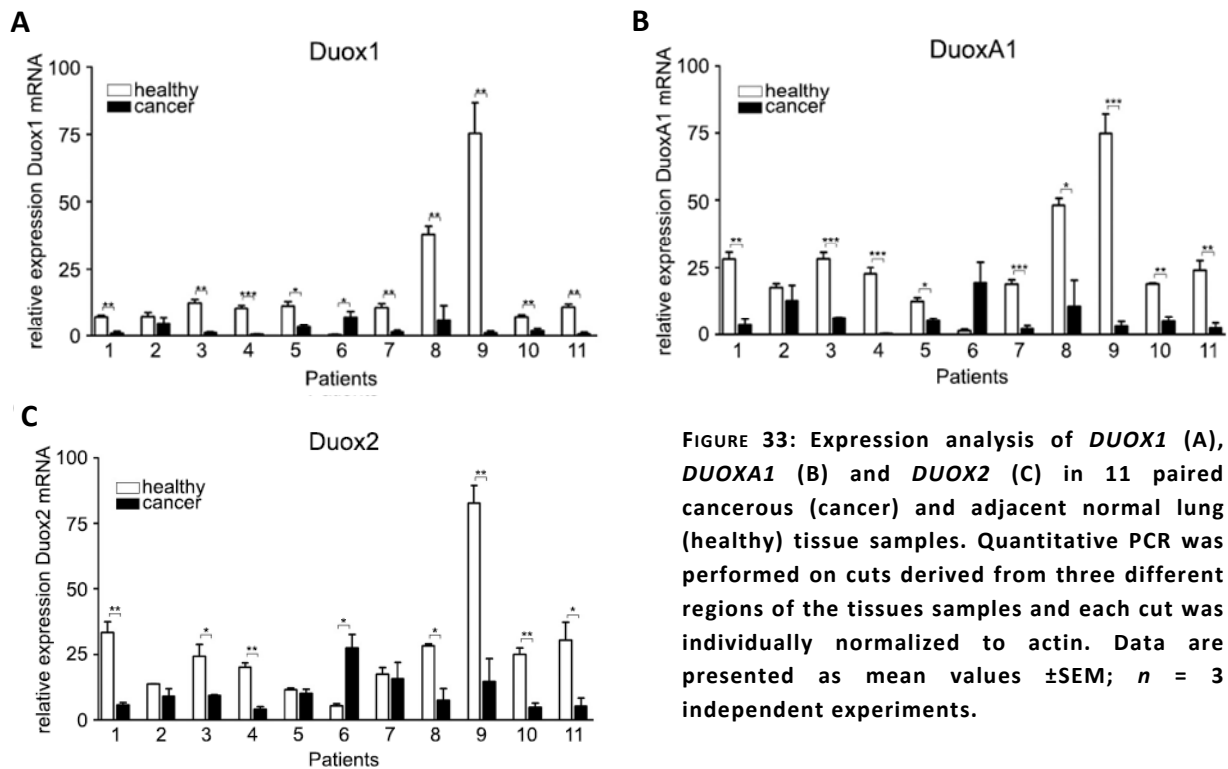


FIGURE 33: Expression analysis of *DUOX1* (A), *DUOX1A1* (B) and *DUOX2* (C) in 11 paired cancerous (cancer) and adjacent normal lung (healthy) tissue samples. Quantitative PCR was performed on cuts derived from three different regions of the tissues samples and each cut was individually normalized to actin. Data are presented as mean values \pm SEM; $n = 3$ independent experiments.

Levels of mRNA do not always directly correlate to total protein, which can arise through differences in mRNA/protein stability or post-transcriptional/-translational modifications (Yoshiko et al., 2002). Therefore, in order to evaluate the relationship between *DUOX* message and protein, total Duox protein was detected via immunohistochemistry in cancerous and adjacent healthy tissues. Duox was detected predominantly in the ciliated airway epithelial cells in the matched normal tissues of patient 11 and 7, where it appears as a red stain (**FIGURE 34A**). A substantially weaker staining was seen in the corresponding tumor-samples of both patients. Limited amounts of tissue samples impeded the analysis of every patient. Moreover, samples without airway crosscuts were removed from further analysis, due to the predominant localization of Duox in airway epithelial cells. No Duox-specific stain was detectable when the sections were stained with Duox preimmune serum, confirming the specificity of the antibody. These results substantiate the real-time data, supporting the hypothesis of Duox being downregulated or even completely absent in lung cancer *in vivo*.

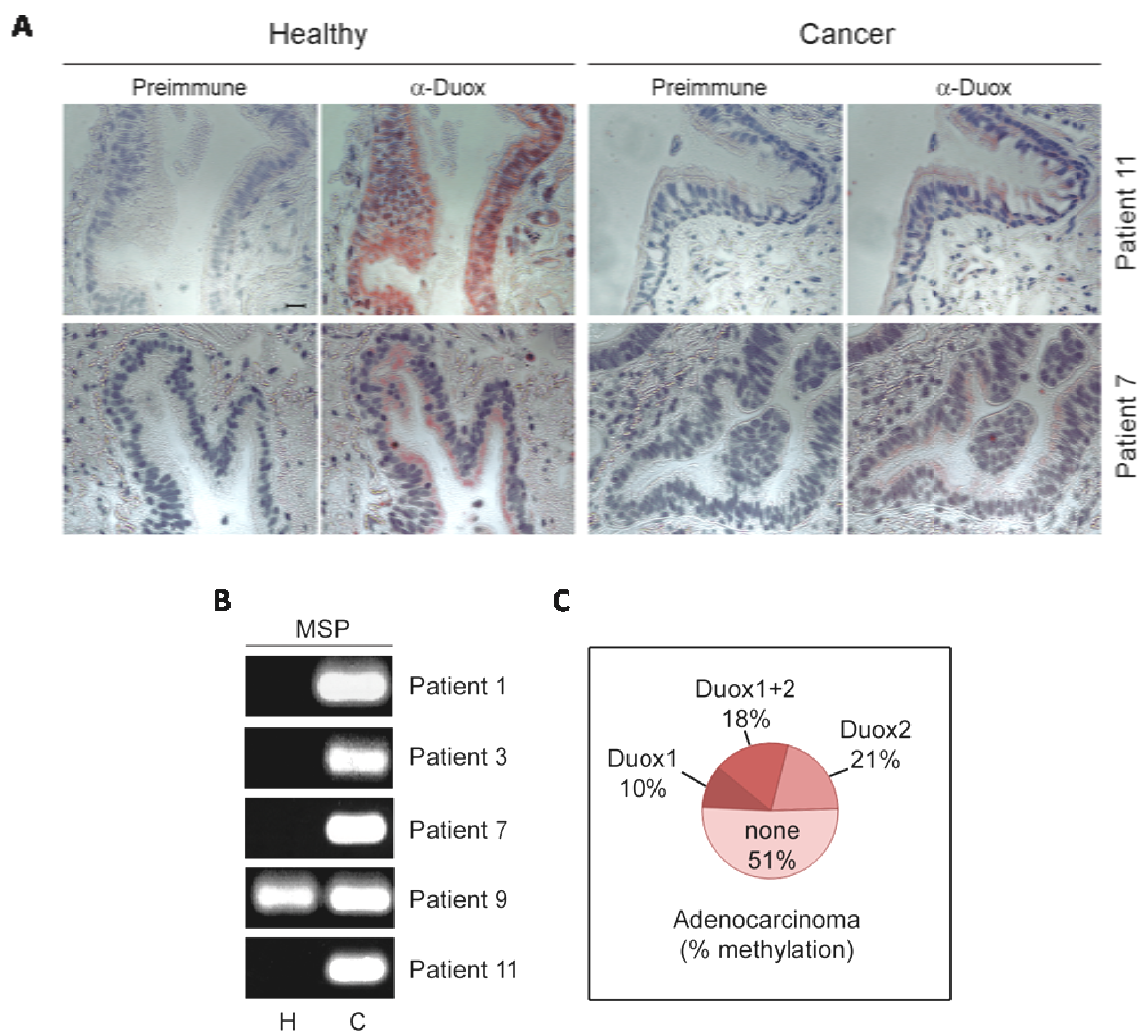


FIGURE 34: Duox expression and promoter analysis in tumor specimen. (A), immunohistochemical detection of Duox protein in matched healthy and cancerous tissue specimen from two NSCLC patients. Duox protein is stained in red and is primarily expressed in the ciliated airway epithelial cells. Bar, 10 μ m. (B), MSP analysis of the *DUOX1* promoter in paired healthy (H) and cancerous (C) tissue samples from 5 patients. Universal and MSP primers were used as described in Figure 31. (C), methylation analysis of the *DUOX1* and *DUOX2* promoters in 39 primary adenocarcinomas. The promoter regions of both genes were amplified with Duox1-Universal-b (-256 and +69) and Duox2-Universal-b (-327 and -76). Methylated sequences were detected with Duox1-MSP-b (-169 and +5) and Duox2-MSP-b (-240 and -108).

Based on the *in vitro* results showing *DUOX1* and *DUOX2* promoter hypermethylation (see **FIGURE 31, 32**), MSP was used to determine if these promoters are also hypermethylated *in vivo*. Five patients, whose tumors displayed significant downregulation of *DUOX1* in real-time PCR, were further analyzed with MSP and USP specific primers (patient 1, 3, 7, 9 and 11). Methylated sequences were detected in all cancer tissues, indicating that these tumors have methylated alleles of the *DUOX1* promoter (**FIGURE 34B**). The absence of a PCR product in the non-cancerous/healthy samples suggests that these tissues have unmethylated alleles only. Only patient 9 was also MSP positive in the healthy tissue, albeit to a much lesser extent than in the matched cancerous tissue. It is possible that the healthy tissue of this patient has been infiltrated with cancerous cells or that the healthy tissue was in close proximity to the tumor and had already undergone some changes towards an abnormal or even pre-cancerous phenotype (Spira and Ettinger, 2004), as evident by the hyperplasia in the healthy tissue of patient 11 (**FIGURE 34A**; compare to histology in **FIGURE 8B**). USP yielded PCR

products in all patient samples, whether of cancerous or healthy origin (data not shown). This most likely arises from contamination of normal cells within the tumor sample (Chang et al., 2007; Krassenstein et al., 2004). Although it is tempting to hypothesize that promoter hypermethylation of *DUOX1* and *DUOX2* is a common event in lung cancer, the sample size of 11 patients is too small for any conclusions. Therefore, this theory was further substantiated through a larger sample size. In collaboration with Steven S. Belinsky at the Lovelace Respiratory Research Institute, the methylation status of the *DUOX1* and *DUOX2* promoter was analyzed via MSP analysis in 39 patients with primary adenocarcinomas (FIGURE 34C). A hypermethylated promoter of *DUOX1* and *DUOX2* was detected in 28% and 39% of the tumors, respectively. And while 50% of the tissues contained at least one methylated gene, 18% displayed promoter hypermethylation for both *DUOX* genes.

In conclusion, these results indicate that downregulation of Duox and DuoxA proteins is a prevalent occurrence in lung cancer cells *in vitro* and *in vivo* and is contingent on non-random aberrant promoter hypermethylation. As the promoter regions of all genes feature CpG islands, it is possible that the whole chromosomal region is prone to this epigenetic event, causing loss or deregulation of these transcriptionally linked enzymes.

3.2.5 Reconstitution of Duox leads to enhanced migration

It has been previously shown that Duox1 is implicated in airway homeostasis and cell migration of lung epithelial cells (Koff et al., 2006; Wesley et al., 2007). As Duox1 is the predominant Duox-isoform in the lung, the impact of Duox1 on lung epithelial cells was investigated. First, two Duox-deficient lung cancer cell lines (A549 and H157) were stably reconstituted with functional Duox1. Control cells were transduced either with empty vector (EV) or DuoxA1-2 alone. As expected, the cells expressing the functional oxidase regained the ability to produce H_2O_2 upon Ca^{2+} mobilization through thapsigargin or ionomycin (FIGURE 35).

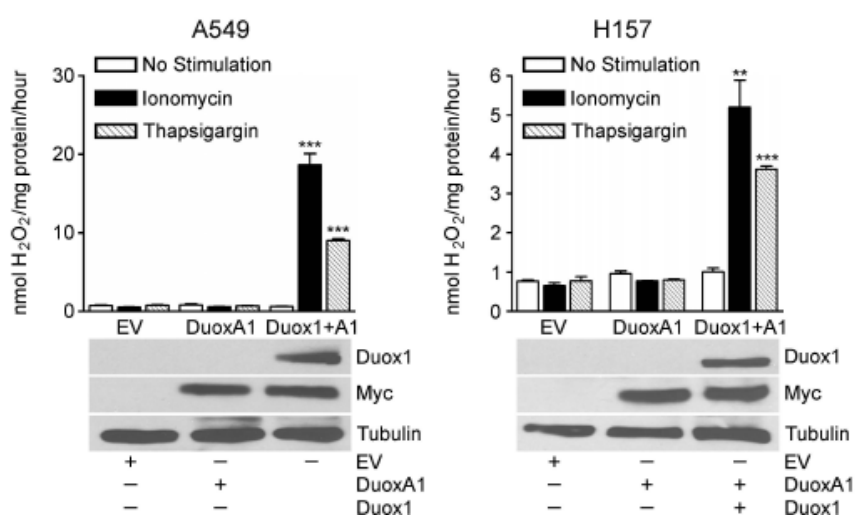


FIGURE 35: Reintroduction of functional Duox into lung cancer cell lines. Duox-deficient lung cancer cells A549 and NCI-H157 were stably transduced with lentivirus encoding for Duox1 and DuoxA1-2 or empty vector (EV) as indicated. Duox1-dependent H_2O_2 production was measured in response to stimulation with ionomycin ($2\mu M$) or thapsigargin ($1\mu M$). TCL were probed for the expression of Duox1, DuoxA1-2 (myc) and tubulin. Data are presented as mean values \pm SEM.

In order to investigate if functional Duox1 influences directional cell migration, cells were seeded in serum-free media into transwell migration chambers and were allowed to migrate to the bottom of the chamber, containing serum-rich medium. In both cell lines, control cells expressing either empty vector (EV) or DuoxA1-2 alone did migrate towards the bottom of the insert, but to a much lesser

extent than cell expressing Duox1/DuoxA1-2 (**FIGURE 36A**). Directional migration was further analyzed under more physiological conditions by wounding a confluent monolayer of transduced A549 and NCI-H157 cells (**FIGURE 36B, top**). This *in vitro* wound closure assay mimics *in vivo* cell migration during wound closure to a certain degree. Upon wounding, cells expressing Duox1/DuoxA1-2 were able to migrate and close the wound faster than Duox1-deficient cells (**FIGURE 36B, bottom**). Wound closure is a process that requires not only cell migration but also cell proliferation, in order to repopulate the injured areas. As cell proliferation has been linked to increased ROS-generation by a variety of sources within the cell, the influence of Duox1 on cellular growth rates was investigated (**FIGURE 33C**). Proliferation was not altered in cells expressing Duox1/DuoxA1-2 compared to control cells, which expressed EV or DuoxA1-2 alone, suggesting that functional Duox1 does not influence proliferation in selected lung cancer cell lines.

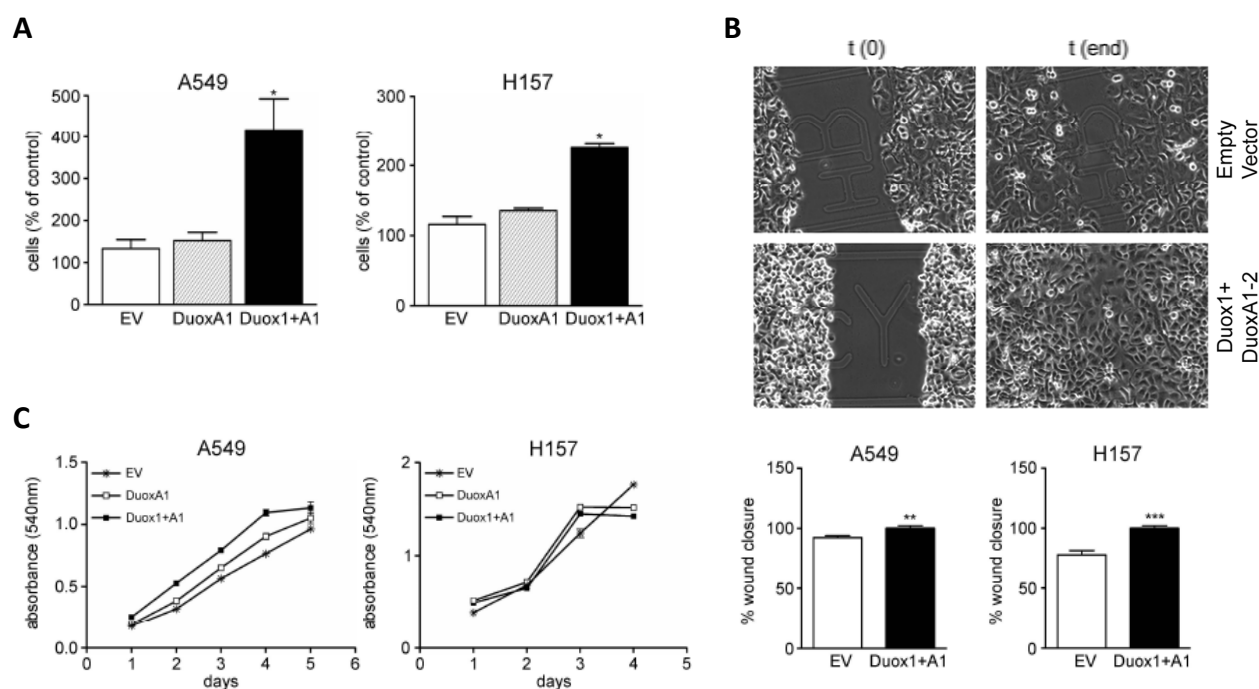


FIGURE 36: Duox1 increases directional migration and wound closure but not proliferation. (A), Cells were seeded in serum-free media on top of the membrane and directional migration was initiated by the addition of FBS to the bottom of the transwell migration chamber. Cells on bottom of the filter were counted after 2 hours and 3.5 hours for A549 and H157 cells, respectively. Values are presented as percent of EV control (\pm SEM) from triplicates of one representative experiment. (B), a confluent monolayer of cells expressing EV or functional Duox1 was injured. *Top*, pictures were taken from the same positions over a time course of several hours. *Bottom*, cell migration into the wound area was analyzed for 9 and 15 h for transduced A549 and NCI-H157 cells. Data were collected from at least 9 random fields and are expressed as percent closed wound of the average wound area of Duox1+A1 (\pm SEM). (C), cells were cultured in low-serum conditions for up to 5 days. Every 24 hours proliferation was spectrophotometrically determined at 540nm based on mitochondria-based reduction of MTT. Shown is a triplicate of one representative experiment.

It has been shown that H_2O_2 production is increased upon wounding of confluent monolayers of aortic endothelial and airway epithelial cells. In addition, the detected ROS was localized to the cells lining the wound edge (Moldovan et al., 1999; Wesley et al., 2007). Treatment with NADPH oxidase inhibitor DPI or siRNA-mediated silencing of Duox1 diminished ROS production in airway epithelial cells (Wesley et al., 2007). Since functional Duox localizes to the plasma membrane of transfected cells (**FIGURE 13**), seems to concentrate on the leading edge of randomly migrating cells (**FIGURE 24 EV/EV**)

and is beneficial for wound closure (**FIGURE 36**), it is conceivable that Duox proteins are targeted to the leading edge during cellular migration. This hypothesis was analyzed in NCI-H661, which stably express both functional oxidases, Duox1/DuoxA1-2 and Duox2/DuoxA2, respectively. Control cells expressed EV, DuoxA1-2 or DuoxA2 alone (see **FIGURE 14A**). In a first step, these cells were analyzed in transwell migration and quantitative wound closure assays to see, if they also feature the same Duox-based migrational advantage as lung cancer cells A549 and NCI-H157. Indeed, cells that expressed functional Duox1 migrated faster towards the bottom of the transwell chamber or into the wound area (**FIGURE 37 A and B**). Surprisingly, Duox2-based transwell migration was greatly increased compared to either control cells as well as Duox1-expressing cells, while wound closure was slightly faster compared to cells expressing functional Duox1. This suggests that the presence of functional Duox1 or Duox2 leads to increased motility of cells and that Duox2 has an even greater impact on cellular movement compared to Duox1. Transwell migration rates in DuoxA2-expressing cells were also improved. This could indicate that the maturation factor alone can already influence migration via yet undefined pathways.

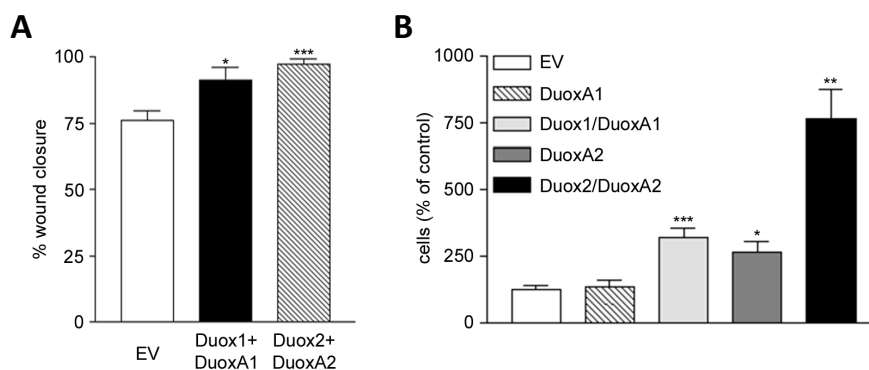


FIGURE 37: Duox1 and Duox2 increase migration in NCI-H661. Cells were stably transduced with either Duox1/DuoxA1-2 or Duox2/DuoxA2. Control cells expressed EV, DuoxA1-2 or DuoxA2. (A), Wounding assay. A confluent monolayer of cells expressing EV, functional Duox1 or functional Duox2 was injured. Cell migration into the wound area was analyzed after 6 h. Data were collected from at least 9 random fields and are expressed as percent closed wound of the average wound area of Duox1+A1 (\pm SEM). (B), Transwell migration assay. Cells were seeded on top of the membrane in serum-free media. Directional migration was initiated by the addition of serum-rich media to the bottom of the chamber. Cells on bottom of the filter were counted after 5.5 hours. Values are presented as percent of EV control (\pm SEM) from triplicates of one representative experiment.

Since both oxidases increased migration rates, their localization was analyzed along wound edges. One hour after generation of a linear injury to a confluent cell layer, both Duox1 and Duox2 localized at the leading edge of cells migrating into the wound, where they co-localized with their respective maturation factor (**FIGURE 38**).

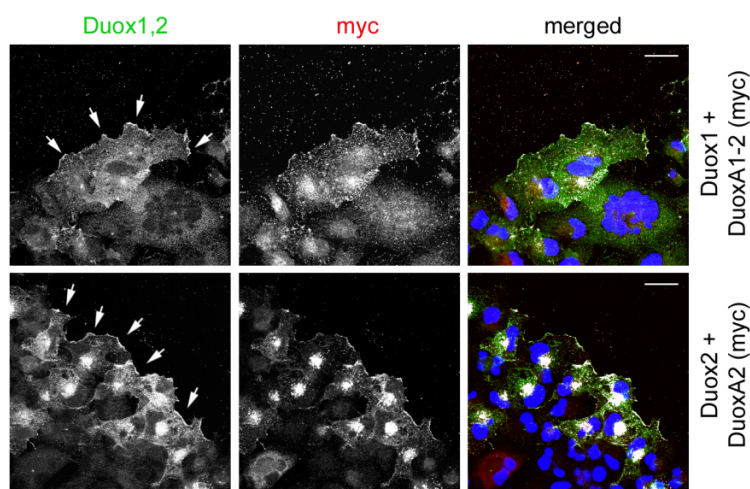


FIGURE 38: Localization of Duox proteins at the leading edge. Confluent mono-layers of lenti-virally-transduced NCI-H661 cells expressing Duox1/DuoxA1-2 or Duox2/DuoxA2 were wounded in a linear fashion. After one hour the localization of Duox and DuoxA was analyzed by immunostaining for Duox (Duox1,2; green) and DuoxA (myc; red). Arrows indicate particular Duox locations. Co-localization is shown in white. Bar, 30 μ m.

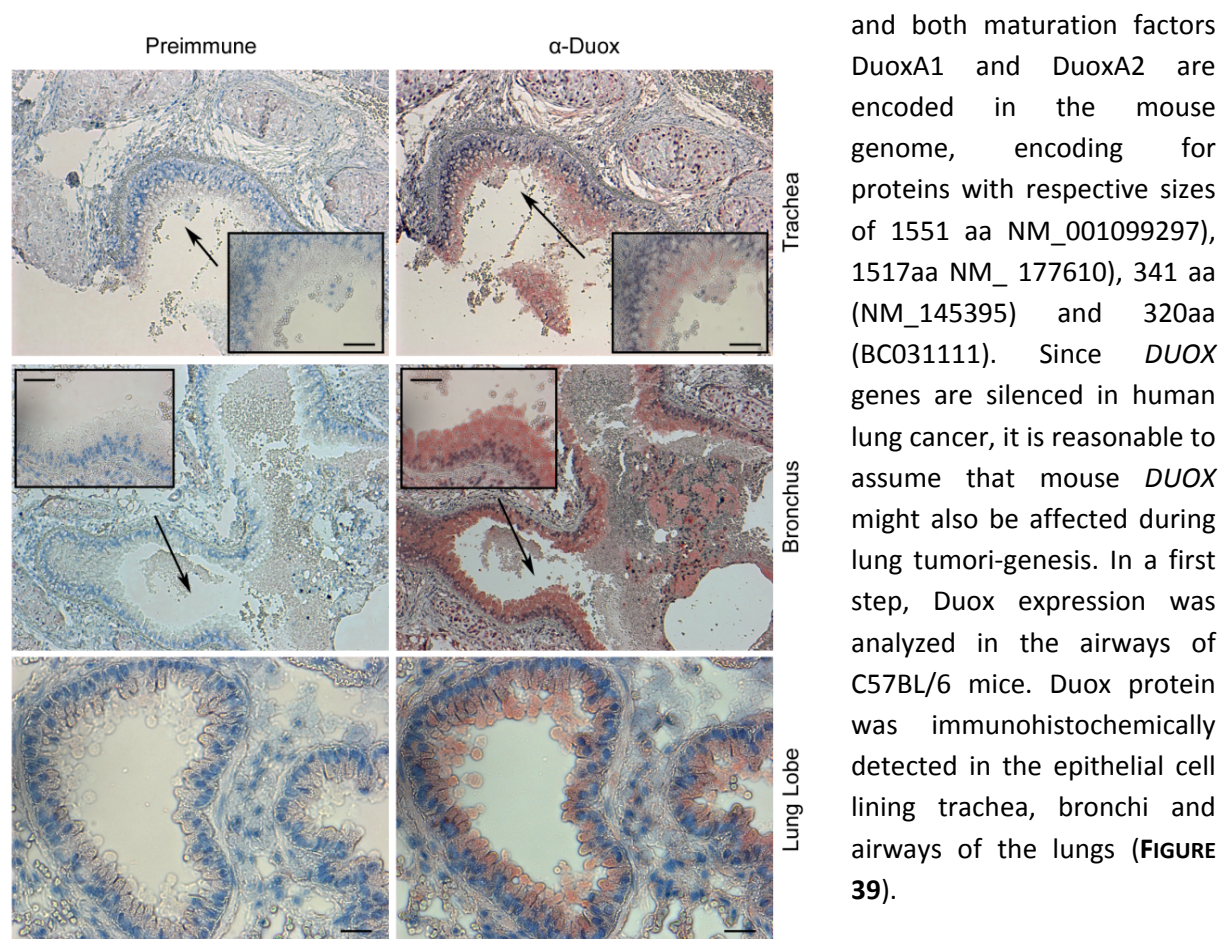
In conclusion, these results suggest an important role for functional Duox enzymes, as they not only increase directional migration but also accelerate wound repair. It is possible that functional Duox allows the airway epithelium to heal faster in response to injury, an ability that is constricted in tissues that have lost Duox as a result of non-random promoter hypermethylation.

3.3 Characterization of Duox expression in Rodents

In human lung cancer, little is known about the cellular origins of the disease or the process of tumor initiation, because early-stage tumors are hardly detectable. Yet, animal models of human lung cancer have helped to improve the understanding of the cellular and molecular changes within lung cells during development and progression of the disease (Kim et al., 2005). Particularly, pulmonary tumor models in rodents are being used, as they are easily inducible and resemble lung carcinomas found in humans.

3.3.1 Duox expression in murine airways

Several models for induction of murine lung carcinomas have been described, which are mostly derived through carcinogen exposure, conditional deletion of tumor suppressors and/or Cre-recombinase-induced activation of proto-oncogenes (Jackson et al., 2001; Meuwissen et al., 2003; Meuwissen et al., 2001; Wang et al., 2006). The selective activation of oncogenic mutations in a subset of cells permits the study of tumor initiation and progression. Moreover, this model allows for the investigation of the cell of origin and the role of cancer stem cells in the preservation of those tumors. An Entrez Protein Database search for murine *DUOX* isoforms confirmed that Duox1, Duox2



and both maturation factors DuoxA1 and DuoxA2 are encoded in the mouse genome, encoding for proteins with respective sizes of 1551 aa (NM_001099297), 1517aa (NM_177610), 341 aa (NM_145395) and 320aa (BC031111). Since *DUOX* genes are silenced in human lung cancer, it is reasonable to assume that mouse *DUOX* might also be affected during lung tumorigenesis. In a first step, Duox expression was analyzed in the airways of C57BL/6 mice. Duox protein was immunohistochemically detected in the epithelial cell lining trachea, bronchi and airways of the lungs (FIGURE 39).

FIGURE 39: Immunohistochemical detection of mouse Duox in C57BL/6 mice. Sections from mouse trachea, bronchus and lung lobe were stained with anti-human Duox1,2 antibody. Duox protein was stained in red and was primarily expressed in the epithelial cells lining the airways. The inserts depict enlarged areas with specific Duox staining. Adjacent sections served as negative controls and were treated with preimmune serum in order to ensure the specificity of the antibody. Bar, 10 μ m.

Since the antibody used for the immunohistochemical detection of endogenous mouse Duox was directed against human Duox1, but also recognizes Duox2, the identity of the Duox isoform in mouse tissues was still unknown. Therefore, specific primers for mouse *DUOX1*, *DUOX2*, *DUOXA1* and *DUOXA2* were designed and expression of these genes was probed in whole tissue lysates from trachea, upper lung and lower lung. The tissues were derived from two different mouse strains, namely C57BL/6 and BALB/c. Both strains are inbred and are commonly used for lung cancer studies; however they are unequally susceptible for lung tumor development. While BALB/c mice are considered to be intermediate sensitive to spontaneous lung tumor incidence and chemically induced lung tumors (through exposure to cigarette smoke, tar or chemical carcinogens), C57BL/6 are almost completely resistant (Meuwissen and Berns, 2005). Surprisingly, *DUOX1* was only expressed in the trachea but not in the lungs of C57BL/6 mice (**FIGURE 40**). In BALB/c mice *DUOX1* was also greatly expressed in the trachea, while some *DUOX1* was also detectable in the lung. In both strains the expression of *DUOXA1* was reduced or completely absent, except for high levels in the trachea of BALB/c mice, suggesting that Duox1 can only be functional in the trachea of those animals, while C57BL/6 mice do not possess a functional Duox1 in their airways per se. *DUOX2* and *DUOXA2* were detectable in all tissues of both mice strains, indicating that Duox2 could be the main oxidase in murine airways.

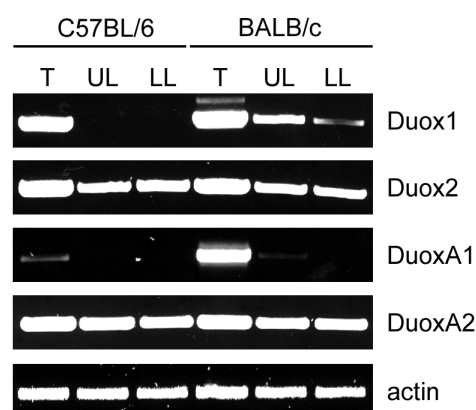


FIGURE 40: Endogenous expression of mouse *DUOX1*, *DUOX2*, *DUOXA1* and *DUOXA2*. RT-PCR with mouse-specific primers was performed in C57BL/6 and BALB/c mice. Whole tissue lysates were obtained from trachea (T), upper lung (UL) and lower lung (LL). Actin was used as internal control.

3.3.2 Duox expression in rat airways

As Duox1 might not to be functional in the murine lung, a mouse model of human lung cancer with regard to *DUOX1* expression is not useful. Fortunately, lung cancer in rats features many cytogenetic and molecular mechanisms involved in tumor evolution, which are similar to the human disease (Dano et al., 2000). As rat lung cancer can easily be induced by exposure to X rays, cigarette smoke, beryllium metal, plutonium-239 oxide, radon or tumor xenografts, it appears to be an excellent model for de novo gene methylation analysis (Dano et al., 2000; March et al., 2001; Swafford et al., 1997). A database search in the rat genome revealed the existence of genes encoding for *DUOX1*, *DUOX2*, *DUOXA1* and *DUOXA2*, translating to proteins with respective sizes of 1551aa (NM_153739.1), 1517aa (NM_024141.1), 340aa (NM_001107767.1) and 320aa (XM_575222.1). Expression of both *DUOX* and *DUOXA* isoforms was analyzed in whole tissue lysates from trachea, upper lung and lower lung of Sprague Dawley rats, a strain commonly used in lung cancer studies (**FIGURE 41A**).

In contrast to the results obtained in murine tissues, both *DUOX1* and *DUOX1A1* were expressed in all analyzed tissues, while *DUOX2* and *DUOX2A2* were only detectable in the trachea.

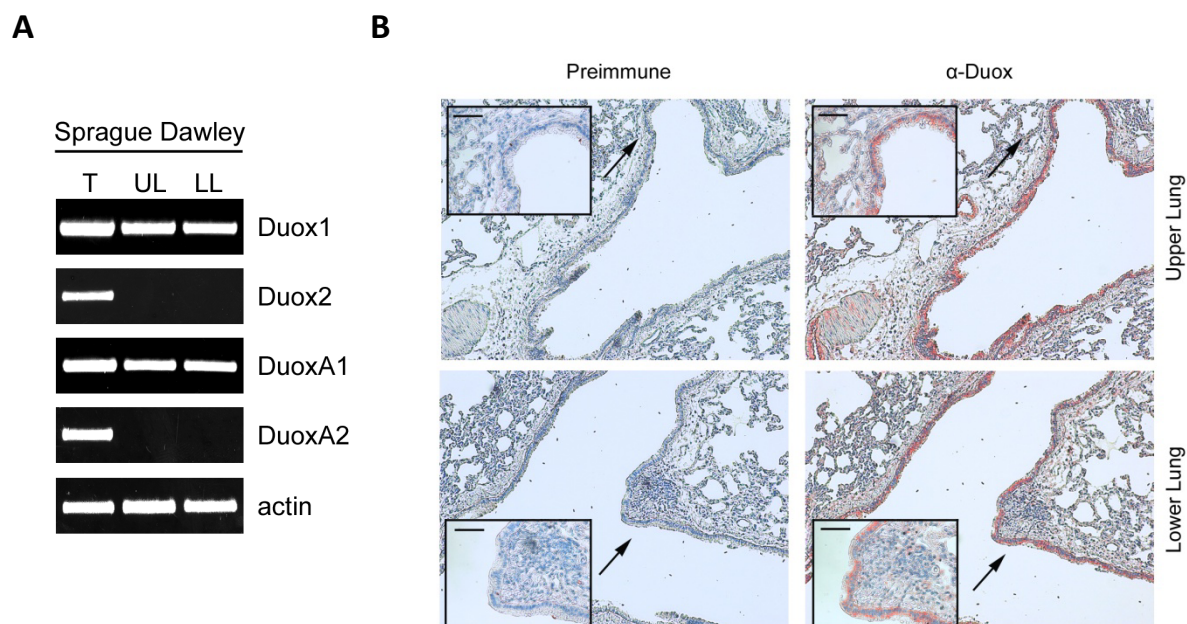


FIGURE 41: Endogenous expression of Duox in rat airways. **(A)** Whole tissue lysates from trachea (T), upper lung (UL) and lower lung (LL) of Sprague Dawley rats were analyzed for expression of *DUOX1*, *DUOX2*, *DUOX1A1* and *DUOX2A2* via RT-PCR. Actin served as internal control. **(B)** Sections of upper lung and lower lung from Sprague Dawley rats were stained anti-human Duox1,2 antibody. Duox protein was stained in red and was primarily expressed in the epithelial cells lining the airways. The inserts depict enlarged areas with specific Duox staining. Adjacent sections served as negative controls and were treated with preimmune serum in order to ensure the specificity of the antibody. Bar, 10µm.

Staining with Duox-specific antibody demonstrated a distinct red stain in the epithelial cells of the airways of upper and lower lung (**FIGURE 41B**). As no *DUOX2* transcript was detected in the lungs of Sprague Dawley rats, the immunohistochemical staining indicates that Duox1 is the main oxidase of the lung.

In conclusion, these results show that *DUOX1* is not expressed in the murine lung, and therefore this species cannot be used for studies of *DUOX1* silencing in the context of lung cancer onset and progression. As rat lungs express *DUOX1*, this species might make a candidate model for the investigation of *DUOX1*-silencing in lung cancer.

4 Discussion

The family of NADPH oxidases (Nox) has been linked to host defense, cell differentiation, transformation and inflammation. Two particular members, termed Duox1 and Duox2, are abundantly expressed in the epithelial cells lining the airways of the lung. To date, their functions are still largely unknown, but involvement in innate immunity and airway homeostasis has been suggested. Duox enzymes were also linked to oxidant-mediated signaling and chronic airway pathologies, based on their ability to produce reactive oxygen species (ROS).

The key findings of my work can be grouped in two categories. With respect to the regulation of the enzymes I discovered that Duox1 and Duox2 are differentially localized and expressed in lung epithelial cells, that they form paired functional heterodimers with their respective maturation factors DuoxA1 and DuoxA2, and that Duox2 functionally interacts with the paralog DuoxA1. In the context of lung cancer, my studies demonstrated that expression of both Duox enzymes as well as their maturation factors is markedly decreased in lung cancer and that their silencing is based on aberrant promoter hypermethylation.

4.1 Regulation of Duox1 and Duox2

The regulation as well as the specific functions of Duox enzymes are largely unknown. Harper and coworkers demonstrated that expression of both Duox enzymes was regulated differently in lung epithelial cells (Harper et al., 2005). While Duox1 mRNA was modestly upregulated through the Th2 cytokines interleukin (IL)-4 and IL-13, the Th1 cytokine interferon (IFN)- γ greatly enhanced expression of Duox2 mRNA. This suggests that Duox enzymes might have different functions in the airways in response to diverse stimuli or insults. It was not determined how much Duox1 or Duox2 protein was expressed or where the proteins were localized in primary or air-liquid differentiated epithelial cells.

Confocal analysis of lung epithelial cells demonstrated different cellular localizations for Duox1 and Duox2, which may indicate distinct cellular function. Duox1 has been linked to increased cellular migration rates in earlier studies (Koff et al., 2006; Wesley et al., 2007). As Duox1 is localized along the plasma membrane, and may generate H_2O_2 on-site, thus facilitating cellular migration via an ERK-activation pathway. For the most part Duox2 remained in the ER; yet, some Duox2 was also localized to the plasma membrane and to intracellular vesicles. The nature of these vesicles is still unresolved. However, they are reminiscent of trafficking vesicles, which can be latent and remain in the cytosol until an activating signal induces their transport to the membrane. These intracellular membrane reservoirs fuse with the plasma membrane and the contents of the vesicle will be released into the extracellular space, while enclosed integral membrane proteins will be exposed on the cell surface. H_2O_2 can actively control exocytosis through inhibition of a protein that regulates membrane fusion events necessary for exocytosis, termed *N*-ethylmaleimide sensitive factor (NSF) (Matsushita et al., 2005). Thus, Duox2-derived H_2O_2 could actively control the release of proteins and compounds stored in transport vesicles, including Duox2 itself.

Peroxisomes are small cellular respiratory organelles located in the cytoplasm that participate in the metabolism of fatty acid and amino acid degradation. They contain a wide variety of enzymes, including catalase, an enzyme that facilitates the decomposition of hydrogen peroxide to water and oxygen (del Rio et al., 1992). It is not surprising that peroxisomes are also a source of reactive oxygen species (Singh, 1997). H_2O_2 is generated in the peroxisomal respiratory pathway by different flavin oxidases, such as D-amino acid oxidase or uric acid oxidase (Corpas et al., 2001; del

Rio et al., 1992; Gootjes et al., 2004). Interestingly, the intracellular staining pattern of catalase and consequently of peroxisomes (Gootjes et al., 2004) is highly similar to the one observed for Duox2. It seems possible that Duox2 is one of the several flavin enzymes enclosed in lung epithelial peroxisomes and that Duox2-mediated H_2O_2 could participate in beta-oxidation, a process that breaks down fatty acids.

The expression of Duox2 was greatly induced upon differentiation in 3D culture, which could indicate that the enzyme is involved in polarization and maturation of airway epithelial cells, or that it performs a function characteristic of differentiated cells. In fact, it has been demonstrated for several other genes (such as mucin MUC3, MUC5AC, MUC5B, and MUC6) that their expression is upregulated through differentiation (Bernacki et al., 1999; Yoshisue et al., 2004). Duox1 has been linked to MUC5AC expression in cultured human airway epithelial cells via a Duox1-ROS-TACE-proligand-EGF receptor cascade (Shao and Nadel, 2005), and it is conceivable that Duox2 could have a similar function in inducing epithelial mucin production.

The development of isoform-specific Duox and DuoxA antibodies allowed localization analysis of Duox1 and Duox2. Interestingly, although both isoforms were localized apically in the *in vitro* polarized airway system, Duox2 was selectively enriched in ciliated cells, where it mainly localized to the cilia. A recent report demonstrated that hyaluronan (HA), a high molecular weight polymer, is synthesized at the apical pole of airway epithelial cell. HA is broken down by ROS, resulting in several low molecular weight fragments that stimulate the ciliary beat frequency (Manzanares et al., 2007). As Duox2 is localized in the cilia of differentiated cells and is also expressed in vesicular structures, it is tempting to speculate that Duox2 will be transported via an intraflagellar mechanism along the microtubules into the cilia (Ainsworth, 2007). Duox2-mediated ROS could induce HA de-polymerization, thus contributing to the beating of cilia during mucociliary clearance. This hypothesis could be tested, for instance, by selectively knocking down either Duox or DuoxA isoforms utilizing lentivirus-mediated shRNA and studying the effect on cilia motility.

The diverse expression and localization patterns suggest different functions for Duox1 and Duox2. As directional migration was strikingly enhanced in cells expressing functional Duox2 compared to functional Duox1, it seems possible that upon insult or injury of the epithelium Duox2 enhances migration and/or wound closure to a larger extent than Duox1. Duox1 may perform a homeostatic function, whereas Duox2 is only expressed and transported to the plasma membrane when its function is needed by the cell. In fact, the promoter of Duox2 contains a putative ATF/CRE-binding site, a stress-responsive element. ROS have also been shown to mediate phosphorylation of cAMP-responsive element-binding protein (CREB) (Bedogni et al., 2003). Expression of Duox2 could be upregulated through activation of stress-pathways and its expression might be sustained via a positive feedback loop.

It has become evident that Duox function is not solely dependent on transcriptional regulation. In fact, Duox function is critically dependent on the presence of the maturation factors DuoxA1 and DuoxA2, allowing the oxidase to exit the ER and translocate to the plasma membrane (Grasberger and Refetoff, 2006). Surprisingly, contrary to the hypothesis that DuoxA1 and DuoxA2 are ER-resident proteins, DuoxA1 and DuoxA2 form heterodimeric complexes with their respective Duox partner. This phenomenon of complex formation had already been described for other members of the Nox family. In particular, the phagocytic oxidase Nox2 forms a heterodimer with p22^{phox} (DeLeo et al., 2000; Yu et al., 1997). Consistent with the concept of the Nox2/p22^{phox}

heterodimer system, my studies unraveled that incorporation of heme into Duox was required for the assembly of the complex with DuoxA. These results suggest that Duox1 as well as Duox2 follow the paradigm of heterodimer formation with an associated subunit in a heme incorporation-dependent manner.

Based on the fact that several DuoxA isoforms exist, one might be tempted to speculate, how this could impact the function of Duox1. Unexpectedly, although Duox1 could form a heterodimeric complex with DuoxA1-3, this DuoxA1 isoform was not expressed in undifferentiated or differentiated airway epithelial cells. DuoxA1-3 expression might be age-dependent and is only expressed in embryonic tissues, as known e.g. for splice variants of G-protein coupled receptors (Pilzer and Gozes, 2006). Alternatively, it is possible that this isoform is not expressed in the lung per se, as it was originally identified from pooled libraries of brain, lung and testis. In addition, the polarized 3D system lacks alveolar type II cells, which could be the source for DuoxA1-3. Those cells are only expressed in the terminal alveoli, where they secrete lung surfactant and serve as progenitor cells for the terminally differentiated alveolar type I cells (Bhaskaran et al., 2005). The primary lung epithelial cells used for 3D differentiation were isolated from the bronchi (NHBE) or the smaller airways (SAEC), which are both localized afar from the terminal bronchioles (Fischer and Widdicombe, 2006). Therefore, these cells can differentiate into goblet, basal or ciliated cells, but not into alveolar type II cells. The identification of two simultaneously expressed splice variants, DuoxA1-1 and DuoxA1-2, could indicate that Duox1 is regulated by both isoforms in a competitive manner. The differential expression of DuoxA1-1 and DuoxA1-2 may modulate Duox1 activity by competing and therefore affecting functional Duox1/DuoxA1-2 heterodimer formation, a scenario identified for p73, a homolog of tumor suppressor p53 (De Laurenzi et al, 1998). In addition, as alternative splicing of mRNA transcripts generates additional genomic complexity from the low number of genes present in the human genome, the different DuoxA1-isoforms may have different roles in various Duox-expressing tissues (such as testis, thyroid, tongue and cerebellum).

The finding that Duox2 is localized differentially depending on its associated subunit (DuoxA2 or DuoxA1-2) might be indicative of a dual assignment for Duox2. It is plausible that by heterodimerization with DuoxA1-2, Duox2 could compensate for Duox1 in case of genetic or mutational inactivation. Based on their high degree of sequence homology, it might also be possible that DuoxA1-2 could substitute for DuoxA2, thus providing another fallback mechanism to maintain Duox2 function when mutational inactivation of DuoxA2 occurs. However, a recent report demonstrated that mutations in DuoxA2 resulted in hypothyroidism (Zamproni et al., 2008), a condition generally attributed to genetic abnormalities in the sodium-iodide symporter (NIS), thyroperoxidase (TPO) or Duox2 (Ris-Stalpers, 2006). This finding contradicts the theory that DuoxA1-2 can generally substitute DuoxA2. Nevertheless, since the study demonstrated that DuoxA2 was still expressed as a truncated version, it is conceivable that the mutant DuoxA2 may not be able to support function anymore, but could still bind to Duox2. It would act as a dominant-negative suppressor of Duox2 function by binding to Duox2 and preventing the formation of a functional mismatch heterodimer with DuoxA1-2. However, the inability to form a mismatch might be confined to the thyroid, while still being applicable to the lung. Functional analysis in thyroid cells transiently reconstituted with the Duox2/DuoxA1-2 heterodimer would shed some light on such mechanism.

Nox5 function is tightly regulated based on its localization within the cell (Kawahara and Lambeth, 2008). This spatial regulation is achieved by phosphorylated phosphatidylinositol (PI) lipids (PI(4,5)P₂ and PI(3,4,5)P₃), which target proteins with polybasic clusters, such as Nox5, to the plasma

membrane (Heo et al., 2006; McLaughlin et al., 2002). In analogy to this observation, Duox enzymes could be regulated in a similar manner. Since all DuoxA-isoforms contain polybasic motifs, it is possible that directed association with a given maturation factor could determine the subcellular location of the oxidase, constituting another form of spatial targeting and therefore regulation. In conclusion, the presence of distinct Duox and DuoxA genes might result in a larger variety of function and in addition, might also secure preservation of Duox function in case of genetic alteration/mutation.

4.2 Duox in lung cancer

A deregulation of Duox enzymes has already been indirectly linked to several lung pathologies, including cystic fibrosis (Wright et al., 2006), chronic obstructive pulmonary disease (COPD) (Nagai et al., 2008) and asthma (van der Vliet, 2008). ROS had been connected to carcinogenesis, as they are important for the initiation and promotion of cells to neoplastic growth (Chung-man Ho et al., 2001). Because Duox enzymes have the ability to produce potentially harmful ROS, which may induce recurring DNA damage, inhibition of apoptosis and activation of proto-oncogenes (Azad et al., 2008), increased Duox expression or function could contribute to the pathogenesis of lung malignancy. However, in contrast to our expectations, this study showed that the expression of both Duox enzymes as well as their DuoxA maturation factors was clearly reduced in lung cancer cell lines as well as non-small cell lung cancer, thus ruling out the hypothesis of Duox being overexpressed or constitutively active.

The functions of many critical genes are lost in lung cancer, which can result from genomic amplification, homozygous deletion, frame shift or other coding-region mutations (Belinsky, 2004; Motiwala et al., 2004). The most common mechanism of gene silencing in lung cancer constitutes aberrant methylation of the 5' promoter region (Zochbauer-Muller et al., 2002). Genomic analysis of the promoters of both *DUOX* as well as *DUOXA* genes disclosed high density of CpG dinucleotides. Aberrant hypermethylation was confirmed for *DUOX1* and *DUOX2* and suggested for *DUOXA1* and *DUOXA2*.

Promoter hypermethylation is frequent in both early-stage and late-stage lung tumor pathogenesis (Bowman et al., 2006; Machida et al., 2006; Palmisano et al., 2000; Tsou et al., 2002; Widschwendter et al., 2004). So far, more than 40 genes have been identified as being inactivated by promoter hypermethylation, many of which are involved in cell cycle regulation (*CDKN2A*, *RAR β* , *PAX5 α,β*), DNA repair (*MGMT*), apoptosis (*Caspase-8*, *Fas*, *DAPK*, *TRAILR1*), Ras signalling (*RASSF1A*, *NORE1A*), and invasion (*H-cadherin*, *E-cadherin*, *TIMP3*, laminin family) (Belinsky, 2004; Bowman et al., 2006; Krunkosky et al., 2003; Tang et al., 2004; Zhou et al., 2005). In fact, it has been shown that aberrant CpG island methylation is not random (Costello et al., 2000). Brena et al. reported that loci at 15q15.1 and 15q22.2, which are located close to the Duox gene cluster at 15q15-21, are aberrantly methylated in lung cancer (Brena et al., 2007). In this regard, it is likely that methylation-based silencing of *DUOX/DUOXA* is not accidental, but rather a lung cancer-associated incident.

In general, promoters of tumor suppressor genes, such as *RB1*, *p53*, *CDKN2A*, *BRCA1*, *BRCA2* and *APC*, are affected by this epigenetic event. Their gene products have pivotal roles in normal cells, as they control cell cycle repression, DNA repair, apoptosis or suppress metastasis (Baylin and Herman, 2000; Belinsky, 2004; Jones and Laird, 1999). Overall, their essential function is to inhibit the process of tumorigenesis. For instance, the gene *CDKN2A*, which encodes for *INK4A* (also known as

p16), is frequently silenced by aberrant methylation in many cancers. As INK4A inhibits cell-cycle progression, the inactivation of *CDKN2A* was proposed to be a first step towards immortalization by allowing cells to escape the immortality checkpoint M0 (Belinsky, 2004). Given that the promoters of both *DUOX* genes are frequently hypermethylated *in vitro* as well as *in vivo*, we hypothesized that Duox enzymes may be involved in a tumor suppressing network. They might transduce growth-inhibiting signals through regulated ROS production, which in turn act as secondary messengers. In fact, accumulation of high levels of intracellular ROS have recently been linked to senescence (Ramsey and Sharpless, 2006). In addition, the peroxidase-homology domain of Duox could be utilized to selectively oxidize target proteins of the tumor suppressing network, resulting in their inhibition or activation.

Reconstitution of functional Duox1 however resulted in improved migration rates. This phenotype is generally attributed to increased malignancy, as cell migration is the first step in metastasis, allowing a cell to spread from the initial site of tumor growth and invade the surrounding tissue. Another hallmark of malignant cells is uncontrolled proliferation (Tfelt-Hansen et al., 2004), which correlates with tumorigenesis and metastasis (Tagliaferri et al., 2000). Other studies have shown that reconstitution of tumor suppressors, such as PTEN (Zhao et al., 2004) or p53 (Marchetti et al., 2004) resulted in decreased cell growth. However, functional Duox1 did not influence cellular growth rates. Furthermore, anchorage-independent growth in soft agar or on poly-HEMA was not altered by reintroduction of Duox1 (data not shown), a function generally attributed to tumor suppressing proteins (Georgescu et al., 1999; Ha et al., 2007). In conclusion, as functional Duox1 did not have any repressive effects on cell migration or cell cycle control, a role for Duox1 as tumor suppressor is not likely.

The fact that functional Duox1 as well as Duox2 lead to increased wound healing, might suggest that these enzymes have a crucial role in facilitating fast and efficient closure of a wounded epithelium. Interestingly, clinical studies and experimental data demonstrated that smokers heal poorly and are more susceptible to incisional wound infection than non-smokers (Wong and Martins-Green, 2004; Yang and Longaker, 2003). Additionally, cigarette smoke has been shown to inhibit repair processes of airway epithelial cells (Kode et al., 2006; Luppi et al., 2005; Wang et al., 2001). It thus seems likely that smoking inhibits Duox function, resulting in sustained tissue injury and inflammation.

In fact, Nagai and coworkers have shown that chronic exposure to cigarette smoke was connected to down-regulation of *DUOX1* (Nagai et al., 2008). Moreover, cigarette smoke has already been associated with promoter hypermethylation in various organs (Enokida et al., 2006; Marsit et al., 2007), especially in the lung (Belinsky et al., 1998; Belinsky et al., 2002; Eguchi et al., 1997; Kim et al., 2003; Kim et al., 2001). Therefore, cigarette smoking might be responsible for hypermethylation of the *DUOX* promoter, potentially leading to silencing of the whole locus harboring the *DUOX/DUOXA* genes. My *in vivo* expression analysis showed a concerted down-regulation of *DUOX1/DUOXA1* in 82% of the patients, while only 64% demonstrated diminished *DUOX2* levels. This could be due to the fact that the *DUOX2* promoter contains less CpG dinucleotides than the *DUOX1* promoter. This increases the probability of aberrant methylation, resulting in more efficient silencing of *DUOX1* than *DUOX2*. Therefore, my findings might provide a first link between smoking-induced promoter hypermethylation and smoking-induced silencing of *DUOX1*.

In summary, Duox enzymes might contribute to tissue repair and thus constitute a prerequisite of the healthy lung epithelium. Upon such injury, a repair process is initiated that includes cell migration, proliferation, and differentiation (Aarbiou et al., 2004). Duox enzymes have already been linked to mucociliary cell differentiation through induction of mucin expression (Shao and Nadel, 2005) as well as to acidification of the airway surface liquid ASL (Schwarzer et al., 2004). My results further substantiate a homeostatic role of Duox enzymes as they enhance cell migration, thereby ensuring epithelial integrity and consequently maintenance of lung tissue functions such as ion transport and ciliary beating. Based on the prevalence of CpG islands within the promoter region of the *DUOX/DUOXA* genes, their genomic location might constitute a hot spot for methylation events that occur in the earliest stages of premalignancy.

As Duox enzymes seem to orchestrate several homeostatic functions, their silencing may lead to an altered lung epithelium without enough mucus, a basic pH change of the ASL and a reduced ability to regenerate from damage.

4.3 Outlook

Future studies should further elucidate the role of epigenetic *Duox* silencing in the development and progression of lung cancer. As the *in vitro* as well as *in vivo* studies demonstrated an overall high occurrence of aberrant *DUOX* promoter hypermethylation – despite a relatively small sample size – we propose that this mechanism is an early event in the development of lung cancer. Therefore, *DUOX* methylation could serve as a biomarker for individual risk assessment of genetic predisposition to lung cancer.

Epigenetically-mediated gene silencing by promoter hypermethylation has been shown to be the most common mechanism for gene silencing in lung cancer and these abnormalities arise in the early stages of lung pathogenesis, even before any pathological changes become apparent (Belinsky, 2004). For instance, research identified the genes for *INK4A* (p16) and *MGMT* as being 100% hypermethylated in patients with squamous cell lung carcinoma three years prior to clinical diagnosis. Several studies have shown that during the gradual change of the normal tissue to hyper-, meta-, dysplasia, and finally to carcinoma, the prevalence for promoter hypermethylation increases as time to lung cancer diagnosis decreases (Belinsky, 2004; Belinsky et al., 2006; Zochbauer-Muller et al., 2002).

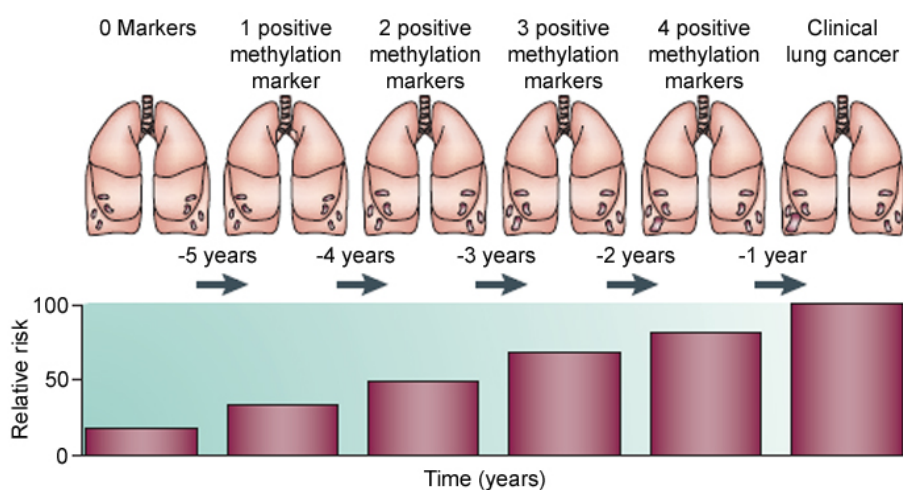


FIGURE 42: Aberrant promoter hypermethylation as biomarker for lung cancer prediction. Accumulation of promoter hypermethylation of several genes could increase the relative risk for clinical lung cancer development. While one positive methylation marker correlates with a lower risk, the occurrence of numerous positive methylation markers amplifies the relative risk for developing lung cancer. Adapted from (Belinsky, 2004).

If our theory is correct, case-control studies should demonstrate that *Duox* hypermethylation is indeed an early event, possibly present in preneoplastic lesions. Therefore, *Duox* would be a biomarker of genetic predisposition to cancer rather than an indicator of current malignancy. As such, *Duox* could be utilized for a highly sensitive, PCR-based sputum screening analysis for examination of high risk individuals, for example heavy smokers or workers exposed to airborne carcinogens (e.g. miners, textile or railroad workers). The probing of exfoliate material constitutes a non-invasive and side effect-free alternative to other more conservative examination methods, such as spiral CT or bronchoscopy.

However, if *DUOX* silencing does not occur during premalignancy, further studies might be able to link *DUOX* silencing directly to a certain tumor stage. *Duox* expression analysis of extensive tissue panels, which include detailed information regarding pathology and disease history, might reveal a connection between *DUOX* methylation and a certain lung cancer subtype and/or stage, thus

allowing the use of Duox as a tumor stage marker for clinical lung cancer. Particularly, linking of Duox silencing to either *K-ras* or *EGFR* mutations, which are present in up to 50-60% and 60% of non-small cell lung cancer (Duarte and Paschoal, 2006; Lynch et al., 2004) may provide an additional marker for tumor classification. As research is currently exploring the efficacy of demethylating agents (Belinsky et al., 2005), hypermethylated *DUOX* could prove to be a key therapeutic target to prevent or reverse malignant transformation in the airways.

Additionally, studies are important which investigate the association of Duox with other lung pathologies that are characterized by high oxidative stress (e.g. asthma, cystic fibrosis, COPD). It is possible that – in contrast to *DUOX* silencing in lung cancer – Duox enzymes are over-expressed or constantly activated in these diseases. To that end, the generation of animal models would allow for a more detailed correlation between Duox function and disease progression.

However, as my preliminary data suggest, both mouse and rat are not appropriate models for analysis of Duox1 and Duox2 in lung disease, as they lack co-expression of both oxidases throughout their pulmonary tract. In addition, transgenic mouse models of cystic fibrosis (CF) have been shown to fail to recapitulate the natural progression of the human disease, as they manifest subtle to no CF lung disease (Guilbault et al., 2007). Ferret and pig have emerged as new models for cystic fibrosis (Li and Engelhardt, 2003; Li et al., 2006; Rogers et al., 2008). Particularly pigs may constitute a better model for human genetic diseases based on the similarity to humans in regard to anatomy, biochemistry, physiology, size and genetics. However, ferrets might be the more appropriate lab model. Nevertheless, the expression patterns of Duox1 and Duox2 as well their maturation factors remain to be identified in ferrets as well as in pigs in order to use these models for Duox-focused research.

Our knowledge of the complex Duox biology will increase through histological assessment of clinical samples for Duox1 and Duox2 expression, utilizing the newly generated specific antibodies. This might identify abnormalities in specific lung diseases, possibly allowing the identification of specific isoform de-regulation. Answers to these questions could move the field towards a better understanding of onset and progression of lung diseases and might provide opportunities to develop novel therapeutic strategies.

5 Summary

Duox NADPH oxidases are the ROS-generating enzymes in the respiratory epithelium and the thyroid. Duox1 and Duox2 generate H₂O₂ at the air-liquid interphase of lung epithelial cells and at apical membranes of thyroid follicular cells. Duox enzymes have been linked to host defense and thyroid hormone biosynthesis. Duox1 was further connected to acidification of the airway surface liquid as well as wound healing. Besides dependence on co-expression of DuoxA maturation factors, not much is known about the spatial expression and regulation of both Duox enzymes in airway epithelial cells.

Here, I demonstrate that Duox enzymes form functional heterodimers with the corresponding DuoxA subunits, in close analogy to the phagocyte NADPH oxidase Nox2. Several DuoxA1-isoforms (DuoxA1-1, DuoxA1-2 and DuoxA1-3) were identified, which do not contribute equally to Duox1 function. Duox1 and Duox2 localize to different cellular compartments in lung epithelial cells, depending on divergent DuoxA co-expression. It is possible that this localization defines the signaling specificity of Duox isoforms. In fact, Duox2 but not Duox1 is expressed in ciliated cells in an *ex vivo* differentiated lung epithelial model.

In addition, based on their ability to produce potentially harmful ROS in the airways, Duox expression was investigated. The expression of *DUOX1*, *DUOX2* and their maturation factors was markedly reduced or absent in lung cancer cell lines as well as in lung cancer tissues. Analysis of the CpG-rich promoter regions of *DUOX1* and *DUOX2* revealed frequent aberrant hypermethylation. Reconstitution of Duox increased cellular migration and wound healing, but did not affect growth rates.

In conclusion, the results suggest that Duox1 and Duox2 have distinct functions in the lung epithelium and that aberrant *DUOX* promoter hypermethylation is a common silencing mechanism of *DUOX1* and *DUOX2* in lung cancer. Therefore, epigenetic modifications of the genomic locus harboring the *DUOX* genes might be a potential biomarker for developing or progressing lung cancer. Further, analysis of isoform expression in other lung diseases might present an initial step towards early screening approaches and drug development.

6 Zusammenfassung

Duox NADPH Oxidasen verfügen über die Möglichkeit reaktive Sauerstoffspezies (reactive oxygen species; ROS) im Lungenepithelium sowie in der Schilddrüse zu produzieren. Duox1 und Duox2 erzeugen Wasserstoffperoxid (H_2O_2) an der luftzugewandten Seite von Lungenepithelzellen und in der apikalen Zellmembran follikulärer Schilddrüsenzellen. Beide Enzyme wurden mit der körpereigenen Immunabwehr sowie der Hormonsynthese in der Schilddrüse in Verbindung gebracht. Weiterhin spielt Duox1 eine Rolle bei der Regulierung des pH-Wertes der Lungenflüssigkeit sowie bei Heilungsprozessen des Lungenepitheliums. Über die Regulierung beider Duox Enzyme ist bisher lediglich bekannt, dass sie zusammen mit den Proteinuntereinheiten DuoxA1 und DuoxA2 expremiert werden müssen, um ihre biologische Aktivität zu entfalten. Die Regulierung von Duox1 und Duox2 ist jedoch bisher nicht geklärt.

Im Rahmen dieser Doktorarbeit konnte gezeigt werden, dass Duox Enzyme funktionelle Einheiten mit ihren jeweiligen DuoxA Proteinuntereinheiten bilden. Dieser Mechanismus findet ebenfalls bei Nox2, der NADPH Oxidase des phagozytischen Systems, statt. Weiterhin wurden mehrere DuoxA1 Isoformen (Duox1-1, DuoxA1-2 und DuoxA1-3) identifiziert, die jedoch nicht alle im gleichen Maße zur Wirkungsweise von Duox1 beitragen. Die beiden Duox Isoformen befinden sich in unterschiedlichen Kompartimenten der Zelle, was bedeuten könnte, dass beide Proteine unterschiedliche Aufgaben in der Zelle besitzen. Speziell im *ex vivo* differenzierten Lungenepithel-Modellsystem stellte sich heraus, dass Duox2 sich in Flimmerepithelzellen befindet und dort entlang der Zilien lokalisiert ist.

Da Duox Proteine die Fähigkeit haben, gesundheitsschädliche ROS zu produzieren, wurde ihre Expression in Lungenkrebszellen untersucht. Duox1 und Duox2, sowie ihre beiden Untereinheiten DuoxA1 und DuoxA2, wurden nicht mehr transkribiert, und die Analyse der CpG-reichen Promotorregionen von *DUOX1* und *DUOX2* zeigte eindeutig, dass diese Abschnitte überdurchschnittlich häufig methyliert sind. Die Wiedereinführung der jeweiligen Duox Enzyme in Lungenkrebszellen führte zu einer beschleunigten Zellwanderung sowie verbesserter Wundheilung *in vitro*, ohne Beeinflussung der Zellteilung.

Zusammenfassend deuten die Ergebnisse darauf hin, dass Duox1 und Duox2 unterschiedliche Aufgaben im Lungenepithel besitzen, und dass beide Enzyme häufig im klinischen Lungenkrebs nicht mehr expremiert werden. Der die *DUOX* Gene umgebende Lokus stellt ein mögliches Ziel für häufige epigenetische Modifikationen im Lungenkrebs dar. Veränderungen in diesem chromosomalen Bereich könnten als potenzielle Biomarker für die Kanzerogenese genutzt und eventuell sogar einer der drei Stufen (Initiation, Promotion, Progression) zugeordnet werden. Darüberhinaus könnte die Analyse der Expressionsmuster von Duox1 und Duox2 Hinweise für neue Entwicklungsansätze von spezifischen Medikamenten liefern, und so die Behandlung verschiedener Lungenkrankheiten ermöglichen.

7 References

- Aarbiou, J., R.M. Verhoosel, S. Van Wetering, W.I. De Boer, J.H. Van Krieken, S.V. Litvinov, K.F. Rabe, and P.S. Hiemstra. 2004. Neutrophil defensins enhance lung epithelial wound closure and mucin gene expression in vitro. *Am J Respir Cell Mol Biol.* 30:193-201.
- Ainsworth, C. 2007. Cilia: tails of the unexpected. *Nature.* 448:638-41.
- Ameziane-El-Hassani, R., S. Morand, J.L. Boucher, Y.M. Frapart, D. Apostolou, D. Agnandji, S. Gnidehou, R. Ohayon, M.S. Noel-Hudson, J. Francon, K. Lalaoui, A. Virion, and C. Dupuy. 2005. Dual oxidase-2 has an intrinsic Ca²⁺-dependent H₂O₂-generating activity. *J Biol Chem.* 280:30046-54.
- Azad, N., Y. Rojanasakul, and V. Vallyathan. 2008. Inflammation and lung cancer: roles of reactive oxygen/nitrogen species. *J Toxicol Environ Health B Crit Rev.* 11:1-15.
- Babior, B.M. 1999. NADPH oxidase: an update. *Blood.* 93:1464-76.
- Banfi, B., F. Tirone, I. Durussel, J. Knisz, P. Moskwa, G.Z. Molnar, K.H. Krause, and J.A. Cox. 2004. Mechanism of Ca²⁺ activation of the NADPH oxidase 5 (NOX5). *J Biol Chem.* 279:18583-91.
- Barnes, P.J. 2000. Chronic obstructive pulmonary disease. *N Engl J Med.* 343:269-80.
- Baylin, S.B., and J.G. Herman. 2000. DNA hypermethylation in tumorigenesis: epigenetics joins genetics. *Trends Genet.* 16:168-74.
- Bedard, K., B. Lardy, and K.H. Krause. 2007. NOX family NADPH oxidases: not just in mammals. *Biochimie.* 89:1107-12.
- Bedogni, B., G. Pani, R. Colavitti, A. Riccio, S. Borrello, M. Murphy, R. Smith, M.L. Eboli, and T. Galeotti. 2003. Redox regulation of cAMP-responsive element-binding protein and induction of manganous superoxide dismutase in nerve growth factor-dependent cell survival. *J Biol Chem.* 278:16510-9.
- Belinsky, S.A. 2004. Gene-promoter hypermethylation as a biomarker in lung cancer. *Nat Rev Cancer.* 4:707-17.
- Belinsky, S.A., D.M. Klinge, J.D. Dekker, M.W. Smith, T.J. Bocklage, F.D. Gilliland, R.E. Crowell, D.D. Karp, C.A. Stidley, and M.A. Picchi. 2005. Gene promoter methylation in plasma and sputum increases with lung cancer risk. *Clin Cancer Res.* 11:6505-11.
- Belinsky, S.A., K.C. Liechty, F.D. Gentry, H.J. Wolf, J. Rogers, K. Vu, J. Haney, T.C. Kennedy, F.R. Hirsch, Y. Miller, W.A. Franklin, J.G. Herman, S.B. Baylin, P.A. Bunn, and T. Byers. 2006. Promoter hypermethylation of multiple genes in sputum precedes lung cancer incidence in a high-risk cohort. *Cancer Res.* 66:3338-44.
- Belinsky, S.A., K.J. Nikula, W.A. Palmisano, R. Michels, G. Saccomanno, E. Gabrielson, S.B. Baylin, and J.G. Herman. 1998. Aberrant methylation of p16(INK4a) is an early event in lung cancer and a potential biomarker for early diagnosis. *Proc Natl Acad Sci U S A.* 95:11891-6.
- Belinsky, S.A., W.A. Palmisano, F.D. Gilliland, L.A. Crooks, K.K. Divine, S.A. Winters, M.J. Grimes, H.J. Harms, C.S. Tellez, T.M. Smith, P.P. Moots, J.F. Lechner, C.A. Stidley, and R.E. Crowell. 2002. Aberrant promoter methylation in bronchial epithelium and sputum from current and former smokers. *Cancer Res.* 62:2370-7.
- Bernacki, S.H., A.L. Nelson, L. Abdullah, J.K. Sheehan, A. Harris, C.W. Davis, and S.H. Randell. 1999. Mucin gene expression during differentiation of human airway epithelia in vitro. Muc4 and muc5b are strongly induced. *Am J Respir Cell Mol Biol.* 20:595-604.
- Bhaskaran, M., H. Chen, Z. Chen, and L. Liu. 2005. Hemoglobin is expressed in alveolar epithelial type II cells. *Biochem Biophys Res Commun.* 333:1348-52.
- Biberstine-Kinkade, K.J., F.R. DeLeo, R.I. Epstein, B.A. LeRoy, W.M. Nauseef, and M.C. Dinauer. 2001. Heme-ligating histidines in flavocytochrome b(558): identification of specific histidines in gp91(phox). *J Biol Chem.* 276:31105-12.
- Bissonnette, S.A., C.M. Glazier, M.Q. Stewart, G.E. Brown, C.D. Ellson, and M.B. Yaffe. 2008. Phosphatidylinositol 3-phosphate-dependent and -independent functions of p40phox in activation of the neutrophil NADPH oxidase. *J Biol Chem.* 283:2108-19.

- Bowman, R.V., I.A. Yang, A.B. Semmler, and K.M. Fong. 2006. Epigenetics of lung cancer. *Respirology*. 11:355-65.
- Brena, R.M., C. Morrison, S. Liyanarachchi, D. Jarjoura, R.V. Davuluri, G.A. Otterson, D. Reisman, S. Glaros, L.J. Rush, and C. Plass. 2007. Aberrant DNA methylation of OLIG1, a novel prognostic factor in non-small cell lung cancer. *PLoS Med*. 4:e108.
- Caillou, B., C. Dupuy, L. Lacroix, M. Nocera, M. Talbot, R. Ohayon, D. Deme, J.M. Bidart, M. Schlumberger, and A. Virion. 2001. Expression of reduced nicotinamide adenine dinucleotide phosphate oxidase (ThoX, LNOX, Duox) genes and proteins in human thyroid tissues. *J Clin Endocrinol Metab*. 86:3351-8.
- Chandel, N.S., E. Maltepe, E. Goldwasser, C.E. Mathieu, M.C. Simon, and P.T. Schumacker. 1998. Mitochondrial reactive oxygen species trigger hypoxia-induced transcription. *Proc Natl Acad Sci U S A*. 95:11715-20.
- Chandel, N.S., D.S. McClintock, C.E. Feliciano, T.M. Wood, J.A. Melendez, A.M. Rodriguez, and P.T. Schumacker. 2000. Reactive oxygen species generated at mitochondrial complex III stabilize hypoxia-inducible factor-1 α during hypoxia: a mechanism of O₂ sensing. *J Biol Chem*. 275:25130-8.
- Chang, H.C., C.Y. Cho, and W.C. Hung. 2007. Downregulation of RECK by promoter methylation correlates with lymph node metastasis in non-small cell lung cancer. *Cancer Sci*. 98:169-73.
- Chung-man Ho, J., S. Zheng, S.A. Comhair, C. Farver, and S.C. Erzurum. 2001. Differential expression of manganese superoxide dismutase and catalase in lung cancer. *Cancer Res*. 61:8578-85.
- Corpas, F.J., J.B. Barroso, and L.A. del Rio. 2001. Peroxisomes as a source of reactive oxygen species and nitric oxide signal molecules in plant cells. *Trends Plant Sci*. 6:145-50.
- Costello, J.F., M.C. Fruhwald, D.J. Smiraglia, L.J. Rush, G.P. Robertson, X. Gao, F.A. Wright, J.D. Feramisco, P. Peltomaki, J.C. Lang, D.E. Schuller, L. Yu, C.D. Bloomfield, M.A. Caligiuri, A. Yates, R. Nishikawa, H. Su Huang, N.J. Petrelli, X. Zhang, M.S. O'Dorisio, W.A. Held, W.K. Cavenee, and C. Plass. 2000. Aberrant CpG-island methylation has non-random and tumour-type-specific patterns. *Nat Genet*. 24:132-8.
- Dano, L., M.N. Guilly, M. Muleris, J.P. Morlier, S. Altmeyer, P. Vielh, A.K. El-Naggar, G. Monchaux, B. Dutrillaux, and S. Chevillard. 2000. CGH analysis of radon-induced rat lung tumors indicates similarities with human lung cancers. *Genes Chromosomes Cancer*. 29:1-8.
- De Deken, X., D. Wang, J.E. Dumont, and F. Miot. 2002. Characterization of ThOX proteins as components of the thyroid H₂O₂-generating system. *Exp Cell Res*. 273:187-96.
- De Deken, X., D. Wang, M.C. Many, S. Costagliola, F. Libert, G. Vassart, J.E. Dumont, and F. Miot. 2000. Cloning of two human thyroid cDNAs encoding new members of the NADPH oxidase family. *J Biol Chem*. 275:23227-33.
- de Jong, P.M., M.A. van Sterkenburg, S.C. Hesselting, J.A. Kempenaar, A.A. Mulder, A.M. Mommaas, J.H. Dijkman, and M. Ponc. 1994. Ciliogenesis in human bronchial epithelial cells cultured at the air-liquid interface. *Am J Respir Cell Mol Biol*. 10:271-7.
- del Rio, L.A., L.M. Sandalio, J.M. Palma, P. Bueno, and F.J. Corpas. 1992. Metabolism of oxygen radicals in peroxisomes and cellular implications. *Free Radic Biol Med*. 13:557-80.
- DeLeo, F.R., J.B. Burritt, L. Yu, A.J. Jesaitis, M.C. Dinauer, and W.M. Nauseef. 2000. Processing and maturation of flavocytochrome b558 include incorporation of heme as a prerequisite for heterodimer assembly. *J Biol Chem*. 275:13986-93.
- Donaldson, S.H., W.D. Bennett, K.L. Zeman, M.R. Knowles, R. Tarran, and R.C. Boucher. 2006. Mucus clearance and lung function in cystic fibrosis with hypertonic saline. *N Engl J Med*. 354:241-50.
- Donko, A., Z. Peterfi, A. Sum, T. Leto, and M. Geiszt. 2005. Dual oxidases. *Philos Trans R Soc Lond B Biol Sci*. 360:2301-8.
- Duarte, R.L., and M.E. Paschoal. 2006. Molecular markers in lung cancer: prognostic role and relationship to smoking. *J Bras Pneumol*. 32:56-65.

- Dupuy, C., R. Ohayon, A. Valent, M.S. Noel-Hudson, D. Deme, and A. Virion. 1999. Purification of a novel flavoprotein involved in the thyroid NADPH oxidase. Cloning of the porcine and human cdnas. *J Biol Chem.* 274:37265-9.
- Edens, W.A., L. Sharling, G. Cheng, R. Shapira, J.M. Kinkade, T. Lee, H.A. Edens, X. Tang, C. Sullards, D.B. Flaherty, G.M. Benian, and J.D. Lambeth. 2001. Tyrosine cross-linking of extracellular matrix is catalyzed by Duox, a multidomain oxidase/oxidoreductase with homology to the phagocyte oxidase subunit gp91phox. *J Cell Biol.* 154:879-91.
- Eguchi, K., Y. Kanai, K. Kobayashi, and S. Hirohashi. 1997. DNA hypermethylation at the D17S5 locus in non-small cell lung cancers: its association with smoking history. *Cancer Res.* 57:4913-5.
- Enokida, H., H. Shiina, S. Urakami, M. Terashima, T. Ogishima, L.C. Li, M. Kawahara, M. Nakagawa, C.J. Kane, P.R. Carroll, M. Igawa, and R. Dahiya. 2006. Smoking influences aberrant CpG hypermethylation of multiple genes in human prostate carcinoma. *Cancer.* 106:79-86.
- Espinosa, A., and J.R. Alfano. 2004. Disabling surveillance: bacterial type III secretion system effectors that suppress innate immunity. *Cell Microbiol.* 6:1027-40.
- Figueiredo, M.D., L.C. Cardoso, A.C. Ferreira, D.V. Campos, M. da Cruz Domingos, R. Corbo, L.E. Nasciutti, M. Vaisman, and D.P. Carvalho. 2001. Goiter and hypothyroidism in two siblings due to impaired Ca(+2)/NAD(P)H-dependent H(2)O(2)-generating activity. *J Clin Endocrinol Metab.* 86:4843-8.
- Finkel, T. 1999. Signal transduction by reactive oxygen species in non-phagocytic cells. *J Leukoc Biol.* 65:337-40.
- Fischer, H., L.K. Gonzales, V. Kolla, C. Schwarzer, F. Miot, B. Illek, and P.L. Ballard. 2007. Developmental regulation of DUOX1 expression and function in human fetal lung epithelial cells. *Am J Physiol Lung Cell Mol Physiol.* 292:L1506-14.
- Fischer, H., and J.H. Widdicombe. 2006. Mechanisms of acid and base secretion by the airway epithelium. *J Membr Biol.* 211:139-50.
- Flatau, E., E. Bogenmann, and P.A. Jones. 1983. Variable 5-methylcytosine levels in human tumor cell lines and fresh pediatric tumor explants. *Cancer Res.* 43:4901-5.
- Forteza, R., M. Salathe, F. Miot, R. Forteza, and G.E. Conner. 2005. Regulated hydrogen peroxide production by Duox in human airway epithelial cells. *Am J Respir Cell Mol Biol.* 32:462-9.
- Geiszt, M., and T.L. Leto. 2004. The Nox family of NAD(P)H oxidases: host defense and beyond. *J Biol Chem.* 279:51715-8.
- Geiszt, M., J. Witta, J. Baffi, K. Lekstrom, and T.L. Leto. 2003. Dual oxidases represent novel hydrogen peroxide sources supporting mucosal surface host defense. *Faseb J.* 17:1502-4.
- Georgescu, M.M., K.H. Kirsch, T. Akagi, T. Shishido, and H. Hanafusa. 1999. The tumor-suppressor activity of PTEN is regulated by its carboxyl-terminal region. *Proc Natl Acad Sci U S A.* 96:10182-7.
- Gerard, A.C., C. Daumerie, C. Mestdagh, S. Gohy, C. De Burbure, S. Costagliola, F. Miot, M.C. Nolleaux, J.F. Deneff, J. Rahier, B. Franc, J.J. De Vijlder, I.M. Colin, and M.C. Many. 2003. Correlation between the loss of thyroglobulin iodination and the expression of thyroid-specific proteins involved in iodine metabolism in thyroid carcinomas. *J Clin Endocrinol Metab.* 88:4977-83.
- Gootjes, J., F. Schmohl, H.R. Waterham, and R.J. Wanders. 2004. Novel mutations in the PEX12 gene of patients with a peroxisome biogenesis disorder. *Eur J Hum Genet.* 12:115-20.
- Grasberger, H., X. De Deken, F. Miot, J. Pohlenz, and S. Refetoff. 2007. Missense mutations of dual oxidase 2 (DUOX2) implicated in congenital hypothyroidism have impaired trafficking in cells reconstituted with DUOX2 maturation factor. *Mol Endocrinol.* 21:1408-21.
- Grasberger, H., and S. Refetoff. 2006. Identification of the maturation factor for dual oxidase. Evolution of an eukaryotic operon equivalent. *J Biol Chem.* 281:18269-72.
- Gray, T.E., K. Guzman, C.W. Davis, L.H. Abdullah, and P. Nettlesheim. 1996. Mucociliary differentiation of serially passaged normal human tracheobronchial epithelial cells. *Am J Respir Cell Mol Biol.* 14:104-12.

- Guilbault, C., Z. Saeed, G.P. Downey, and D. Radzioch. 2007. Cystic fibrosis mouse models. *Am J Respir Cell Mol Biol.* 36:1-7.
- Ha, E.M., C.T. Oh, Y.S. Bae, and W.J. Lee. 2005. A direct role for dual oxidase in *Drosophila* gut immunity. *Science.* 310:847-50.
- Ha, L., T. Ichikawa, M. Anver, R. Dickins, S. Lowe, N.E. Sharpless, P. Krimpenfort, R.A. Depinho, D.C. Bennett, E.V. Sviderskaya, and G. Merlino. 2007. ARF functions as a melanoma tumor suppressor by inducing p53-independent senescence. *Proc Natl Acad Sci U S A.* 104:10968-73.
- Harper, R.W., C. Xu, J.P. Eiserich, Y. Chen, C.Y. Kao, P. Thai, H. Setiadi, and R. Wu. 2005. Differential regulation of dual NADPH oxidases/peroxidases, Duox1 and Duox2, by Th1 and Th2 cytokines in respiratory tract epithelium. *FEBS Lett.* 579:4911-7.
- Henricks, P.A., and F.P. Nijkamp. 2001. Reactive oxygen species as mediators in asthma. *Pulm Pharmacol Ther.* 14:409-20.
- Heo, W.D., T. Inoue, W.S. Park, M.L. Kim, B.O. Park, T.J. Wandless, and T. Meyer. 2006. PI(3,4,5)P3 and PI(4,5)P2 lipids target proteins with polybasic clusters to the plasma membrane. *Science.* 314:1458-61.
- Jackson, E.L., N. Willis, K. Mercer, R.T. Bronson, D. Crowley, R. Montoya, T. Jacks, and D.A. Tuveson. 2001. Analysis of lung tumor initiation and progression using conditional expression of oncogenic K-ras. *Genes Dev.* 15:3243-8.
- Jagnandan, D., J.E. Church, B. Banfi, D.J. Stuehr, M.B. Marrero, and D.J. Fulton. 2007. Novel mechanism of activation of NADPH oxidase 5. calcium sensitization via phosphorylation. *J Biol Chem.* 282:6494-507.
- Jaimes, E.A., E.G. DeMaster, R.X. Tian, and L. Raij. 2004. Stable compounds of cigarette smoke induce endothelial superoxide anion production via NADPH oxidase activation. *Arterioscler Thromb Vasc Biol.* 24:1031-6.
- Jones, P.A., and P.W. Laird. 1999. Cancer epigenetics comes of age. *Nat Genet.* 21:163-7.
- Kamio, K., I. Matsushita, M. Hijikata, Y. Kobashi, G. Tanaka, K. Nakata, T. Ishida, K. Tokunaga, Y. Taguchi, S. Homma, K. Nakata, A. Azuma, S. Kudoh, and N. Keicho. 2005. Promoter analysis and aberrant expression of the MUC5B gene in diffuse panbronchiolitis. *Am J Respir Crit Care Med.* 171:949-57.
- Kawahara, T., and J.D. Lambeth. 2008. Phosphatidylinositol (4,5)-bisphosphate Modulates Nox5 Localization via an N-Terminal Polybasic Region. *Mol Biol Cell.*
- Kawahara, T., M.T. Quinn, and J.D. Lambeth. 2007. Molecular evolution of the reactive oxygen-generating NADPH oxidase (Nox/Duox) family of enzymes. *BMC Evol Biol.* 7:109.
- Kim, C.F., E.L. Jackson, D.G. Kirsch, J. Grimm, A.T. Shaw, K. Lane, J. Kissil, K.P. Olive, A. Sweet-Cordero, R. Weissleder, and T. Jacks. 2005. Mouse models of human non-small-cell lung cancer: raising the bar. *Cold Spring Harb Symp Quant Biol.* 70:241-50.
- Kim, D.H., J.S. Kim, Y.I. Ji, Y.M. Shim, H. Kim, J. Han, and J. Park. 2003. Hypermethylation of RASSF1A promoter is associated with the age at starting smoking and a poor prognosis in primary non-small cell lung cancer. *Cancer Res.* 63:3743-6.
- Kim, D.H., H.H. Nelson, J.K. Wiencke, S. Zheng, D.C. Christiani, J.C. Wain, E.J. Mark, and K.T. Kelsey. 2001. p16(INK4a) and histology-specific methylation of CpG islands by exposure to tobacco smoke in non-small cell lung cancer. *Cancer Res.* 61:3419-24.
- Kode, A., S.R. Yang, and I. Rahman. 2006. Differential effects of cigarette smoke on oxidative stress and proinflammatory cytokine release in primary human airway epithelial cells and in a variety of transformed alveolar epithelial cells. *Respir Res.* 7:132.
- Koff, J.L., M.X. Shao, S. Kim, I.F. Ueki, and J.A. Nadel. 2006. *Pseudomonas* lipopolysaccharide accelerates wound repair via activation of a novel epithelial cell signaling cascade. *J Immunol.* 177:8693-700.
- Krassenstein, R., E. Sauter, E. Dulaimi, C. Battagli, H. Ehya, A. Klein-Szanto, and P. Cairns. 2004. Detection of breast cancer in nipple aspirate fluid by CpG island hypermethylation. *Clin Cancer Res.* 10:28-32.

- Krunkosky, T.M., L.D. Martin, B.M. Fischer, J.A. Voynow, and K.B. Adler. 2003. Effects of TNF α on expression of ICAM-1 in human airway epithelial cells in vitro: oxidant-mediated pathways and transcription factors. *Free Radic Biol Med.* 35:1158-67.
- Kuwahara, I., E.P. Lillehoj, T. Koga, Y. Isohama, T. Miyata, and K.C. Kim. 2007. The signaling pathway involved in neutrophil elastase stimulated MUC1 transcription. *Am J Respir Cell Mol Biol.* 37:691-8.
- Kyle, H., J.P. Ward, and J.G. Widdicombe. 1990. Control of pH of airway surface liquid of the ferret trachea in vitro. *J Appl Physiol.* 68:135-40.
- Lacroix, L., M. Nocera, C. Mian, B. Caillou, A. Virion, C. Dupuy, S. Filetti, J.M. Bidart, and M. Schlumberger. 2001. Expression of nicotinamide adenine dinucleotide phosphate oxidase flavoprotein DUOX genes and proteins in human papillary and follicular thyroid carcinomas. *Thyroid.* 11:1017-23.
- Laemmli, U.K. 1970. Cleavage of structural proteins during the assembly of the head of bacteriophage T4. *Nature.* 227:680-5.
- Lambeth, J.D. 2004. NOX enzymes and the biology of reactive oxygen. *Nat Rev Immunol.* 4:181-9.
- Lavigne, M.C., and M.J. Eppihimer. 2005. Cigarette smoke condensate induces MMP-12 gene expression in airway-like epithelia. *Biochem Biophys Res Commun.* 330:194-203.
- Li, Z., and J.F. Engelhardt. 2003. Progress toward generating a ferret model of cystic fibrosis by somatic cell nuclear transfer. *Reprod Biol Endocrinol.* 1:83.
- Li, Z., X. Sun, J. Chen, X. Liu, S.M. Wisely, Q. Zhou, J.P. Renard, G.H. Leno, and J.F. Engelhardt. 2006. Cloned ferrets produced by somatic cell nuclear transfer. *Dev Biol.* 293:439-48.
- Lin, K.T., R.L. Momparler, and G.E. Rivard. 1981. High-performance liquid chromatographic analysis of chemical stability of 5-aza-2'-deoxycytidine. *J Pharm Sci.* 70:1228-32.
- Luppi, F., J. Aarbiou, S. van Wetering, I. Rahman, W.I. de Boer, K.F. Rabe, and P.S. Hiemstra. 2005. Effects of cigarette smoke condensate on proliferation and wound closure of bronchial epithelial cells in vitro: role of glutathione. *Respir Res.* 6:140.
- Lynch, T.J., D.W. Bell, R. Sordella, S. Gurubhagavatula, R.A. Okimoto, B.W. Brannigan, P.L. Harris, S.M. Haserlat, J.G. Supko, F.G. Haluska, D.N. Louis, D.C. Christiani, J. Settleman, and D.A. Haber. 2004. Activating mutations in the epidermal growth factor receptor underlying responsiveness of non-small-cell lung cancer to gefitinib. *N Engl J Med.* 350:2129-39.
- Machida, E.O., M.V. Brock, C.M. Hooker, J. Nakayama, A. Ishida, J. Amano, M.A. Picchi, S.A. Belinsky, J.G. Herman, S. Taniguchi, and S.B. Baylin. 2006. Hypermethylation of ASC/TMS1 is a sputum marker for late-stage lung cancer. *Cancer Res.* 66:6210-8.
- Manzanares, D., M.E. Monzon, R.C. Savani, and M. Salathe. 2007. Apical oxidative hyaluronan degradation stimulates airway ciliary beating via RHAMM and RON. *Am J Respir Cell Mol Biol.* 37:160-8.
- March, T.H., P.G. Marron-Terada, and S.A. Belinsky. 2001. Refinement of an orthotopic lung cancer model in the nude rat. *Vet Pathol.* 38:483-90.
- Marchetti, A., B. Cecchinelli, M. D'Angelo, G. D'Orazi, M. Crescenzi, A. Sacchi, and S. Soddu. 2004. p53 can inhibit cell proliferation through caspase-mediated cleavage of ERK2/MAPK. *Cell Death Differ.* 11:596-607.
- Marsit, C.J., E.A. Houseman, A.R. Schned, M.R. Karagas, and K.T. Kelsey. 2007. Promoter hypermethylation is associated with current smoking, age, gender and survival in bladder cancer. *Carcinogenesis.* 28:1745-51.
- Matsushita, K., C.N. Morrell, R.J. Mason, M. Yamakuchi, F.A. Khanday, K. Irani, and C.J. Lowenstein. 2005. Hydrogen peroxide regulation of endothelial exocytosis by inhibition of N-ethylmaleimide sensitive factor. *J Cell Biol.* 170:73-9.
- McLaughlin, S., J. Wang, A. Gambhir, and D. Murray. 2002. PIP(2) and proteins: interactions, organization, and information flow. *Annu Rev Biophys Biomol Struct.* 31:151-75.
- Meuwissen, R., and A. Berns. 2005. Mouse models for human lung cancer. *Genes Dev.* 19:643-64.

- Meuwissen, R., S.C. Linn, R.I. Linnoila, J. Zevenhoven, W.J. Mooi, and A. Berns. 2003. Induction of small cell lung cancer by somatic inactivation of both Trp53 and Rb1 in a conditional mouse model. *Cancer Cell*. 4:181-9.
- Meuwissen, R., S.C. Linn, M. van der Valk, W.J. Mooi, and A. Berns. 2001. Mouse model for lung tumorigenesis through Cre/lox controlled sporadic activation of the K-Ras oncogene. *Oncogene*. 20:6551-8.
- Mills, P.C., and A.J. Higgins. 1997. Oxidant injury, nitric oxide and pulmonary vascular function: implications for the exercising horse. *Vet J*. 153:125-48.
- Moldovan, L., K. Irani, N.I. Moldovan, T. Finkel, and P.J. Goldschmidt-Clermont. 1999. The actin cytoskeleton reorganization induced by Rac1 requires the production of superoxide. *Antioxid Redox Signal*. 1:29-43.
- Morand, S., D. Agnandji, M.S. Noel-Hudson, V. Nicolas, S. Buisson, L. Macon-Lemaitre, S. Gnidehou, J. Kaniewski, R. Ohayon, A. Virion, and C. Dupuy. 2004. Targeting of the dual oxidase 2 N-terminal region to the plasma membrane. *J Biol Chem*. 279:30244-51.
- Morand, S., M. Charaoui, J. Kaniewski, D. Deme, R. Ohayon, M.S. Noel-Hudson, A. Virion, and C. Dupuy. 2003. Effect of iodide on nicotinamide adenine dinucleotide phosphate oxidase activity and Duox2 protein expression in isolated porcine thyroid follicles. *Endocrinology*. 144:1241-8.
- Moreno, J.C., H. Bikker, M.J. Kempers, A.S. van Trotsenburg, F. Baas, J.J. de Vijlder, T. Vulsma, and C. Ris-Stalpers. 2002. Inactivating mutations in the gene for thyroid oxidase 2 (THOX2) and congenital hypothyroidism. *N Engl J Med*. 347:95-102.
- Moskwa, P., D. Lorentzen, K.J. Excoffon, J. Zabner, P.B. McCray, Jr., W.M. Nauseef, C. Dupuy, and B. Banfi. 2007. A novel host defense system of airways is defective in cystic fibrosis. *Am J Respir Crit Care Med*. 175:174-83.
- Motiwala, T., H. Kutay, K. Ghoshal, S. Bai, H. Seimiya, T. Tsuruo, S. Suster, C. Morrison, and S.T. Jacob. 2004. Protein tyrosine phosphatase receptor-type O (PTPRO) exhibits characteristics of a candidate tumor suppressor in human lung cancer. *Proc Natl Acad Sci U S A*. 101:13844-9.
- Nagai, K., T. Betsuyaku, M. Suzuki, Y. Nasuhara, K. Kaga, S. Kondo, and M. Nishimura. 2008. Dual oxidase 1 and 2 expression in airway epithelium of smokers and patients with mild/moderate chronic obstructive pulmonary disease. *Antioxid Redox Signal*. 10:705-14.
- Nauseef, W.M. 2008. Biological roles for the NOX family NADPH oxidases. *J Biol Chem*. 283:16961-5.
- Nisimoto, Y., S. Motalebi, C.H. Han, and J.D. Lambeth. 1999. The p67(phox) activation domain regulates electron flow from NADPH to flavin in flavocytochrome b(558). *J Biol Chem*. 274:22999-3005.
- Ohye, H., S. Fukata, A. Hishinuma, T. Kudo, E. Nishihara, M. Ito, S. Kubota, N. Amino, T. Ieiri, K. Kuma, and A. Miyauchi. 2008. A novel homozygous missense mutation of the dual oxidase 2 (DUOX2) gene in an adult patient with large goiter. *Thyroid*. 18:561-6.
- Pachucki, J., D. Wang, D. Christophe, and F. Miot. 2004. Structural and functional characterization of the two human ThOX/Duox genes and their 5'-flanking regions. *Mol Cell Endocrinol*. 214:53-62.
- Pacquelet, S., M. Lehmann, S. Luxen, K. Regazzoni, M. Frausto, D. Noack, and U.G. Knaus. 2008. Inhibitory action of Noxa1 on Duox activity in airway cells. *J Biol Chem*.
- Palmisano, W.A., K.K. Divine, G. Saccomanno, F.D. Gilliland, S.B. Baylin, J.G. Herman, and S.A. Belinsky. 2000. Predicting lung cancer by detecting aberrant promoter methylation in sputum. *Cancer Res*. 60:5954-8.
- Panda, K., M. Chawla-Sarkar, C. Santos, T. Koeck, S.C. Erzurum, J.F. Parkinson, and D.J. Stuehr. 2005. Visualizing inducible nitric-oxide synthase in living cells with a heme-binding fluorescent inhibitor. *Proc Natl Acad Sci U S A*. 102:10117-22.
- Pfarr, N., E. Korsch, S. Kaspers, A. Herbst, A. Stach, C. Zimmer, and J. Pohlenz. 2006. Congenital hypothyroidism caused by new mutations in the thyroid oxidase 2 (THOX2) gene. *Clin Endocrinol (Oxf)*. 65:810-5.

- Pilzer, I., and I. Gozes. 2006. A splice variant to PACAP receptor that is involved in spermatogenesis is expressed in astrocytes. *Ann N Y Acad Sci.* 1070:484-90.
- Raha, S., and B.H. Robinson. 2000. Mitochondria, oxygen free radicals, disease and ageing. *Trends Biochem Sci.* 25:502-8.
- Ramsey, M.R., and N.E. Sharpless. 2006. ROS as a tumour suppressor? *Nat Cell Biol.* 8:1213-5.
- Ris-Stalpers, C. 2006. Physiology and pathophysiology of the DUOXes. *Antioxid Redox Signal.* 8:1563-72.
- Rizzi, M., M.P. Tschan, C. Britschgi, A. Britschgi, B. Hugli, T.J. Grob, N. Leupin, B.U. Mueller, H.U. Simon, A. Ziemiecki, B.E. Torbett, M.F. Fey, and A. Tobler. 2007. The death-associated protein kinase 2 (DAPK2) is up-regulated during normal myeloid differentiation and enhances neutrophil maturation in myeloid leukemic cells. *J Leukoc Biol.*
- Rogers, C.S., Y. Hao, T. Rokhlina, M. Samuel, D.A. Stoltz, Y. Li, E. Petroff, D.W. Vermeer, A.C. Kabel, Z. Yan, L. Spate, D. Wax, C.N. Murphy, A. Rieke, K. Whitworth, M.L. Linville, S.W. Korte, J.F. Engelhardt, M.J. Welsh, and R.S. Prather. 2008. Production of CFTR-null and CFTR-DeltaF508 heterozygous pigs by adeno-associated virus-mediated gene targeting and somatic cell nuclear transfer. *J Clin Invest.* 118:1571-7.
- Ryter, S.W., H.P. Kim, A. Hoetzel, J.W. Park, K. Nakahira, X. Wang, and A.M. Choi. 2007. Mechanisms of cell death in oxidative stress. *Antioxid Redox Signal.* 9:49-89.
- Schwarzer, C., T.E. Machen, B. Illek, and H. Fischer. 2004. NADPH oxidase-dependent acid production in airway epithelial cells. *J Biol Chem.* 279:36454-61.
- Shao, M.X., and J.A. Nadel. 2005. Dual oxidase 1-dependent MUC5AC mucin expression in cultured human airway epithelial cells. *Proc Natl Acad Sci U S A.* 102:767-72.
- Singh, D.K., D. Kumar, Z. Siddiqui, S.K. Basu, V. Kumar, and K.V. Rao. 2005. The strength of receptor signaling is centrally controlled through a cooperative loop between Ca²⁺ and an oxidant signal. *Cell.* 121:281-93.
- Singh, I. 1997. Biochemistry of peroxisomes in health and disease. *Mol Cell Biochem.* 167:1-29.
- Smith, P.K., R.I. Krohn, G.T. Hermanson, A.K. Mallia, F.H. Gartner, M.D. Provenzano, E.K. Fujimoto, N.M. Goeke, B.J. Olson, and D.C. Klenk. 1985. Measurement of protein using bicinchoninic acid. *Anal Biochem.* 150:76-85.
- Spira, A., and D.S. Ettinger. 2004. Multidisciplinary management of lung cancer. *N Engl J Med.* 350:379-92.
- Stadtman, E.R. 2006. Protein oxidation and aging. *Free Radic Res.* 40:1250-8.
- Swafford, D.S., S.K. Middleton, W.A. Palmisano, K.J. Nikula, J. Tesfaigzi, S.B. Baylin, J.G. Herman, and S.A. Belinsky. 1997. Frequent aberrant methylation of p16INK4a in primary rat lung tumors. *Mol Cell Biol.* 17:1366-74.
- Swan, C.H., B. Buhler, P. Steinberger, M.P. Tschan, C.F. Barbas, 3rd, and B.E. Torbett. 2006. T-cell protection and enrichment through lentiviral CCR5 intrabody gene delivery. *Gene Ther.* 13:1480-92.
- Tagliaferri, F., L. Teodori, M.G. Valente, F. Stipa, A. Cucina, W. Gohde, D. Colettii, P. Alo, and S. Stipa. 2000. In vitro proliferation and in vivo malignancy of cell lines simultaneously derived from a chemically-induced heterogeneous rat mammary tumor. *In Vitro Cell Dev Biol Anim.* 36:163-6.
- Takai, D., and P.A. Jones. 2003. The CpG island searcher: a new WWW resource. *In Silico Biol.* 3:235-40.
- Tang, X., W. Wu, S.Y. Sun, Wistuba, II, W.K. Hong, and L. Mao. 2004. Hypermethylation of the death-associated protein kinase promoter attenuates the sensitivity to TRAIL-induced apoptosis in human non-small cell lung cancer cells. *Mol Cancer Res.* 2:685-91.
- Tfelt-Hansen, J., N. Chattopadhyay, S. Yano, D. Kanuparthi, P. Rooney, P. Schwarz, and E.M. Brown. 2004. Calcium-sensing receptor induces proliferation through p38 mitogen-activated protein kinase and phosphatidylinositol 3-kinase but not extracellularly regulated kinase in a model of humoral hypercalcemia of malignancy. *Endocrinology.* 145:1211-7.

- Thrasher, A.J., N.H. Keep, F. Wientjes, and A.W. Segal. 1994. Chronic granulomatous disease. *Biochim Biophys Acta*. 1227:1-24.
- Torres, M.A., H. Onouchi, S. Hamada, C. Machida, K.E. Hammond-Kosack, and J.D. Jones. 1998. Six *Arabidopsis thaliana* homologues of the human respiratory burst oxidase (gp91phox). *Plant J*. 14:365-70.
- Trinklein, N.D., S.F. Aldred, S.J. Hartman, D.I. Schroeder, R.P. Otilar, and R.M. Myers. 2004. An abundance of bidirectional promoters in the human genome. *Genome Res*. 14:62-6.
- Tsou, J.A., J.A. Hagen, C.L. Carpenter, and I.A. Laird-Offringa. 2002. DNA methylation analysis: a powerful new tool for lung cancer diagnosis. *Oncogene*. 21:5450-61.
- Valko, M., C.J. Rhodes, J. Moncol, M. Izakovic, and M. Mazur. 2006. Free radicals, metals and antioxidants in oxidative stress-induced cancer. *Chem Biol Interact*. 160:1-40.
- van der Vliet, A. 2008. NADPH oxidases in lung biology and pathology: host defense enzymes, and more. *Free Radic Biol Med*. 44:938-55.
- Varela, V., C.M. Rivolta, S.A. Esperante, L. Gruneiro-Papendieck, A. Chiesa, and H.M. Targovnik. 2006. Three mutations (p.Q36H, p.G418fsX482, and g.IVS19-2A>C) in the dual oxidase 2 gene responsible for congenital goiter and iodide organification defect. *Clin Chem*. 52:182-91.
- Vigone, M.C., L. Fugazzola, I. Zamproni, A. Passoni, S. Di Candia, G. Chiumello, L. Persani, and G. Weber. 2005. Persistent mild hypothyroidism associated with novel sequence variants of the DUOX2 gene in two siblings. *Hum Mutat*. 26:395.
- Virtanen, C., Y. Ishikawa, D. Honjoh, M. Kimura, M. Shimane, T. Miyoshi, H. Nomura, and M.H. Jones. 2002. Integrated classification of lung tumors and cell lines by expression profiling. *Proc Natl Acad Sci U S A*. 99:12357-62.
- Wallach, T.M., and A.W. Segal. 1996. Stoichiometry of the subunits of flavocytochrome b558 of the NADPH oxidase of phagocytes. *Biochem J*. 320 (Pt 1):33-8.
- Wang, D., X. De Deken, M. Milenkovic, Y. Song, I. Pirson, J.E. Dumont, and F. Miot. 2005. Identification of a novel partner of duox: EFP1, a thioredoxin-related protein. *J Biol Chem*. 280:3096-103.
- Wang, H., X. Liu, T. Umino, C.M. Skold, Y. Zhu, T. Kohyama, J.R. Spurzem, D.J. Romberger, and S.I. Rennard. 2001. Cigarette smoke inhibits human bronchial epithelial cell repair processes. *Am J Respir Cell Mol Biol*. 25:772-9.
- Wang, Y., Z. Zhang, R.A. Lubet, and M. You. 2006. A mouse model for tumor progression of lung cancer in ras and p53 transgenic mice. *Oncogene*. 25:1277-80.
- Wesley, U.V., P.F. Bove, M. Hristova, S. McCarthy, and A. van der Vliet. 2007. Airway epithelial cell migration and wound repair by ATP-mediated activation of dual oxidase 1. *J Biol Chem*. 282:3213-20.
- Widschwendter, M., G. Jiang, C. Woods, H.M. Muller, H. Fiegl, G. Goebel, C. Marth, E. Muller-Holzner, A.G. Zeimet, P.W. Laird, and M. Ehrlich. 2004. DNA hypomethylation and ovarian cancer biology. *Cancer Res*. 64:4472-80.
- Wistuba, II, D. Bryant, C. Behrens, S. Milchgrub, A.K. Virmani, R. Ashfaq, J.D. Minna, and A.F. Gazdar. 1999. Comparison of features of human lung cancer cell lines and their corresponding tumors. *Clin Cancer Res*. 5:991-1000.
- Wong, J.L., R. Creton, and G.M. Wessel. 2004. The oxidative burst at fertilization is dependent upon activation of the dual oxidase Udx1. *Dev Cell*. 7:801-14.
- Wong, L.S., and M. Martins-Green. 2004. Firsthand cigarette smoke alters fibroblast migration and survival: implications for impaired healing. *Wound Repair Regen*. 12:471-84.
- Wright, J.M., C.A. Merlo, J.B. Reynolds, P.L. Zeitlin, J.G. Garcia, W.B. Guggino, and M.P. Boyle. 2006. Respiratory epithelial gene expression in patients with mild and severe cystic fibrosis lung disease. *Am J Respir Cell Mol Biol*. 35:327-36.
- Wu, R., Y.H. Zhao, and M.M. Chang. 1997. Growth and differentiation of conducting airway epithelial cells in culture. *Eur Respir J*. 10:2398-403.
- Yang, C.M., J.M. Farley, and T.M. Dwyer. 1988. Acetylcholine-stimulated chloride flux in tracheal submucosal gland cells. *J Appl Physiol*. 65:1891-4.

- Yang, G.P., and M.T. Longaker. 2003. Abstinence from smoking reduces incisional wound infection: a randomized, controlled trial. *Ann Surg.* 238:6-8.
- Yeh, H.C., C.M. Puleo, T.C. Lim, Y.P. Ho, P.E. Giza, R.C. Huang, and T.H. Wang. 2006. A microfluidic-FCS platform for investigation on the dissociation of Sp1-DNA complex by doxorubicin. *Nucleic Acids Res.* 34:e144.
- Yoshiko, Y., J.E. Aubin, and N. Maeda. 2002. Stanniocalcin 1 (STC1) protein and mRNA are developmentally regulated during embryonic mouse osteogenesis: the potential of stc1 as an autocrine/paracrine factor for osteoblast development and bone formation. *J Histochem Cytochem.* 50:483-92.
- Yoshisue, H., S.M. Puddicombe, S.J. Wilson, H.M. Haitchi, R.M. Powell, D.I. Wilson, A. Pandit, A.E. Berger, D.E. Davies, S.T. Holgate, and J.W. Holloway. 2004. Characterization of ciliated bronchial epithelium 1, a ciliated cell-associated gene induced during mucociliary differentiation. *Am J Respir Cell Mol Biol.* 31:491-500.
- Yu, L., L. Zhen, and M.C. Dinauer. 1997. Biosynthesis of the phagocyte NADPH oxidase cytochrome b558. Role of heme incorporation and heterodimer formation in maturation and stability of gp91phox and p22phox subunits. *J Biol Chem.* 272:27288-94.
- Zamproni, I., H. Grasberger, F. Cortinovis, M.C. Vigone, G. Chiumello, S. Mora, K. Onigata, L. Fugazzola, S. Refetoff, L. Persani, and G. Weber. 2008. Biallelic inactivation of the dual oxidase maturation factor 2 (DUOXA2) gene as a novel cause of congenital hypothyroidism. *J Clin Endocrinol Metab.* 93:605-10.
- Zhao, H., J. Dupont, S. Yakar, M. Karas, and D. LeRoith. 2004. PTEN inhibits cell proliferation and induces apoptosis by downregulating cell surface IGF-IR expression in prostate cancer cells. *Oncogene.* 23:786-94.
- Zhou, X.M., S.J. Shao, G.D. Xu, R.T. Zhong, D.Y. Liu, J.W. Tang, Y.N. Gao, S.J. Cheng, and B.C. Lin. 2005. Highly sensitive determination of the methylated p16 gene in cancer patients by microchip electrophoresis. *J Chromatogr B Analyt Technol Biomed Life Sci.* 816:145-51.
- Zochbauer-Muller, S., J.D. Minna, and A.F. Gazdar. 2002. Aberrant DNA methylation in lung cancer: biological and clinical implications. *Oncologist.* 7:451-7.

8 Acknowledgments

My sincere gratitude goes to two people: Prof. Ulla G. Knaus of The Scripps Research Institute and Prof. Arnd Baumann of the University of Cologne/Forschungszentrum Jülich. I would like to thank Ulla for the opportunity to work in her lab and providing me with all the projects I worked on since I joined the lab. I learned so much during my time in your lab. Thank you for your endless advice and constant support! I am also grateful to Arnd for being an extraordinary „external“ supervisor. Thanks for always taking the time to meet with me and all of your support from overseas!

I also would like to thank Prof. Dr. Sigrun Korsching, Prof. Dr. Siegfried Roth and Dr. Ingo Weyand for agreeing to be part of my thesis committee.

Furthermore I want to thank Monika Frausto, Kat Schreiber, Monica Ruse, Mandy Lehmann, Julie Lamothe, Mike Ye and Suzel Davanture for their continuous support, helpful discussions and advice. Thank you for providing an extraordinary atmosphere at work! I also would like to acknowledge Paul Monnier, who performed many studies on the animal models.

Besonderer Dank gilt Saskia Hemmers und Edward Lemke. Danke für eure unermüdliche Freundschaft und Unterstützung! Danke auch für eure wissenschaftlichen Ratschläge (extremely significant) sowie für eure Hilfe beim Korrigieren dieser Arbeit. Thanks to Jessica Houghton, for being the person that you are!

Vielen Dank speziell an Jochen Pelsler, Meike Hausmanns und Dirk Oedekoven, dafür, dass ihr mich auch nach all den Jahren in San Diego nicht vergessen habt. Und was wäre ich ohne meinen BSPF Michael Maue (aka Milchi)?

Mein größter Dank gilt meiner Familie. Ohne eure vielfältige Hilfe wäre ich nicht da wo ich heute bin! Danke an meine Schwester Katrin Skelnik, die sich in den letzten Jahren so aufopferungsvoll um Tammi gekümmert hat. Schlußendlich danke ich meinen Eltern Regina Skelnik und Walter Luxen, sowie meiner Großmutter Hermine Barthel. Danke, dass ihr immer an mich geglaubt habt (bis auf die Geschichte mit dem Nobelpreis vielleicht) und stets meine Ziele bedingungslos unterstützt habt.

Danke für alles!

9 Erklärung

Ich versichere, daß ich die von mir vorgelegte Dissertation selbständig angefertigt, die benutzten Quellen und Hilfsmittel vollständig angegeben und die Stellen der Arbeit - einschließlich Tabellen, Karten und Abbildungen -, die anderen Werken im Wortlaut oder dem Sinn nach entnommen sind, in jedem Einzelfall als Entlehnung kenntlich gemacht habe; daß diese Dissertation noch keiner anderen Fakultät oder Universität zur Prüfung vorgelegen hat; daß sie - abgesehen von unten angegebenen Teilpublikationen - noch nicht veröffentlicht worden ist, sowie, daß ich eine solche Veröffentlichung vor Abschluß des Promotionsverfahrens nicht vornehmen werde. Die Bestimmungen dieser Promotionsordnung sind mir bekannt. Die von mir vorgelegte Dissertation ist von Herrn Prof. Dr. Arnd Baumann (Forschungszentrum Jülich) Frau Prof. Dr. Ulla G. Knaus (The Scripps Research Institute) betreut worden.

San Diego im August 2008

Sylvia Luxen

Teilpublikationen:

- (1) Sylvia Luxen, Steven A. Belinsky and Ulla G. Knaus. (2008) Silencing of DUOX NADPH oxidases by promoter hypermethylation in lung cancer. *Cancer Research*. 68:1037-1045
- (2) Sandrine Pacquelet, Mandy Lehmann, Sylvia Luxen, Karine Regazzoni, Monika Frausto, Deborah Noack, and Ulla G. Knaus. (2008) Inhibitory action of Noxa1 on Duox activity in airway cells. *Journal of Biological Chemistry*. 283(36):24649-24658
- (3) Sylvia Luxen, Deborah Noack, Monika Frausto, Bruce E. Torbett, and Ulla G. Knaus. (2008) Heterodimerization controls localization of ROS-producing Duox/DuoxA enzymes in airway cells. *Journal of Cell Science* (accepted)

10 Curriculum Vitae

Persönliche Daten

Name	Sylvia Luxen
Geburtsdatum	29. November 1979
Geburtsort	Krefeld
Adresse	St.-Matthias-Str. 17, 47809 Krefeld
Nationalität	deutsch
Email	sylvia.luxen@gmx.de

Bildungsweg

04/2005 – 10/2008	auswärtige Promotion am Scripps Research Institute (La Jolla, USA) im Department of Immunology and Microbial Science in der Arbeitsgruppe von Prof. Dr. Ulla G. Knaus; betreut durch Prof. Dr. Arnd Baumann
03/2005	Diplom in Biologie, Universität zu Köln
03 - 12/2004	Auswärtige Diplomarbeit am Scripps Research Institute (La Jolla, USA) im Department of Immunology and Microbial Science in der Arbeitsgruppe von Prof. Ulla G. Knaus zum Thema: "The expression of the novel NADPH oxidase Duox1 in lung cells & lung cancer cell lines"; betreut durch Prof. Dr. Benno Müller-Hill
02/2004	Diplomprüfungen im Hauptfach Genetik und in den Nebenfächern Biochemie und Organische Chemie
09/2001	Vordiplom in Biologie, Universität zu Köln
1999 - 2005	Studium der Biologie an der Mathematisch-Naturwissenschaftlichen Fakultät der Universität zu Köln
1999	Abitur
1990 - 1999	Gymnasium Fabritianum, Krefeld

Praktika/Auslandsaufenthalte

04 - 08/2003	Altana Research Institute, Waltham, MA, USA
06/2002	Institut für Biochemie der Universität zu Köln
05/2002	Institut für Virologie der Universität zu Köln
03 - 04/2002	Bayer AG, Leverkusen, Zentrale Forschung
08 - 09/2000	Bayer AG, Uerdingen, Forschung und Entwicklung